Department of Signal Processing and Acoustics

Development of digital predistorters for broadband power amplifiers in OFDM systems using the simplicial canonical piecewise linear function

Mei Yen Cheong

Aalto University

DOCTORAL DISSERTATIONS

Aalto University publication series
DOCTORAL DISSERTATIONS 38/2014

Development of digital predistorters for broadband power amplifiers in OFDM systems using the simplicial canonical piecewise linear function

Mei Yen Cheong

A doctoral dissertation completed for the degree of Doctor of Science (Technology) to be defended, with the permission of the Aalto University School of Electrical Engineering, at a public examination held at the lecture hall S1 of the school on 25 April 2014 at 12.

Aalto University
School of Electrical Engineering
Department of Signal Processing and Acoustics

Supervising professor
Prof. Risto Wichman

Thesis advisor
Dr. Stefan Werner

Preliminary examiners
Prof. Paulo S. R. Diniz, Universidade Federal do Rio de Janeiro, Brazil
Prof. Pedro Julian, Universidad Nacional del Sur, Bahia Blanca, Argentina

Opponents
Prof. Markku Renfors, Tampere University of Technology, Tampere, Finland
Prof. Paulo S. R. Diniz, Universidade Federal do Rio de Janeiro, Brazil

Aalto University publication series
DOCTORAL DISSERTATIONS 38/2014

ISBN 978-952-60-5619-7
ISBN 978-952-60-5620-3 (pdf)
ISSN-L 1799-4934
ISSN 1799-4934 (printed)
ISSN 1799-4942 (pdf)
http://urn.fi/URN:ISBN:978-952-60-5620-3

Unigrafia Oy
Helsinki 2014

Finland

441 697
Printed matter

Aalto University

Abstract

Aalto University, P.O. Box 11000, FI-00076 Aalto www.aalto.fi

Author
Mei Yen Cheong

Name of the doctoral dissertation
Development of digital predistorters for broadband power amplifiers in OFDM systems using the simplicial canonical piecewise linear function

Publisher School of Electrical Engineering

Unit Department of Signal Processing and Acoustics

Series Aalto University publication series DOCTORAL DISSERTATIONS 38/2014

Field of research Signal Processing for Communications

Manuscript submitted 8 November 2013 **Date of the defence** 25 April 2014

Permission to publish granted (date) 15 January 2014 **Language** English

☐ **Monograph** ☒ **Article dissertation (summary + original articles)**

Abstract

Power amplifiers (PAs) are inherently nonlinear devices. Linearity of a PA can be achieved by backing off the PA to its linear region at the expense of power efficiency loss. For signals with high envelope fluctuation such OFDM system, large backoff is required, causing significant loss in power efficiency. Thus, backoff is not a favourable solution. Digital predistorters (PDs) are widely employed for linearizing PAs that are driven to the nonlinear regions. In broadband systems where PAs exhibit memory effects, the PDs are also required to compensate the memory effects.

This thesis deals with the development of digital PDs for broadband PAs in OFDM systems using the Simplicial Canonical Piecewise Linear (SCPWL) function. The SCPWL function offers a few advantages over polynomial models. It imposes a saturation after the last breakpoint, making it suitable for modelling nonlinearities of PA and PD. The breakpoints of the function can be freely placed to allow optimum fitting of a given nonlinearity. It is suitable for modeling strong nonlinearities. Analysis of the SCPWL spectra property shows that the function models infinite order of intermodulation distortion, even with small number of breakpoints. The accuracy of the model can be improved by increasing the number of breakpoints.

The original real-valued SCPWL function is extended to include memory structure and complex-valued coefficients, resulting in the proposed baseband SCPWL model with memory. The model is adopted in the development of the Hammerstein-SCPWL PD and memory-SCPWL PD. Vector projection methods are developed for static SCPWL PDs identification. Adaptive algorithms employing the indirect and direct learning architectures are developed for identifying the Hammerstein-SCPWL PD and memory-SCPWL PD. By exploiting the properties of the SCPWL function, the algorithms are simplified. A modified Wiener model estimator is employed to circumvent the non-convex cost function problem of block models. This further reduces the complexity of the Hammerstein PD algorithms. The thesis also analyses the effects of measurement noise on indirect learning SCPWL filter. Due to its linear basis function, the SCPWL filter coefficients do not suffer the coefficient bias effects which are observed in polynomial models. The performance of the proposed SCPWL PDs are compared with state-of-the-art polynomial-based PDs by simulations and measurements.

Keywords Predistorter, power amplifier, nonlinear distortion, memory effects, adaptive linearization, piecewise linear function, OFDM

ISBN (printed) 978-952-60-5619-7 **ISBN (pdf)** 978-952-60-5620-3

ISSN-L 1799-4934 **ISSN (printed)** 1799-4934 **ISSN (pdf)** 1799-4942

Location of publisher Helsinki **Location of printing** Helsinki **Year** 2014

Pages 191 **urn** http://urn.fi/URN:ISBN:978-952-60-5620-3

Preface

The research leading to this thesis has been carried out in the Department of Signal Processing and Acoustics, Aalto University (formerly known as Signal Processing Laboratory, Helsinki University of Technology) from 2004 - 2012. The early stage of the research was supervised by Prof. Timo Laakso and the later stage was supervised by Prof. Risto Wichman.

First, I would like to express my sincere gratitude to my supervisors. I am grateful to Prof. Risto Wichman for taking my research under his supervision and for helping me finish this work. I thank him for his many constructive comments which have helped improve this manuscript. I am also grateful to Prof. Timo Laakso for his encouragement, guidance and advice during the early stage of this work. I would also like to extend my sincere gratitude to Dr. Stefan Werner for his guidance and help in this work. The insightful discussions, suggestions and constructive comments he provided have contributed to the quality of this thesis. I also thank Prof. Juan Cousséau for the insightful discussions and suggestions during his visits at the laboratory. The help from Prof. José Luis Figueroa and Marcelo Bruno are also highly appreciated. Prof. Markus Rupp and Dr. Ernst Aschbacher are also acknowledged for their advice and collaboration during my research visit at the Vienna University of Technology.

I would like to thank the preliminary examiners, Prof. Paulo Diniz and Prof. Pedro Julián for their time and effort in reviewing the manuscript. Their comments and suggestions have helped improve the quality and clarity of this manuscript.

I am grateful to my former colleagues at the Department of Signal Processing and Acoustic who have created an exceptionally nice and friendly working atmosphere. Besides your being always helpful and supportive, I miss those lunch conversations which were funny, smart and most of all, inspiring at times. I thank Dr. Màrio Jorge Costa, Dr. Alexandra Oborina, Dr. Traian Abrudan, Dr. Jussi Salmi, Dr. Fernando Hugo Gregorio, Dr. Andreas Richter, Dr. Fabio Belloni, Dr. Sachin Chaudhari, Dr. Pekka Jänis, Tuomas Aittomäki, Marian Bică, Taneli Riihonen, Pramod

Mathecken, Jayaprakash Rajasekharan, Azadeh Haghparast and Mobien Shoaib. I thank our laboratory secretary Mirja Lemetyinen for her help and support in many practical matters. Dilek and Chiara deserve my special thanks for being exceptionally supportive and for lending their listening ears when frustration took over. I also acknowledge Anu, Nuch, Timppa, Mikä, Erkin, Tomi, Lasse, Kalle, Markku, Shengye, Arlene, Sari, Yanli and Jing for their support and friendship. Special thanks also go to my Malaysian friends for making hanging out fun and relaxing, and every time, without exception, fantastic food are involved.

A part of this research work was funded by the Graduate School of the Electrical and Communications Engineering department of Helsinki University of Technology. The financial support granted by HPY:n Tutkimussäätiö and the Research Foundation of Helsinki University of Technology (Teknillisen koerkeakoulu tutkisäätiö) are also gratefully acknowledge.

I thank my family in Malaysia for their love and constant support. I am indebted to them for not being able to spend more time with them. Finally, thank you Janne for your unconditional support and love. You bring to my life abundance of happiness and meaning with simplicity. Let's still try to tackle the unsplitted wave function together!

Espoo, March 27, 2014,

Mei Yen Cheong

Contents

List of Publications

[**I**] Mei Yen Cheong, Stefan Werner, Juan Cousséau and Timo I. Laakso, "Predistorter identification using the simplicial canonical piecewise linear function," *in Proceedings of the 12th International Conference on Telecommunications (ICT)*, Cape Town, South Africa, May 3-6, 2005.

[**II**] Mei Yen Cheong, Ernst Aschbacher, Peter Brunmayr, Markus Rupp and Timo I. Laakso,"Comparison and experimental verification of two low-complexity digital predistortion methods," *in Proceedings of the 39th Asilomar Conference on Signals, Systems and Computers*, Pacific Grove, CA., USA, pp. 432-436, 30 October-2 November, 2005.

[**III**] Mei Yen Cheong, Stefan Werner, Timo Laakso, Juan Cousséau, and Jose L. Figueroa, "Predistorter design employing parallel piecewise linear structure and inverse coordinate mapping for broadband communications," *in Proceedings of the 14th European Signal Processing Conference (EUSIPCO)*, Florence, Italy, September 4-8, 2006.

[**IV**] Mei Yen Cheong, Helka-Liina Määttänen, Stefan Werner and Sven-Gustav Häggman, "A combined PAPR reduction and predistorter scheme for OFDM systems in nonlinear channels," *in Proceedings of the IEEE Radio and Wireless Symposium (RWS)*, Long Beach, CA., USA, pp. 309-312, January 9-11, 2007.

[**V**] Ernst Aschbacher, Mei Yen Cheong, Peter Brunmayr, Markus Rupp and Timo I. Laakso, "Prototype implementation of two efficient low-complexity digital predistortion algorithms," *EURASIP Journal on Advanced Signal Processing*, vol. 2008, pp. 15, 2008.

[**VI**] Mei Yen Cheong, Stefan Werner, Juan Cousséau, Risto Wichman, "Spectral characteristics of a piecewise linear function in modeling power amplifier type nonlinearities," *in Proceedings of the IEEE 21st International Symposium on Personal Indoor and Mobile Radio Communications (PIMRC)*, Istanbul, Turkey, pp. 639-644, September 26-30, 2010.

[**VII**] Mei Yen Cheong, Stefan Werner, Marcelo J. Bruno, Jose L. Figueroa, Juan Cousséau and Risto Wichman, "Adaptive piecewise linear predistorters for nonlinear power amplifiers with memory," *IEEE Transaction on Circuits and Systems–I*: Regular Papers, vol.59, no.7, pp. 1519-1532, July 2012.

List of Abbreviations

2G	second generation
3G	third generation
4G	fourth generation
ACP	adjacent channel power
ACPR	adjacent channel power ratio
ADC	analog-to-digital conversion
ADS	advanced design system
AM/AM	amplitude-to-amplitude conversion
AM/PM	amplitude-to-phase conversion
BER	bit-error-rate
CCDF	complementary cumulative distribution function
CDMA	code division multiple access
DAC	digital-to-analog conversion
DC	direct current
DFT	discrete Fourier transform
DSP	digital signal processor
EVM	error vector magnitude
FFT	fast Fourier transform
FIR	finite impulse response
GSM	global system for mobile communications
IBO	input backoff
ICI	intercarrier interference
ICM	inverse coordinate mapping
IDFT	inverse discrete Fourier transform
IEL	instantaneous equivalent filter
IFFT	inverse fast Fourier transform
IMD	intermodulation distortion
IP3	third order intercept point

ISI	intersymbol interference
LMS	least mean square
LS	least squares
LTE	Long Term Evolution
MC-CDMA	multi-carrier CDMA
MSE	mean squared error
NFxLMS	nonlinear filtered-x least mean square
NFxRLS	nonlinear filtered-x recursive least squares
NG	Narrendra-Gallman
OBO	output backoff
OFDM	orthogonal frequency division multiplexing
PA	power amplifier
PAE	power added efficiency
PD	predistorter
PSB	Poza-Sarkozy-Berger
PSD	power spectral density
PSK	phase shift keying
PTS	partial transmit system
PWL	piecewise linear
QAM	quadrature amplitude modulation
RF	radio frequency
SCPWL	simplicial canonical piecewise linear
SLM	selected mapping
SNR	signal-to-noise ratio
SSPA	solid state power amplifier
TD	total degradation
TWTA	traveling wave tube amplifier
WCDMA	wideband code division multiple access
WiMAX	Worldwide Interoperability for Microwave Access

List of Symbols

$\hat{a}$	estimate of scalar a
a^*	conjugate of scalar a
$\lvert a \rvert$	modulus of scalar a
$\mathbf{a}^H$	conjugate transpose of vector $\mathbf{a}$
$\mathbf{A}^{-1}$	inverse of matrix $\mathbf{A}$
c_i	the i-th coefficient of SCPWL function
$\mathbf{c}$	coefficient vector of SCPWL function
$c_{\ell i}$	the i-th coefficient of memory-SCPWL function of the ℓ-th branch
$\mathbf{c}_\ell$	coefficient vector of the ℓ-th delay branch of memory-SCPWL function
$\mathbb{C}$	complex domain
d_i	the i-th digital symbol sequence
$d_{n,i}$	delay of the i-th pulse of a pulse train associated with the n-th SCPWL basis
D_n	the n-th reference symbol
$E[\cdot]$	expectation operator
f_k	the k-th OFDM subcarrier frequency
f_s	sampling frequency
$f_A(\cdot)$	AM/AM function
$f_p(\cdot)$	AM/PM function
G	desired linear gain at the PD-PA output
$\mathscr{G}(k)$	derivative of the PA nonlinear function associated with the k-th sample
$\mathbb{H}$	linear filter function of the PA
m_i	slope of the i-th SCPWL segment
M_n	the number of pulses in the pulse train associated with the n-th SCPWL basis

n	sample number
N	number of discrete samples in one OFDM symbol
N_b	total number of transmitted bits
N_e	total number of erroneous bits
N_s	number OFDM subcarriers
$\mathbb{N}[\cdot]$	nonlinear function of the PA
P_{dc}	DC power
P_i	RF input power
$P_{\text{i,avg}}$	mean input signal power
$P_{\text{i,sat}}$	input saturation power
P_o	RF output power
$P_{\text{o,avg}}$	mean output signal power
$P_{\text{o,sat}}$	output saturation power
$\mathbb{P}[\cdot]$	nonlinear function of the PD
$\mathbf{Q}$	vector projection matrix
$\mathbb{Q}$	linear filter function of the PD
$s(t)$	baseband representation of OFDM symbol
s_i	length of the i-th SCPWL segment
$\hat{\mathbf{S}}(f)$	estimate of the spectrum of the SCPWL function
t	time index
t_s	OFDM symbol start time
T	OFDM symbol duration
T_s	sampling period
$u(t)$	input signal of the PA or output signal of the PD
$\mathbf{u}_k$	the discrete sample set of the k-th OFDM symbol
$W_{n,i}$	pulse width of the i-th pulse of a pulse train associated with the n-th SCPWL basis
$x(t)$	input signal of the PD
$y(t)$	output signal of the PA
$\tilde{z}(t)$	generic RF signal
$z(t)$	complex envelope of a generic RF signal
$z[n]$	discrete-time equivalent of a generic RF signal complex envelope
$\hat{Z}_n$	the n-th demodulated received symbol
β_i	the i-th breakpoint of SCPWL function
β_σ	the last breakpoint of the SCPWL function
γ	conduction angle of the PA
$\Gamma[\cdot]$	pulse train corresponding to the sign of the argument

$\mathbf{\Gamma}(f)$	Fourier transform of a
η	power efficiency of the PA
η_{PAE}	power added efficiency of the PA
$\vartheta_z(t)$	phase of a generic complex baseband signal
$\lambda_i(\cdot)$	the i-th SCPWL basis function
$\boldsymbol{\lambda}(\cdot)$	SCPWL basis function vector
$\mathbf{\Lambda}(\cdot)$	SCPWL basis function matrix
$\mathbf{\Lambda}(\cdot)^{-1}$	inverse of the SCPWL basis function matrix
$\mathbf{\Pi}_n(f)$	Fourier transform of a rectangular pulse train function associated with the n-th SCPWL basis
σ^2	variance of a random variable
$\otimes$	convolution
$\|\cdot\|_\infty$	infinity-norm
$\|\cdot\|_2$	2-norm
$\left(\frac{E_b}{N_0}\right)_{\text{NL}}$	bit-energy-to-noise ratio in nonlinear channel
$\left(\frac{E_b}{N_0}\right)_{\text{Lin}}$	bit-energy-to-noise ratio in AWGN channel

1. Introduction

1.1 Motivation

Power amplifier (PA) is an essential component in the wireless transmitter. It amplifies the transmitted signal so that the signal power attenuation caused by path loss can be compensated. On the other hand, PAs are inherently nonlinear in their response. The undesired effects of nonlinear distortion caused by a PA include inband signal distortion and spectral spreading into adjacent channels, in which, the latter may cause adjacent channel interference [1, 2]. The easiest way to avoid nonlinear distortion is by backing off the PA to its linear region. However, this solution comes at the cost of power efficiency loss. Systems that employ multicarrier schemes such as orthogonal frequency division multiplexing (OFDM) and multi-carrier code division multiple access (MC-CDMA), produce high peak-to-average power ratio (PAPR) signals. Due to the high PAPR signal, large backoff is required to avoid nonlinear distortion, resulting in significant power efficiency loss. Poor power efficiency translates to heat dissipation problem, higher power consumption and increased carbon footprint. In mobile networks, power efficient operation of the base stations is crucial for operational cost saving and reduction of carbon footprint [3, 4]. On the mobile terminal side, the incentive of power efficiency is a prolonged battery life. Thus, external linearization techniques for compensating nonlinear effects of efficiently operated PAs are required.

There are a variety of linearization techniques for radio frequency (RF) PAs, such as feedback and feedforward linearizers and predistorter (PD). Among these techniques, digital PD is known to be the most appealing method [1, 2] due to its relatively good performance, broader operating bandwidth, cost effectiveness and flexibility, when compared to the other

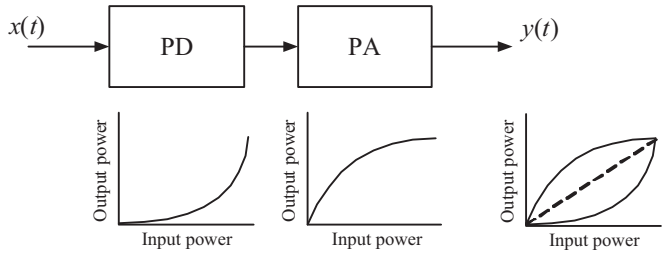

Figure 1.1. The operational principle of a predistortion linearizer

techniques. In the recent literature, digital PDs are widely proposed for linearization of PAs in third generation (3G) [5, 6], WiMAX [7, 8] and long term evolution (LTE)/LTE-Advanced (LTE-A) [9] systems.

The working principle of predistortion linearizer is illustrated in Fig. 1.1. The characteristic of the PD $\mathbb{P}[\cdot]$ is ideally the exact inverse of the PA nonlinearity, $\mathbb{N}[\cdot]$. The PD is placed before the PA, predistorting the input signal so that the resultant output of the PA is a linearly amplified version of the input signal given by

$$y(t) = \mathbb{N}\big[\mathbb{P}[x(t)]\big] = Gx(t), \tag{1.1}$$

where G is ideally a linear gain. From this simple illustration of PD operation, it is easy to follow that accurate modeling of $\mathbb{N}[\cdot]$, and thus $\mathbb{P}[\cdot]$ is essential for obtaining an effective PD. This, in turn, requires a suitable function to be chosen for modeling the nonlinearities and an efficient method for identifying the model parameters.

In narrowband systems such as the second generation (2G) GSM system, PA nonlinearities are characterized by the amplitude-modulation-to-amplitude-modulation conversion (AM/AM) and amplitude-modulation-to-phase-modulation conversion (AM/PM). Thus, memoryless nonlinear models are adequate for characterizing the PA and PD. In broadband systems such as 3G, LTE/LTE-A and WiMAX systems, the nonlinear behaviour of the PA becomes frequency-dependent, which is also known as memory effect. Thus, nonlinear models with memory are required in order to capture the frequency-dependency of PAs and PDs in broadband systems. In the literature, much research efforts are made in development of nonlinear models with memory for the purpose of PD design. Most of the models proposed are simplified Volterra models or polynomial-based models [5, 10–12]. Blocks models such as Wiener and Hammerstein models and the cascades of them are also commonly adopted for modeling nonlinear PAs and PDs with memory [13–17]. The nonlinear blocks

of these block models are also most commonly characterized by polynomial models. A weakness of polynomial models is their limitation in modeling strong nonlinearities. High order polynomials exhibit Runge phenomenon [18, Chapter 4.3.4] when used for modeling strong nonlinearities and pose numerical problems associated with parameter estimation. Orthogonal polynomial [19] and more recently, Zernike polynomial [12], which possess better numerical property are proposed for PD implementation. The piecewise linear (PWL) nonlinear model proposed in this thesis is another alternative nonlinear model suitable for modeling strong nonlinearity without posing numerical problems.

It is well-understood that PA characteristics slowly drift as the device ages. In addition, in LTE/LTE-A systems, advanced techniques such as adaptive modulation [20] and scalable bandwidth [21] schemes are adopted to enhance throughput and optimize spectrum sharing. The operating signal condition of these systems (e.g., operating bandwidth, power level and digital modulation size) undergo frequent changes, and thus, causing variation in the PA characteristics. In order for the PD to be effective, the time-varying characteristics of the PA must be tracked, leading to the recent focus on development of adaptive PD identification algorithms. The indirect [5,10] and direct learning [16,22–24] methods are most commonly employed for PD training, with the former being more popular due to its simplicity and efficiency.

A major issue of the indirect learning method is its sensitivity to measurement noise at the feedback path [25, 26]. An analysis in [25] shows that measurement noise at the feedback path of an indirect learning filter induces a bias in the estimates of polynomial filter coefficients. The effect is known as coefficient bias effect. The authors proposed a technique for reducing the bias. However, the technique increases the complexity of the PD algorithm significantly. A more efficient method based on the modified least squares (LS) method for reducing the noise induced bias is proposed in [27]. The direct learning algorithm is not affected by measurement noise. However, the downside of the direct learning method is its computational complexity, incurred by the need for the PA model estimation and filtering of the reference input signal with the PA estimates [22, 28, 29]. In [16, 23], the authors simplified their proposed direct learning PD identification algorithm by assuming that the PA model is known. It is shown that the optimal performance of a direct learning PD can only be obtained when both PA and PD models are identified iteratively [30].

In summary, in order to obtain an effective PD, models with simple structure and sufficient support for characterizing the essential modes of the PA and PD behaviour are required. Then, efficient algorithms needs to be developed for identifying the PD model parameters. In addition, issues that hinder the performance of the PD have to be addressed, for instance, measurement noise and computational complexity issues associated with the indirect learning or direct learning architectures, respectively.

1.2 Scope of the thesis

This thesis considers development of digital PDs for broadband PA in OFDM systems using the Simplicial Canonical Piecewise Linear (SCPWL) function [31, 32]. The scope of the thesis includes characterization of broadband PAs and PDs, development of efficient PD identification algorithms and performance evaluation of the proposed PDs.

The SCPWL function is used as a basis for developing baseband piecewise linear (PWL) models that are suitable for modeling baseband nonlinearities with memory. The proposed baseband SCPWL model is employed for modeling Hammerstein-SCPWL PDs and memory-SCPWL PDs. PD identification algorithms based on vector projection method and adaptive filtering method employing the indirect and direct learning architectures, are developed. By exploiting the properties of the SCPWL function, methods are developed to improve the efficiency of the identification algorithms. The performance of the proposed SCPWL PDs are evaluated and compared with well-known state-of-the-art digital PDs in the literature. The performance evaluation and comparison are performed by computer simulations in MATLAB® environment, circuit level simulations in the Agilent Advanced Design System (ADS), and by measurements on a practical PA in a testbed.

1.3 Contributions

The contribution of this thesis work are as follows.

The original real-valued SCPWL function proposed in [32] is employed in this work for developing digital PDs. As digital PDs operate in baseband, using complex-valued functions for modeling the nonlinear PA and PD is more convenient. Otherwise, the in-phase and quadrature-phase

components of the baseband signal will have to be modeled separately using two real-valued functions. In this work, a complex-valued baseband SCPWL model is proposed. In order to cater for broadband characteristics of the PAs and PDs, the model also includes memory structure, as expressed in (3.19). The proposed SCPWL model is suitable for modeling strong nonlinearity and does not pose numerical problems during parameter estimation. It is particularly suitable for modeling PA and PD types of nonlinearities as the model imposes a saturation after a given maximum input signal level. The proposed SCPWL model is adopted in the development of Hammerstein model PDs and memory-SCPWL PD.

The properties of the SCPWL function are studied and its linear affine property is found to be a useful for simplifying the PD algorithms. The spectral property of the SCPWL function is analyzed and some insights are gained on how the function introduces intermodulation products (IMD). The operation of the SCPWL basis functions is found to spread the spectrum of the input signal, producing infinite IMD products. In other words, the SCPWL function is capable of modeling nonlinearity of infinite order. The accuracy of the model improves as the number of segments is increased.

For identification of the SCPWL PDs, two approaches are proposed. Firstly, vector projection based methods, namely, the image projection method and inverse coordinate mapping (ICM) method are developed for efficient identification of static SCPWL PDs. In the second approach, adaptive filtering method based on the least mean square (LMS) algorithm (see e.g., [33]), adopting both the indirect and direct learning architectures, are developed for adaptive identification of SCPWL PDs with memory, i.e., the Hammerstein-SCPWL PD and memory-SCPWL PD. In order to improve computational efficiency in these algorithms, the properties of the SCPWL function are exploited for techniques to simplify these algorithms. In addition, for identification of Wiener and Hammerstein models, which is often hindered by non-convex cost function problem [34–36], the thesis adopts a modified Wiener model estimator leading to reduced computational complexity.

Acknowledging the issue of measurement noise at the feedback path of indirect learning filters, the thesis also provides an analysis on the effects of noise on the indirect learning SCPWL filter. It is found that, due to its linear basis functions, the SCPWL filter coefficients are not affected by noise-induced coefficient bias effect which affects polynomial filters

The performance of the proposed SCPWL PDs are evaluated and compared with well-referenced polynomial based PDs by extensive system level simulations in MATLAB® environment and circuit-level simulations in the Agilent ADS environment. The memoryless SCPWL PD is also evaluated on a real PA (ZVE8G) by Minicircuits. The main metrics used for evaluating the performance of the PDs are the adjacent channel power ratio (ACPR), error vector magnitude of received digital symbols and bit-error rate (BER). Results showed that the SCPWL PDs performances are comparable to the state-of-the-art polynomial based PDs.

1.4 Structure of the thesis

The thesis consists of an introductory part and seven original publications. The introductory part consisting of Chapter 2 through Chapter 6.

Chapter 2 provides a review on the problems of nonlinear distortion and memory effects caused by PAs and their effects on broadband communications systems. Then, factors that affect the linearity and efficiency of a PA are discussed and metrics commonly used for evaluating PD performance are defined. The high PAPR of OFDM signal and the problems it causes are also discussed.

Chapter 3 summarizes the contribution on modeling of PA and PD nonlinearities using the SCPWL function. The chapter begins with a review of the most employed nonlinear models for modeling broadband nonlinear PAs. Then, the proposed complex-valued baseband SCPWL model with memory is presented. The findings on the studies of the SCPWL function properties and the advantages of modeling PAs and PDs using the SCPWL function are outlined. The chapter concludes with a summary of the thesis contribution in the aspects of broadband PAs and PDs characterization.

Chapter 4 presents the SCPWL PD identification algorithms developed in this work. First, the PD identification algorithms found in the literature are reviewed. Then, the proposed vector projection based methods for mapping of the static SCPWL PD from the static SCPWL PA and the indirect learning and direct learning adaptive algorithms for adapting the SCPWL PDs with memory are presented. An analysis of measurement noise effects on indirect learning filters is provided. The convergence issues of the direct learning method are also discussed.

The results of performance evaluations and comparisons of the proposed

SCPWL PDs and well-referenced polynomial based PDs are summarized in Chapter 5. The simulation environments and measurement testbed used are illustrated.

The thesis contribution is summarized and concluded in Chapter 6.

1.5 Summary of publications

This section provides a summary for the original publications included in this thesis.

In all the publications, equations/algorithms derivation, experiment design, programming of simulations software in MATLAB® and writing related to the proposed SCPWL PD designs have been performed by the author. In [II] and [V], the measurement system setup and all parts involving the polynomial based Secant-PD were performed by the co-authors, Peter Brunmyr and Ernst Ashbacher, respectively. In [VII], the setup of the MATLAB® ADS-Ptolemy co-simulation has been performed by co-author Marcelo Bruno. The rest of the co-authors have contributed by providing constructive comments to the writing and/or supervising of the research work.

Publication [I] introduces the application of the simplicial canonical piecewise linear (SCPWL) function in predistorter (PD) design for nonlinear power amplifiers (PAs). The operation of the SCPWL function on an input signal is reviewed and its linear affine property, which is characterized by the user-defined breakpoints, is studied. The linear affine property gives rise to a special structure in the SCPWL basis function matrix. With the special structure, matrix inversion associated with least squares (LS) parameter identification can be avoided. Instead, the inverse of the matrix, which is a tri-diagonal full rank matrix, can be constructed from the known values of the user-defined breakpoints. Due to the linear affine property, an orthogonal projection method, which identifies the PD characteristic from that of the PA using a 2-by-2 projection matrix, is also developed. The real-valued SCPWL function was used to characterize the static nonlinearity (AM/AM) of a Wiener model PA. The orthogonal projection method and the constructed inverse basis function matrix are used in the PD parameter identification. It is shown that the overall computational complexity of SCPWL PD parameter identification is reduced compared to conventional LS identification of a polynomial PD.

Publication [II] is a short conference article reporting part of the work

in [V], where the proposed SCPWL PD and polynomial PD are tested on a practical PA in a testbed.

In [III], the orthogonal projection method in [I], which requires the linearized gain of the PD-PA to be normalized to 1, is extended in this paper to allow any arbitrary linearized gain. The enhanced PA-to-PD characteristic projection method is called the inverse coordinate mapping (ICM) method. In this paper, a Hammerstein model PD is used for linearizing a Wiener model PA. The nonlinear parts of the PA and PD are characterized as a quasi-static nonlinearities (AM/AM and AM/PM). The SCPWL parameters of the PD nonlinear block (AM/AM and AM/PM) are identified by the non-iterative approach using the ICM method and the inverse basis function matrix constructed from the known values of the function breakpoints. The dynamic blocks of the PA and PD are modeled using linear filters. The PD linear filter parameters are iteratively identified using the indirect learning architecture with least mean square (LMS) algorithm. A comparison in performance is made between the proposed SCPWL PD and one that the nonlinear parts are modeled using orthogonal polynomials [19].

In [IV], we categorize nonlinear distortion caused by the PA in systems that transmit high peak-to-average-power ratio (PAPR) signal such as OFDM into compressive gain distortion (nonlinear amplification) or signal peak clipping distortion. Linearization technique can be employed for compensating compressive gain distortion. However, considerable level of backoff is still required to avoid signal peak clipping, leading to power efficiency loss. This paper considers a combined peak-to-average-power ratio (PAPR) reduction and predistorter (PD) scheme for compensating nonlinear distortion and improving power efficiency. A simple static nonlinear PA modeled by a traveling wave tube amplifier (TWTA) is simulated in order to demonstrate the improvement in linearization performance and total degradation (TD) provided by the combined scheme as compared to either PD or PAPR reduction alone. While the PAPR reduction technique is effective in reducing clipping noise, it is ineffective in reducing adjacent channel power ratio (ACPR). The combined scheme is shown to provide an ACPR improvement twice as good as when the PD is applied alone. The TD gain obtained by combining the two methods is equal to the sum of the gains obtained by the PD and PAPR reduction individually.

Publication [V] presents the measurement results of testing a memoryless SCPWL PD and a memoryless polynomial PD on a practical PA, Mini-

circuit ZVE-8G. The measurement testbed consists of a signal processing part (MATLAB®, ADC, DAC) and an RF part (up/down-converter, preamps.) and the output of the PA is measured using a spectrum analyzer. Both the PDs are identified in the signal processing part using input-output data obtained by exciting the PA with a 5 MHz random phase multitone signal. The parameter of the SCPWL PD is identified using the reduced-complexity non-iterative method outlined in [I]. The inverse coordinate mapping method (ICM) detailed in [III] is used instead of the orthogonal projection method. The output signal of the polynomial PD is iteratively searched using the secant method for root-finding. The PDs are tested under two PA operating scenarios, i.e., in a mildly nonlinear region and driven into the nonlinear region. The SCPWL PD is found to be more effective for the PA with stronger nonlinearity. The comparison of computational complexity for the two PDs during PD identification and operation are provided.

Publication [VI] investigates how intermodulation distortion (IMD) components are introduced by the SCPWL function. This information is important for reflecting if an SCPWL function with a given number of parameters is sufficient for capturing all the significant IMD components generated by a PA. The operation of the SCPWL basis function on sinusoids and multi-tone signals are analyzed. It is shown that, in frequency domain, each SCPWL basis spreads the spectrum of the input signal resulting in an output signal with infinite IMD order. From the analysis, expressions that can be used to predict the output spectrum of the SCPWL basis is derived. It follows that the modeling accuracy of the function is determined by the number of linear affine segments (i.e., number of SCPWL parameters) used to define the SCPWL function. Increasing the number of model parameters improves the accuracy of function in modeling each IMD component. Unlike polynomial models, increasing the number of segments above the optimum order does not degrade the SCPWL model quality.

In [VII], a novel complex-valued SCPWL function with memory structure suitable for modeling baseband PA and PD nonlinearities is introduced. The new memory-SCPWL model can be reduced to a quasi-static model by choosing a memory length of 1. The proposed model is used for implementing a memory-SCPWL PD and a Hammerstein-SCPWL PD. Adaptive algorithms based on the indirect and direct learning methods are derived for PD parameter identification. The linear affine property

of the function and the knowledge of the user-defined breakpoint values are exploited for simplifying the algorithms. For instance, the derivative of the PA model appears in the expression of the direct learning algorithm. Using the known SCPWL parameters, an expression for approximating the derivative of the PA model is derived. For analysis of the effects of noise at the feedback path of the indirect learning filter, we derived an expression for the error induced by noise in the SCPWL basis. The expression shows that measurement noise does not cause coefficient bias effects on SCPWL coefficients, as it does to polynomial coefficients. This finding is confirmed by simulation results. The proposed adaptive SCPWL PDs are evaluated on broadband PAs (modeled as Wiener or Wiener-Hammerstein systems) by MATLAB®simulations. The performance of the proposed SCPWL PDs are compared with that of well-known state-of-the-art memory polynomial and generalized memory polynomial PDs, in terms of error vector magnitude (EVM) and adjacent channel power ratio (ACPR). The indirect learning memory-SCPWL PD is also evaluated on the Freescale MRF6S23100H LDMOS PA in 802.16d system by circuit level simulations in the ADS-Ptolemy co-simulation environment.

2. Effects of nonlinear PA and High PAPR of OFDM signal

Power efficiency and linearity are two contradicting requirements in PA design. A design aiming at improving efficiency is inevitably compromising the linearity of the PA [1,37,38]. The effects of nonlinear amplification include distortion of the inband signal and interference to the adjacent channels. As discussed earlier, power backoff is not an ideal solution for reducing nonlinear distortion as it trades off the power efficiency of the PA. Particularly, for systems which signal exhibits high envelop fluctuation, or high peak-to-average power ratio (PAPR), power backoff leads to substantial power efficiency loss. Furthermore, in broadband systems, PAs also exhibit memory effects which give rise to frequency-dependent nonlinear behaviour. Compensation of nonlinear distortion in these systems becomes more complicated. In order to maintain a good tradeoff between power efficiency and linearity, it is best to drive to PA to a sufficiently power efficient region and leave an acceptable level of nonlinear distortion for compensation using an external device such as a digital PD.

This chapter provides background on the effects of nonlinear PA and high PAPR of OFDM signal on communications signal. Linearity and efficiency of a PA and the factors that affect the tradeoff between these figures are discussed. The effects of nonlinear distortion on communications signal are reviewed and the high PAPR of OFDM signal is also discussed. In Section 2.1, factors that influence the power efficiency of PAs, i.e., PA operating classes and power backoff, are reviewed. Section 2.2 discusses the linearity measures of PAs. The nonlinear distortion caused by broadband PAs and the impact on the communications signals are outlined in Section 2.3. Memory effects are discussed separately in Section 2.4. Finally, OFDM and its high PAPR signal are discussed in Section 2.5.

2.1 Power efficiency

Power efficiency is a measure of a PA's ability to convert DC power P_{dc} provided by a DC supply to RF power P_o delivered to the load,

$$\eta = \frac{P_o}{P_{dc}}. \tag{2.1}$$

Another common figure of merit for measuring PA power efficiency is the power added efficiency (PAE) given by

$$\eta_{\text{PAE}} = \frac{P_o - P_i}{P_{dc}}. \tag{2.2}$$

The PAE equation has the RF input power subtracted from the RF output power. Thus, it gives a better indication of the PA efficiency in terms of RF power gain compared to the general power efficiency η. Direct current (DC) power that is not converted to useful RF output power is dissipated as heat.

Without adopting external efficiency enhancement or linearization techniques, the main factors that determines the power efficiency range of a PA are its operating class and power backoff of the PA.

2.1.1 PA operating classes

The power class of a PA is determined by the quiescent bias point of a PA, which defines the conduction angle of the PA (the portion of RF cycle that the transistor conducts). A lower bias level renders higher power efficiency, at the expense of the PA linearity, as illustrated in Figure 2.1. The relationship of conduction angle γ and the maximum efficiency of a PA is given by [1]

$$\eta = \frac{2\gamma - \sin 2\gamma}{4\left(\sin\gamma - \gamma\cos\gamma\right)}. \tag{2.3}$$

A class-A PA is biased such that its conduction angle is $360\,^\circ$, i.e., the transistor conducts for the full cycle of the input signal. This makes a class-A PA highly linear as it reproduces an output signal that closely resembles the input signal. However, the maximum power efficiency of the class-A PA is only 50%. A class-B PA is significantly more efficient than a class-A PA, at the expense of linearity. The maximum power efficiency of class-B PAs is 78.5%. This is due to its lower bias level, having a conduction angle of only $180\,^\circ$, i.e., conducting only half of the time, either during the positive cycle or the negative cycle. A push-pull configuration is normally employed so that the entire input signal can be reproduced at the

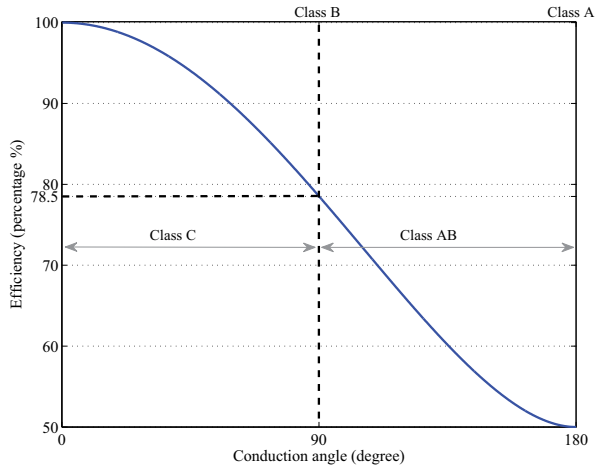

Figure 2.1. Conduction angle vs. Efficiency [1]

output. In this configuration one transistor conducts during the positive half cycle of the input signal and the second transistor conducts during the negative half cycle.

As a compromise between class-A and class-B PAs, a class-AB amplifier operates at bias level that gives the transistor a conduction angle between $180\,^\circ$ and $360\,^\circ$. Class-AB PAs produce more nonlinear distortion, generating odd order intermodulation distortion (IMD) as compared to only even order IMD caused by class-A PAs. The power efficiency of class-AB PAs is between 50% and 78.5%. A significant improvement in power efficiency can be achieved when a PA is biased towards class-C operation, with a conduction angle of less than $180\,^\circ$. The maximum power efficiency of a class-C PA is 85%, but its linearity is poor.

There are other PA classes such as D, E, F, G, H and S which efficiency approaching 100% but are highly nonlinear in their responses. Interested readers are referred to [1, 2] for further reading.

2.1.2 Power backoff

Power backoff imposed on a PA is a method employed to avoid driving the PA to its nonlinear region, thus maintaining the linear operation. It is commonly measured by input backoff (IBO) or output backoff (OBO), defined in Equations (2.4) and (2.5), respectively.

$$IBO = 10\log_{10}\left(\frac{P_{\text{i,sat}}}{P_{\text{i,avg}}}\right), \tag{2.4}$$

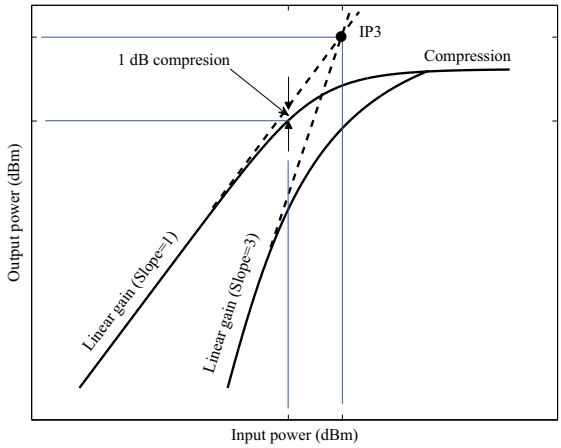

Figure 2.2. PA linearity figures of merit : 1 dB compression point and third order intercept point (IP3)

where $P_{\text{i,sat}}$ is the input saturation power and $P_{\text{i,avg}}$ is the mean power of the input signal.

$$OBO = 10\log_{10}(\frac{P_{\text{o,sat}}}{P_{\text{o,avg}}}), \tag{2.5}$$

where $P_{\text{o,sat}}$ is the output saturation power and $P_{\text{o,avg}}$ is the mean power of the output signal.

2.2 Linearity measures of PAs

An ideal PA is one that amplifies the input signal with a constant gain for all input signal level, i.e., exhibiting a linear behaviour. In practice, a PA amplifies linearly for a range of low signal level (linear region) and then the gain reduces as the signal level increases (nonlinear region) and finally saturates (saturation region). This behaviour is illustrated in Figure 2.2.

Besides gain compression, PA nonlinear distortion also causes the generation of frequency components which are not present in the input signal. The amount of new frequency components introduced depends on the degree of nonlinearity and is typically analyzed using a two-tone signal fed to a polynomial model PA, see e.g., [1,37,38]. Figure 2.3 shows the frequency components in the output signal of a two-tone test on a third order polynomial system (dc and envelope tones not shown). The quadratic nonlinearity produces the second harmonic components and the dc and envelop terms. The cubic nonlinearity generates not only harmonic terms

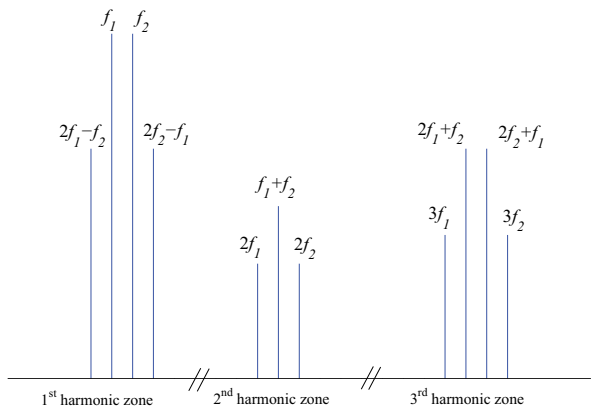

Figure 2.3. Spectral regrowth generated by a PA with third order nonlinearity

but also intermodulation distortion (IMD) terms $2f_1 - f_2$ and $2f_2 - f_1$. All odd order nonlinearities produce IMD, thus are considered more harmful than even order nonlinearities. The frequency components that appear at the second and third harmonic zones can be easily filtered out. The IMD products that fall in the first harmonic zone appear too close to the fundamental tones, making them difficult to be filtered out.

The classical figures of merit used as measures of linearity of a PA are the 1 dB compression point, and the third order intercept point (IP3) as illustrated in Figure 2.2. These figures indicates the amount of nonlinearity caused by the PA.

1-dB compression point

The 1 dB compression point of a nonlinear PA is defined as the output level at which the gain of the PA output is 1 dB below the expected linear output. This figure indicates the effects of the PA nonlinearity on the fundamental-tone signal.

Third order intercept point

Among the IMD products, the third order IMD is normally the strongest. The IP3 is the power level at the interception between the linear gain of the fundamental component and the linear gain of the third order component. It is used for measuring distortion of the fundamental signal caused by the third order IMD.

2.3 Distortions caused by nonlinear PAs

Depending on the signal bandwidth, the characteristics of a PA can be categorized into static nonlinear system or nonlinear system with memory. A memoryless RF PA have memory duration close to the period of the RF carrier and the input signal is a narrowband signal [39]. The envelope characteristics of the PA are constant over the band of interest. Thus, a strictly memoryless system responds to an excitation instantaneously without any delay. Strictly memoryless nonlinear PA exhibits only AM/AM distortion. However, in practice, this kind of systems do not exist. A large class of narrowband systems fall into the quasi-static category. In a quasi-memoryless nonlinear PA, the memory time constant is in the order of the RF carrier period, thus exhibits short-term memory effects. Quasi-memoryless PAs are characterized by both the AM/AM and AM/PM conversions. When the signal bandwidth is comparable to the carrier frequency of the system [1], nonlinear PAs exhibit memory effects which are manifested as frequency-dependent or bandwidth-dependent nonlinear responses.

This section discusses the effects of distortion caused by nonlinear PAs on communications signals transmitted through them. Memory effects are discussed in more details in the following section.

2.3.1 Amplitude and phase conversions

Typically the gain of a PA decreases as the input level increases, giving a compressive AM/AM response. In a similar way, the phase conversion at the output is not a constant as the input amplitude changes. As an example, Figure 2.4 shows the AM/AM and AM/PM responses obtained from simulated Wiener model PA with an FIR filter followed by a Saleh model [40] nonlinear block. The red plots are the PA responses to a single-tone signal with ramping power level.

2.3.2 Distortion in digital symbols

In modern 3G, LTE and WiMAX systems, linear modulations schemes are employed in order to gain throughput of information bits. The larger the constellation size of the modulation scheme, the more sensitive it is to the nonlinearity of the PA. Figure 2.5 shows the distortion of the 16-QAM digital symbols transmitted through a nonlinear PA. The blue dots and

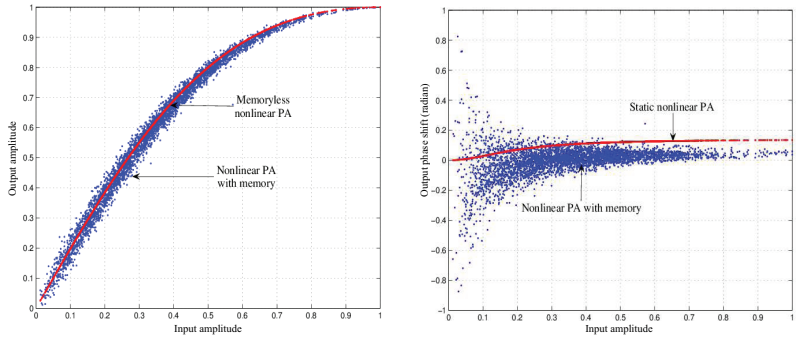

(a) AM/AM characteristics (b) AM/PM characteristics

Figure 2.4. AM/AM and AM/PM conversions of a PA : Red plots indicate memoryless PA and blue plots indicate PA with memory

the red dots represent the original transmitted symbols and the symbols transmitted through the PA, respectively. Due to the nonlinear amplitude conversion, the transmitted symbols are typically scattered around their respective original symbol constellation point and the symbols at the edges of the constellation appear to be pushed inward, resulting in what is known as constellation warping, as shown in Figure 2.5(a). Figure 2.5(b) shows the constellation rotation caused by AM/PM conversion. These effects, severe enough, can cause the received symbols to be shifted into adjacent detection regions, causing detection error and therefore increased bit-error rates.

In the following, the metrics commonly used to measure degradation/losses due to distortion caused by PAs are introduced.

Error vector magnitude

The error vector magnitude (EVM) is used to measure the error between the demodulated digital symbol (e.g., QPSK, 4-QAM, 16-QAM) and the reference symbol. The root mean square (rms) EVM for constellation point error is given by

$$\text{EVM}_{const} = 10\log_{10}\left\{\sqrt{\frac{\sum_{n=1}^{N}|\hat{Z}_n - D_n|^2}{\sum_{n=1}^{N}|D_n|^2}}\right\}, \tag{2.6}$$

where D_n is the n-th reference symbol and $\hat{Z}_n$ is the n-th demodulated symbol.

Bit error rate

The bit error rate (BER) is a performance metric that measures the quality of the communication link. It is also used to measure the degradation

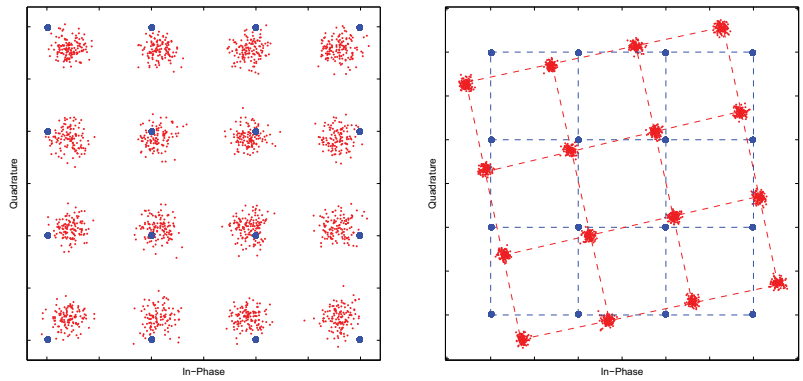

(a) Constellation scattering and warping at the edges of the constellation, due to AM/AM conversion

(b) Constellation rotation due to AM/PM conversion

Figure 2.5. Digital symbols constellation distortion

in the transmitted signal due to the nonlinear distortion caused by the PA. The BER is calculated as

$$\text{BER} = \log_{10}\left(\frac{N_e}{N}\right), \tag{2.7}$$

where N_e and N_b are the total number of erroneous bits and total number of transmitted bits, respectively.

Total degradation

The total degradation (TD) is a metric that measures the power loss due to the nonlinear distortion and the PA efficiency loss in order to meet a BER target. In other words, TD indicates the extra transmit power needed to overcome the nonlinear distortion for achieving a given BER target. The TD as a function of the output backoff (OBO) is given by [41]

$$\text{TD} = \left(\frac{E_b}{N_0}\right)_{\text{NL}} - \left(\frac{E_b}{N_0}\right)_{\text{Lin}} + OBO, \tag{2.8}$$

where $\left(\frac{E_b}{N_0}\right)_{\text{NL}}$ and $\left(\frac{E_b}{N_0}\right)_{\text{Lin}}$ are the bit-energy-to-noise ratio required to achieve a targeted BER in the nonlinear and linear AWGN channel, respectively. Note that all values in the equation are measured in dB.

2.3.3 Spectral spreading

In the frequency domain, the response to nonlinear distortion is the introduction of frequency components that are not present in the input signal. This effect is known as spectral regrowth. Figure 2.6 shows an example

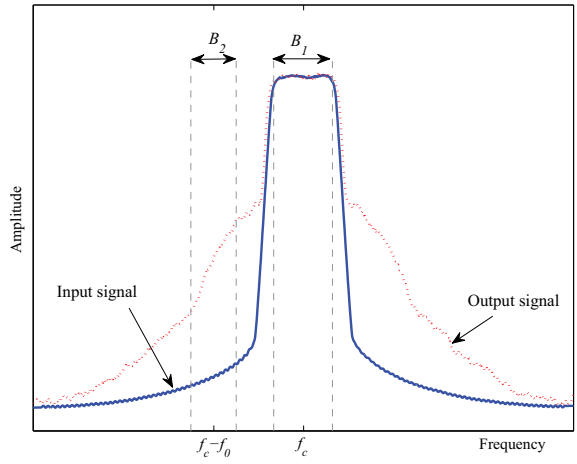

Figure 2.6. Spectral regrowth generated by a nonlinear PA

of typical power spectra density (PSD) of the signals measured at the input and output of a nonlinear PA. The output PSD of the signal without any linearization applied (red plot) shows significant amount of spectral regrowth. If left uncontrolled, spectral regrowth can cause distortion to the transmitted signal as well as interference to the adjacent channels. A linearizer such as a PD can be employed for reducing the spectral spilling into the adjacent channel (blue and cyan plots).

Adjacent channel power ratio

The adjacent channel power ratio (ACPR) or adjacent channel leakage ratio (ACLR) is used to measure the amount of spectral spilling into an adjacent channel. It is defined as the ratio between the power contained within a defined bandwidth B_2 at a defined offset f_o from the channel center frequency f_c, and the power contained within a defined bandwidth B_1 around f_c (refer to Figure 2.6). The bandwidth B_1 and B_2 need not be the same.

2.4 Memory effects in PAs

Memory effects in PAs are caused by the intrinsic electrical and thermal properties of the PAs [37,38,42,43]. PA memory can be divided into linear memory and nonlinear memory. Linear memory contributes to short-term memory effects [39]. It is attributed to the bandpass characteristics of the input and output matching networks in the PA system and the low-pass

characteristics of the transistor.

Nonlinear memory describes the dynamic processes that take place in the presence of some nonlinear processes [39]. These processes contribute to long-term memory effects and can be viewed as some complicated dynamic interaction between two or more nonlinearities within a dynamic network. These effects are attributed to the low-frequency dispersion of the active device, the interactions between the active device and the PA bias circuitry and electrothermal effects (including the device self-heating) [15, 39].

2.4.1 Observation of PA memory effects

Memory effects can be observed in the AM/AM and AM/PM characteristics when broadband signal is fed to a PA. The AM/AM and AM/PM conversions generated with a multitone signal (broadband signal) are no longer continuous lines (red plots) as obtained using a single-tone signal (narrowband signal), as shown in Figure 2.4. Instead the responses are scattered (blue plots) around the static nonlinear curves. Alternatively, the frequency-dependent behaviour can also be observed by measuring the AM/AM and AM/PM responses with single-tone signals at different carrier frequencies, as shown in Figure 2.7. The response curves measured at different carrier frequencies may have almost the same shape but appear vertically or horizontally displaced from each other.

Another common observation of memory effects is the asymmetrical IMD sidebands at the output of RF PA. Bandwidth dependency of memory effects is analysed using two-tone input signal with varying tone spacing in [42]. It is shown that by varying the tone spacing of a two-tone signal fed to a PA, the phase of the IM3 deviates from that of a polynomial model at low and high tone spacing, as shown in Figure 2.8. Another analysis on asymmetrical IMD sidebands in [37] concluded that the effect is due to the time lag between the AM/AM and AM/PM responses, which is caused by a phase shift in the AM/PM response.

2.4.2 Impact on PD performance

Although memory effect normally does not cause huge changes in the PA nonlinearity, e.g., the level of IMD components, it affects the performance of linearizers [38]. The performance of a simple linearizer that do not take into account memory effects, e.g., an RF PD implemented using diodes,

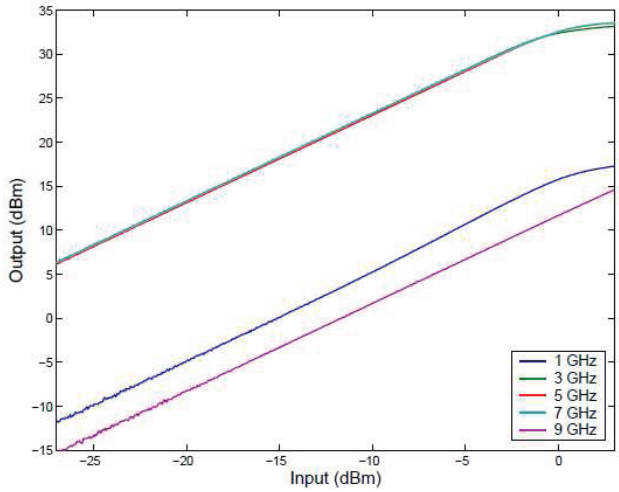

(a) Frequency-dependent AM/AM conversion

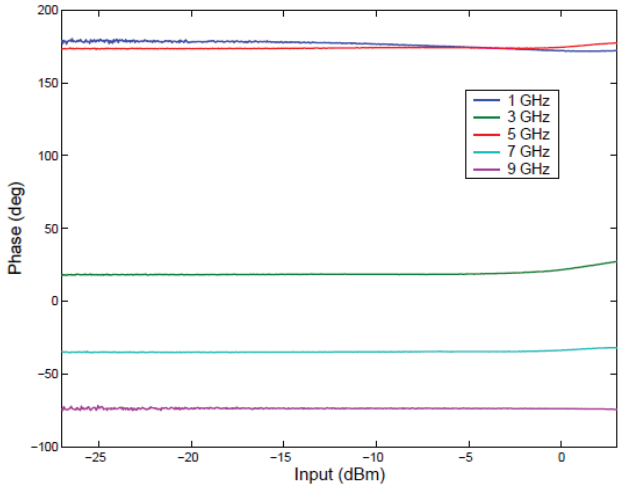

(b) Frequency-dependent AM/PM conversion

Figure 2.7. Measured swept-tone AM/AM and AM/PM conversions of the Minicircuit ZVE-8G PA [44].

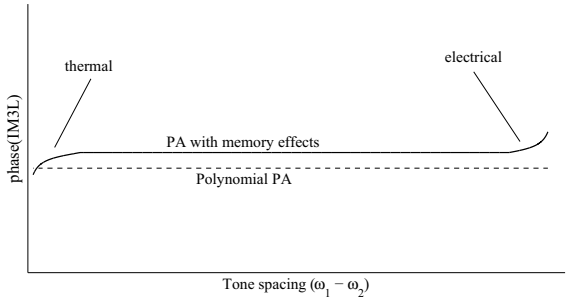

Figure 2.8. Phase of the IM3 component. Solid line indicates system with memory effects; Dotted line indicates system without memory effects [42].

can be greatly deteriorated in broadband systems. As discussed above, the amplitude and phase of the PA IMD components vary as a function of modulation frequency (tone spacing of the two-tone signal). A PD that fails to detect and adjust to the non-constant phase of the IMD may cause more spectral spilling and distortion to the signal. An effective PD is required to include memory structure in its model so that it can generate IMD components of the equal amplitudes but with opposite phase shifts as those generated by the PA.

2.5 High Peak-to-Average Power Ratio of OFDM signal

Orthogonal Frequency Division Multiplexing (OFDM) is known to be a robust transmission scheme in dispersive radio environment. It divides a broadband frequency-selective channel into many flat-fading narrowband subchannels. Each subchannel can then be compensated with a simple equalization scheme. It can also be described as a transmission scheme that divides a high-bit-rate data stream into many parallel lower bit-rate streams that are transmitted simultaneously over multiple subcarriers, each spanning a fraction of the entire bandwidth. This way, the symbol duration of the lower rate data streams increases and therefore decreasing the relative amount of dispersion in time caused by the channel delay spread. By adding a sufficient guard time to the OFDM symbol such that the symbol duration is larger than the delay spread, intersymbol interference (ISI) can be eliminated almost completely. In contrast with conventional frequency division multiplexing (FDM), which employs

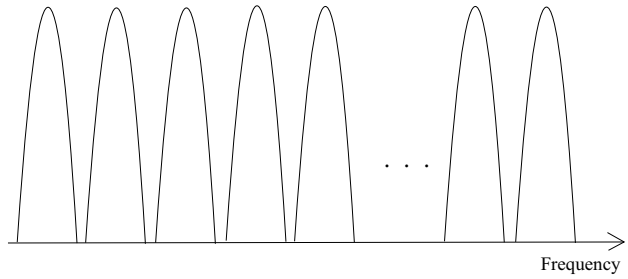

(a) FDM carriers

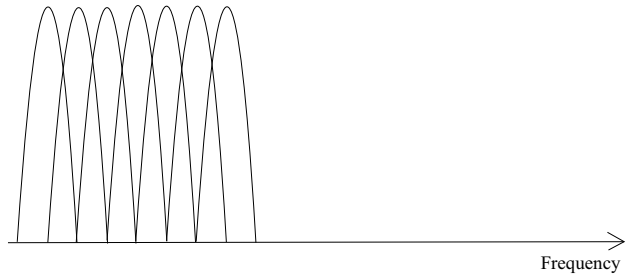

(b) OFDM sub-carriers

Figure 2.9. Carrier spacing of conventional FDM and OFDM.

a guard-band between subcarriers to avoid intercarrier interference (ICI), OFDM divides a bandlimited channel into overlapping orthogonal subcarriers. As illustrated in Figure 2.9, OFDM is spectrally more efficient than the FDM scheme. With all the advantages OFDM offers, it also brings t a few drawbacks, including its receiver sensitivity to frequency offset and phase noise, and its high peak-to-average power ratio (PAPR) signal.

The following subsections first give an overview on OFDM signal generation and reception and its implementation using inverse fast Fourier transform (IFFT). Then, the PAPR of OFDM signal is defined and the cause of high PAPR in OFDM signal is discussed.

2.5.1 OFDM signal generation and demodulation

An OFDM symbol is constructed by summing up N_s overlapping subcarriers, each independently modulated by a complex-valued digital symbol d_i, e.g., phase shift keying (PSK) or M-ary quadrature amplitude modulation (M-QAM) symbol.

The baseband representation of an OFDM symbol is given by [45]

$$s(t) = \begin{cases} \sum_{i=-\frac{N_s}{2}}^{\frac{N_s}{2}-1} d_{i+\frac{N_s}{2}} \exp\left\{j2\pi\left(\frac{i}{T}\right)(t-t_s)\right\}, & t_s \le t \le t_s + T \\ 0, & \text{otherwise} \end{cases}, \tag{2.9}$$

where T is the OFDM symbol duration and t_s is the starting time of the symbol. The carrier orthogonality, which makes it possible for the subcarriers to overlap without causing ICI, is a result of a specific mathematical relationship between the subcarriers. This mathematical relationship is attained by choosing the carrier frequency of each subcarrier such that it is an integer multiple of the lowest subcarrier frequency. For example, the frequency of the k-th subcarrier $f_k = kf_1$, where f_1 is the lowest subcarrier frequency.

At the OFDM receiver, which consists of a bank of demodulators, the demodulation of the k-th subcarrier is performed by multiplying the received OFDM symbol with a carrier $\exp\left(-j2\pi\frac{k}{T}(t-t_s)\right)$ and integrating over an interval of T, given by

$$\begin{aligned} &\int_{t_s}^{t_s+T} \exp\left(-j2\pi\frac{k}{T}(t-t_s)\right) \sum_{i=-\frac{N_s}{2}}^{\frac{N_s}{2}-1} d_{i+\frac{N_s}{2}} \exp\left(j2\pi\frac{i}{T}(t-t_s)\right) dt \\ &= \sum_{i=-\frac{N_s}{2}}^{\frac{N_s}{2}-1} d_{i+\frac{N_s}{2}} \int_{t_s}^{t_s+T} \exp\left(j2\pi\frac{i-k}{T}(t-t_s)\right) dt. \end{aligned} \tag{2.10}$$

From the RHS of (2.10), when $i \neq k$, the carrier $\exp\left(j2\pi\frac{i-k}{T}(t-t_s)\right)$ has an integer number of cycles within the integration interval T, resulting in a zero contribution. However, when $i = k$, the integration process recovers the digital symbol $d_{k+\frac{N_s}{2}}$. This illustrates the orthogonality property of the OFDM subcarriers.

In the frequency domain, the spectrum of an OFDM symbol is a convolution of a group of Dirac pulses at the subcarrier frequencies and the spectrum of a unit square pulse of T seconds period. A square pulse with a period of T in time domain translates to the function $\mathrm{sinc}(\pi f_k T)$ in frequency domain. Figure 2.10 shows the spectrum of an OFDM symbol. The function $\mathrm{sinc}(\pi f_k T)$ returns a zero for all f_k that is not integer multiple of $\frac{1}{T}$. Therefore, at the maximum of each subcarrier spectrum, the spectra of all other subcarriers are zero. This illustrates the carrier orthogonality in the frequency domain.

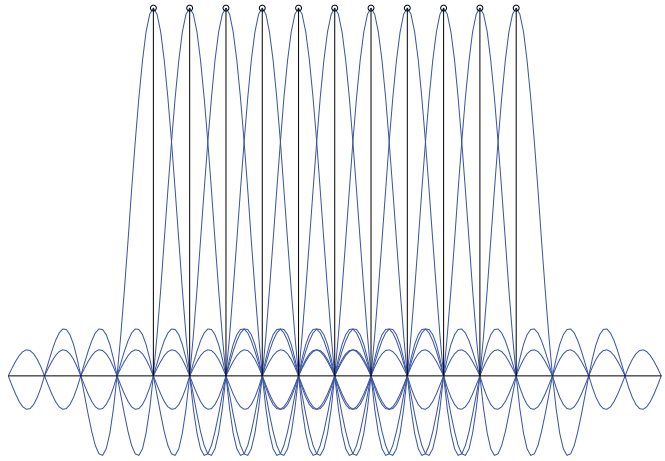

Figure 2.10. Spectrum of an OFDM.

The natural appearance of discrete Fourier transform (DFT) for baseband modulation and demodulation [46] and the advance in digital signal processor (DSP) technologies have made the implementation of OFDM transceiver more feasible. By rewriting (2.9) in discrete-time equivalent form, where time t is replaced by the sample number n, we get

$$s[n] = \sum_{i=0}^{N_s-1} d_i \exp\big(j2\pi \frac{in}{N_s}\big). \tag{2.11}$$

Equation (2.11) is the inverse DFT (IDFT) of the N_s digital symbols $\{d_i\}_0^{N_s-1}$. This eliminates the banks of analog modulators in the OFDM transceiver, significantly reducing the implementation complexity of OFDM transceiver. In practice, the transform is implemented with inverse fast Fourier transform (IFFT) which is computationally more efficient compared to IDFT.

2.5.2 Peak-to-Average Power Ratio

The high PAPR of OFDM signal poses a stringent requirement for PA linearity and thus affects the efficiency of the PA. The time domain OFDM signal in (2.9) is a superposition of N_s complex exponential functions. The amplitude and phase of these carriers are determined by the modulating complex-valued digital symbols d_i. Assuming random data symbols, then the N parallel modulated subcarriers are independently and identically distributed. Based on the central limit theorem, for large N_s, the probability density function (pdf) of $s(t)$ approaches the complex Gaussian distribution with zero mean and variance $\sigma^2 = \frac{1}{2}(|\Re\{s(t)\}|^2 + |\Im\{s(t)\}|^2)$.

Thus, the amplitude of the OFDM signal $|s(t)|$ follows the Rayleigh distribution, which has a long tail. This relates to the high PAPR of OFDM signal, understandably, the PAPR increases as N_s gets larger.

The PAPR of the baseband OFDM symbol is defined as

$$PAPR = \frac{\max_{0 \le t \le T} |s(t)|^2}{E\left(|s(t)|^2\right)}. \tag{2.12}$$

For discrete-time expression, the PAPR of the k-th OFDM symbol can be expressed as

$$PAPR = 10 \log_{10}\left(\frac{1}{N} \frac{\|\mathbf{u}_k\|_\infty^2}{E\left[\|\mathbf{u}_k\|_2^2\right]}\right). \tag{2.13}$$

where N is the number of discrete samples in one OFDM symbol, $E[\cdot]$ is the expectation operator, and $\|\cdot\|_\infty^2$ and $\|\cdot\|_2^2$ are infinity-norm and 2-norm, respectively. The signal PAPR of practical systems that employ OFDM scheme such as WiMAX and 4G LTE downlink, is approximately 10 - 12 dB. This dynamic range requires a large power backoff from the PA peak power in order to avoid clipping of signal peaks which occurs infrequently. Power backoff reduces the power efficiency of the PA tremendously. On the other hand, left unattended, signal peak clipping causes inband distortion, spectral regrowth and destroys the orthogonality of the subcarriers.

2.5.3 PAPR reduction techniques

Many PAPR reduction techniques for OFDM system have been proposed in the literature. An obvious way to reduce the peak power of a signal is by signal peak clipping follow by filtering [47,48]. However, this technique causes distortion to the signal leading to BER degradation and increased out-of-band radiation. In order to reduce the amount of resultant out-of-band radiation, peak windowing techniques [49, 50] have been proposed. In these methods, the signal peaks are multiplied with a certain non-rectangular window function in order to avoid hard clipping. Examples of good spectral characteristics window functions are such as Gaussian, Hamming and Kaiser functions [50].

Methods which manipulate the phases of the OFDM subcarriers in order to obtain low signal PAPR such as multiple signal representation and tone reservation do not cause distortion to the transmitted signal. Multiple signal representation approaches such as partial transmit sequence (PTS) [51, 52] and selected mapping (SLM) [53–56] are known to

achieve good PAPR reduction performance. In PTS, the input digital symbol stream is divided into several blocks. Each block is multiplied with a phase sequence which has been optimized for minimum PAPR after the IDFT operation. In SLM scheme, each input digital data stream is directly multiplied with several random phase sequences before IDFT operation. The signal with the least PAPR is then selected for transmission. A drawback of these methods is the need for side information transmission, i.e., the phase sequence that produces the lowest PAPR signal. Computational complexity is also increased as IDFT operations are required. Another phase optimization scheme know as tone reservation [57] does not require transmission of side information to the receiver. A number of subcarriers are reserved for phase optimization to produce a signal that cancels the high peaks of the composite signal of the data-bearing subcarriers. The computational cost of this method are mainly attributed to the algorithm for finding an effective peak-cancelling signal using a few reserved tones.

Another distortionless approach for PAPR reduction is coding methods where the transmitted bit stream is encoded to obtain low PAPR signal. Some researchers focused on finding codes that produce low PAPR signal, e.g., the Golay complementary sequence [58] and Reed-Muller code [58, 59]. However, the error correction performance of these codes are poor. Turbo codes and low density parity check (LDPC) code which have strong error correction performance are have been proposed in [60] and [61], respectively, for generating low PAPR candidate codewords. The codeword with the lowest PAPR is selected for transmission. Unlike SLM/PTS, no side information is needed at the receiver as the transmitted codewords are valid codewords. The drawback of coding methods are the increased in computational complexity for searching the lowest PAPR candidate and reduced data rate due to encoding.

Constellation extension/modification is a PAPR reduction method that do not reduce data rate. Tone injection and active constellation extension (ACE) are examples of constellation extension methods. In tone injection, the original constellation set is repeated cyclically around the original constellation set. Each original symbol can then be mapped to the original and several equivalent points in the extended constellation. This way, alternative constellation point can be chosen for constructing low PAPR signal. The problem of searching the optimal constellation points for producing the lowest PAPR signal is an integer-programming problem [57],

which is computationally heavy to solve. For practical applications, researchers proposed faster and reduced complexity algorithms, e.g., an iterative quantized-gradient method and a linear programming algorithm are proposed in [62] and [63], respectively. ACE [64, 65] is similar to tone injection, but only exterior constellation points are extended. The ACE optimization is formulated as a minimax problem in [64], which is again, tedious to solve. An approximate gradient-project method is developed in [64] which find a sub-optimal solution that gives good performance in a efficient way. In [65], first the authors define a unique constellation extension pattern for the exterior constellation points. Each exterior constellation point can either be represented by the original point or an extended point. Then, an efficient de-randomization algorithm based on the method of conditional probability is developed to solve for a sub-optimal ACE solution. Due to the extended constellation of these schemes, the average transmit power is slightly increased in these system.

3. Modeling PA and PD using the SCPWL function

An essential step in predistorter (PD) design is the characterization of the PA to be linearized, either explicitly, or implicitly in the process of PD identification. The characteristics of a PA can be captured as physical model or behavioural model. Physical models are built based on the electronic elements that constitute the PA. They are also known as the circuit-level models and are employed for example in circuit-level simulations during PA design. A circuit-level model captures the full RF circuit bandpass properties and information. On the other hand, the knowledge of the circuit level components of the device is not required in behavioural models. A behavioural model captures the input-output relationship of a system by observing a set of input-output measurement data. Therefore, it is also known as the system-level model. In this work, the behavioural model is employed for modeling the PA and PD.

In order to obtain an effective PD, the functions employed for characterizing the PA and PD must have sufficient structure for capturing the essential characteristics of the devices. For instance, the degree of nonlinearity and the type of memory effects exihbit by the nonlinear devices. A variety of nonlinear models have been proposed in the literature for modeling baseband PAs and PDs characteristics. This chapter reviews the most commonly employed behavioural models for PAs and PDs. Then, the proposed complex-valued baseband SCPWL model with memory is introduced. The properties of the SCPWL function and the application of the proposed SCPWL model in PD design are discussed.

The discrete-time complex baseband signal model used throughout this work is first outlined in Section 3.1. In Section 3.2, a review of static and dynamic nonlinear behavioural models commonly employed for PA modeling and PD identification is provided. In Section 3.3, the proposed complex-valued SCPWL model with memory suitable for modeling base-

band PA and PD is introduced. The properties of the SCPWL function studied in this thesis are reviewed in Section 3.4. Finally, a summary of contribution concerning modeling broadband PAs and PDs using the proposed SCPWL model is presented in Sec 3.5.

3.1 Baseband representation of passband signal

In this work, the baseband equivalent of passband characteristics of the PA and PD are modeled. Thus, discrete-time equivalent baseband signals which represent the complex-envelope of the RF input-output signals are first obtained.

Given a generic RF signal with carrier frequency ω_c, expressed as [66]

$$\begin{aligned} \tilde{z}(t) &= \Re\Big\{ |z(t)| e^{j\left(\omega_c t + \vartheta_{\tilde{z}}(t)\right)} \Big\}, \\ &= \Re\Big\{ |z(t)| e^{j\vartheta_{\tilde{z}}(t)} e^{j\omega_c t} \Big\}, \end{aligned} \tag{3.1}$$

the complex-envelope can be written as

$$z(t) = |z(t)| e^{j\vartheta_z(t)}. \tag{3.2}$$

where $|z(t)|$ and $\vartheta_z(t)$ are the time-varying amplitude and phase of the complex baseband signal, respectively. Then, the discrete-time equivalent of the complex baseband signal can be obtained by sampling the baseband signal. In linear systems, in order to avoid aliasing effects, the minimum sampling frequency is at least twice the highest frequency component of the signal, i.e., the Nyquist rate [67, Chap. 3]. However, due to the nonlinear behaviour of the PD, the bandwidth of the PD output signal is larger than the original input signal. In order to capture and counter the IMD effects of the PA, the sampling rate for PA and PD signals have to be several times higher than the Nyquist rate of the original input signal. In this work, a sampling rate of eight times the input signal bandwidth is employed.

Finally, the discrete-time equivalent baseband signal can be obtained by replacing the time variable t in (3.2) with the sample number n,

$$z[n] = |z[n]| e^{j\vartheta_z[n]}, \tag{3.3}$$

where $n = \frac{t}{T_s}$ and $T_s = \frac{1}{f_s}$ is the sampling period. The representation in (3.2) and (3.3) are used throughout this work, which are used to obtain the behavioural models of the PA and PD.

3.2 A review of nonlinear models for PAs and PDs

Nonlinear models can be divided into memoryless nonlinear models and nonlinear models with memory. Memoryless nonlinear models are good approximation for narrowband PAs, in which the AM/AM and AM/PM functions are independent of frequency. A strictly memoryless PA exhibits only AM/AM distortion. A quasi-memoryless PA has a memory time constant in the order of the RF carrier period. Thus, it exhibits short term memory effects and is described by both AM/AM and AM/PM distortions.

In broadband system, the AM/AM and AM/PM characteristics vary over the bandwidth of the PA. The frequency-dependent gains and phase shifts in these PAs are known as memory effects [38]. Nonlinear models with memory are divided into models with linear memory and with nonlinear memory. Models with linear memory assume that the system dynamics are separable from the nonlinear processes. Linear memory effects contribute to short-term memory effects which are attributed to the characteristics of the matching networks [39]. They are typically modeled using cascade of a static nonlinearity and linear filters at the input and output of a static nonlinearity. On the other hand, nonlinear PA with nonlinear memory exhibits also dynamic effects that occur only in the presence of nonlinear processes [39]. Thus, these PAs require nonlinear models with structures that can model the interactions between the nonlinearities and the system dynamics.

The nonlinear behavioural models with and without memory that are most often employed in the literature are reviewed in the following.

3.2.1 Memoryless and quasi-memoryless nonlinear models

The output of a static nonlinear PA $y[n]$ is commonly written in two different baseband equivalent forms in the literature. The first one represents AM/AM $f_A\big(|x[n]|\big)$ and AM/PM $f_p\big(|x[n]|\big)$ functions separately and the output is written in polar form as

$$y[n] = f_A\big(|x[n]|\big)e^{j\left(\vartheta_x[n]+f_p\left(|x[n]|\right)\right)}, \tag{3.4}$$

where $x[n]$ is the PA input signal. With this representation, parametric models with real-valued coefficients are used to model the AM/AM and AM/PM functions.

The second representation of the baseband output is written as

$$y[n] = f\big(|x[n]|\big)e^{j\left(\vartheta_x[n]\right)}. \tag{3.5}$$

The function $f\big(|x[n]|\big)$ has complex-valued coefficients when quasi-memoryless nonlinearity (AM/AM and AM/PM) is modeled. When strictly memoryless nonlinearity (AM/AM only) is considered, the function coefficients become real-valued.

A memoryless PA model can be extracted from the AM/AM and AM/PM response measured by exciting the PA using a single-tone input signal, typically at the centre frequency of the RF PA, with ramping input level. Then, memoryless PA models in the form of (3.4) or (3.5), presented in the following, can be used to fit the AM/AM and AM/PM curves.

3.2.1.1 Polynomial model

Polynomial model is most extensively employed for modeling PAs and PDs. An advantage of the polynomial model is that it lends a hand for easy analysis of spectral regrowth as each model coefficient is directly related to an IMD of a given order. Its model output is linear with respect to its coefficients, making it possible to extract the model coefficients using well-established linear system identification algorithms such as least squares (LS) method or least mean square (LMS) adaptive algorithm [33].

The AM/AM and AM/PM characteristics can be modeled using separate polynomials with real-valued coefficients when the baseband model in (3.4) is employed. Alternatively, when the representation in (3.5) is considered, a polynomial with complex coefficients can be used to describe a baseband P-th order nonlinearity as [68]

$$\begin{aligned} y[n] &= \sum_{p=0}^{P} a_{2p+1}\big(x[n]\big)^{p+1}\big(x^*[n]\big)^{p}, \\ &= x[n]\sum_{p=0}^{P} a_{2p+1}\big|x[n]\big|^{2p}, \end{aligned} \tag{3.6}$$

where $(\cdot)^*$ stands for conjugation. Here, we note that the conjugation is important to ensure correct representation of the baseband signal as discussed in [68]. Equation (3.6) includes only odd order terms as the DC and even-order terms are filtered out by the low-pass filter [69].

However, it is shown in [70] that by including the even order terms in the baseband polynomial model, modeling error can be significantly reduced. It should be emphasized that the even order terms merely improve the quality of the model (thus the linearization performance of the PD), but by no means indicate that the model includes the even order terms from the passband. By writing $x[n] = |x[n]|e^{j\vartheta_x[n]}$, (3.6) can be rearranged to

include the even order terms as

$$y[n] = e^{j\vartheta_x[n]}\left(\sum_{p=1}^{P} a_p|x[n]|^p\right). \tag{3.7}$$

The expression in the bracket is a function of the input signal amplitude only, and it is equivalent to $f(|x[n]|)$ in (3.5). The coefficients a_n are complex-valued when quasi-memoryless nonlinearity is modeled and reduce to real-valued when strictly memoryless PA is considered.

3.2.1.2 Orthogonal polynomials

A drawback of employing polynomial model is the limitation of modeling only weakly nonlinear PAs, which are dominated by the third-order nonlinearity. For PA that exhibits strong nonlinearities, higher order polynomials are required, which leads to increase in computational complexity and the well-known numerical instability problem associated with parameter estimation. Orthogonal polynomials are known to possess better numerical properties. Examples of orthogonal polynomials are Hermite polynomials, Chebyshev polynomials of the first and second kind, Laguerre polynomials and Legendre polynomials. In [19], the authors derived an orthogonal polynomial basis function for the purpose of modeling baseband PA and PD nonlinearities. The p-th order basis function given by [19]

$$\Psi_p\Big(x[n]\Big) = \sum_{\ell=1}^{p}(-1)^{\ell+p}\frac{(p+\ell)!}{(\ell-1)!(\ell+1)!(p-\ell)!}x^{\ell-1}[n]x[n], \tag{3.8}$$

is derived using complex-valued baseband input signal with amplitude $|x[n]|$ uniformly distributed in $[0, 1]$. Their results show the numerical property of the orthogonal polynomial is greatly improved in terms of the autocorrelation matrix condition number as compared to conventional polynomials [71].

3.2.1.3 Saleh model

Another widely employed memoryless nonlinear PA model in the literature is the Saleh model. The Saleh model was proposed in [40] to approximate the AM/AM and AM/PM characteristics of the TWTA using two formulas. The polar representation of the Saleh model is given by

$$\begin{aligned} A(|x[n]|) &= \frac{\alpha_a|x[n]|}{1+\xi_a|x[n]|^2}, \\ \Phi(|x[n]|) &= \frac{\alpha_\theta|x[n]|^2}{1+\xi_\theta|x[n]|^2}, \end{aligned} \tag{3.9}$$

where $A(|x[n]|)$ is the AM/AM function, $\Phi(|x[n]|)$ is the AM/PM function, α_a and α_θ are amplitude and phase gain factors, respectively, and ξ_a and ξ_θ

are amplitude and phase compression factors, respectively. The model coefficients are real-valued. For strictly static nonlinearity PA, the AM/AM function alone is used for representing the PA behaviour. Whereas, for quasi-static nonlinear PA, both the AM/AM and AM/PM functions must be employed.

The corresponding quadrature form of the Saleh model is given by

$$\begin{aligned} I(|x[n]|) &= \frac{\alpha_I |x[n]|}{1+\xi_I |x[n]|^2}, \\ Q(|x[n]|) &= \frac{\alpha_Q |x[n]|^3}{[1+\xi_Q |x[n]|^2]^2}, \end{aligned} \tag{3.10}$$

where $I(|x[n]|)$ represents the in-phase component of the nonlinear conversion and $Q(|x[n]|)$ is the quadrature component of the nonlinear conversion.

The Saleh model has been widely employed for modeling quasi-static nonlinear PAs such as class A and class AB TWTAs. The accuracy of the model deteriorates when highly nonlinear PA such as class C is modeled [1]. This model has often been used as a reference PA in the literature for the study of PA nonlinearities and its compensation [72–74].

3.2.2 Nonlinear models with memory

The Volterra series is well-known as a general expression for nonlinear system with memory [75, 76]. However, due to the number of coefficients required, the classical Volterra series is limited for modeling weak nonlinearities with short memory. Thus, extensive research effort has been made to simplify the structure of Volterra series in order to reduce computational complexity. In the following, some of the most commonly employed variants of simplified Volterra systems and their ability to describe memory effects are discussed.

3.2.2.1 Volterra series

The Volterra series provides a general expression for any nonlinear system with memory [75, 76]. The series is formulated as a combination of linear convolution and nonlinear power series. The input-output relationship of an n-order causal Volterra series with memory length L is given

as

$$\begin{aligned} y[n] = h_0 &+ \sum_{\ell_1=0}^{L} h_1(\ell_1)x[n-\ell_1] \\ &+ \sum_{\ell_1=0}^{L}\sum_{\ell_2=0}^{L} h_2(\ell_1,\ell_2)x[n-\ell_1]x^*[n-\ell_2] + \cdots \\ &+ \sum_{\ell_1=0}^{L}\cdots\sum_{\ell_k=0}^{L} h_k(\ell_1,\cdots,\ell_k)x[n-\ell_1]x[n-\ell_2]\cdots x^*[n-\ell_k], \end{aligned} \tag{3.11}$$

where $h_k(\ell_1,\ell_2,\cdots,\ell_k)$ is the k-order Volterra kernel and $(\cdot)^*$ stands for conjugate transpose. The kernels can completely describe all orders of distortion caused by the system and allow comparisons of different distortion components. Thus, the Volterra series provides convenience for nonlinear system analysis, see e.g., in [77, 78]. Another advantage of the Volterra series is that it has a linear-in-the-parameter expression. The model coefficients can be extracted directly using well-establish linear system identification methods such as LS method.

However, a drawback of Volterra series is the huge number of coefficients involved in a complete series. Furthermore, it is also difficult to compute the higher-order kernels from measurement data. Due to the high computational complexity of the series, it is unattractive for practical implementation. Several approaches have been proposed for simplifying the Volterra series and are discussed in the rest of this section.

3.2.2.2 Memory polynomial

For practical implementation, many methods have been proposed to truncate/prune the Volterra series [76] in order to reduce the complexity of the classical Volterra series. In practice, all PAs are affected by different degree of nonlinearities and memory effects. For a real PA, a significant amount of the Volterra coefficients are very small and can be pruned in order to simplify the model.

A straightforward way is to prune the off-diagonal kernels of the series, resulting in the memory polynomial given by [5]

$$y[n] = \sum_{k=0}^{K}\sum_{q=0}^{Q} a_{kq}x[n-q]|x[n-q]|^k, \tag{3.12}$$

where K and Q are the highest order of nonlinearity and memory length, respectively. It can be implemented as an FIR filter where the gain taps are polynomial functions of the delayed input signal instead of constants. For further reduction of the number of coefficients, sparse delay taps were employed in [79].

Broadband signal can be directly applied for model extraction. Thus, nonlinear memory effects can be captured. The model also has a linear-in-the-parameter expression, making it practical for PA modeling and PD implementation.

3.2.2.3 *Modified / Dynamic Volterra series*

For some systems, the off-diagonal coefficients of the Volterra series may have significant contribution to the model accuracy. In order to improve model accuracy, some authors include some off-diagonal terms, typically those close to the main diagonal [80].

The modified Volterra series [81–83] and the dynamic Volterra series [84], provide a systematic way to prune off insignificant dynamic terms of the series. In these series, a dynamic deviation function $e[n,i] = x[n-i] - x[n]$ is utilized in order to reformulate the Volterra series into a purely static term and a dynamic part, $y[n] = y_s[n] + y_d[n]$, given by the first term and second term of (3.13), respectively.

$$\begin{aligned} y[n] = &\sum_{p=1}^{P} a_p x^p[n] \; + \\ &\sum_{p=1}^{P}\sum_{r=1}^{p} x^{(p-r)}[n] \sum_{\ell_1}^{L}\cdots\sum_{\ell_r}^{L} w_{p,r}(\ell_1,\cdots,\ell_r)\prod_{j=1}^{r} e(n,\ell_j), \end{aligned} \tag{3.13}$$

where a_p is the pth-order coefficient of the static polynomial function and $w_{p,r}$ represents the rth-order dynamic kernel of the pth-order nonlinearity. Then, the dynamic order of the model can be controlled using r, thus reducing the series complexity while maintaining a high modeling accuracy.

However, separate measurements, which involved complicated procedures, are required for extracting the two parts of the model, see [83, 84]. In addition, these series are no longer linear-in-the-parameter, hindering the use of linear system parameter estimation methods.

3.2.2.4 *Dynamic deviation reduction-based (DDR) Volterra series*

In [85], the modified Volterra series is rearranged in order to retain the linear-in-the-parameter property. By substituting the dynamic deviation function $e[n,i] = x[n-i] - x[n]$ into (3.13) and regrouping the coefficients a_p and $w_{p,r}$, the authors arrived at the new representation known as the

dynamic deviation reduction-based Volterra series,

$$y[n] = \sum_{p=1}^{P} h_{p,0}(0,\cdots,0)x^p[n] + \sum_{p=1}^{P}\left\{\sum_{r=1}^{p}\left[x^{(p-r)}[n]\sum_{\ell_1=1}^{L}\cdots\sum_{\ell_r=\ell_{r-1}}^{L} h_{p,r}(0,\cdots,0,\ell_1,\cdots,\ell_r)\prod_{j=1}^{r}x(n-\ell_j)\right]\right\}. \tag{3.14}$$

In this series, the coefficients $h_{p,r}(0,\cdots,0,\ell_1,\cdots,\ell_r)$ are the same as the pth-order Volterra kernel, but with $p-r$ first indices equal to zero. Similar to the modified/dynamic Volterra series, by adjusting r, the number of dynamic terms of the pth order kernel can be reduced. In other words, diagonal and off-diagonal terms up to the rth dynamic order are retained, leading to improved modeling accuracy compared to memory polynomial.

3.2.2.5 Generalized memory polynomial

In an independent development [86], a series which has similar structure as the dynamic deviation reduction-based Volterra series was formulated. The author started by changing the "diagonal" index variables in the classical Volterra series and rearranging the coefficients according to their dynamic orders. An expression [86, Eq. 4] similar to the pth-order term in (3.14) (term between the curly bracket) is obtained, except without the dynamic deviation variable r. Then, by manually choosing the time shift between the signal and its exponential envelope, including both negative and positive time-shift, the generalized memory polynomial is obtained as

$$\begin{aligned} y_{\text{GMP}}[n] = &\sum_{k=0}^{K_a-1}\sum_{\ell=0}^{L_a-1} a_{k\ell}x[n-\ell]\Big|x[k-\ell]\Big|^k + \\ &\sum_{k=0}^{K_b}\sum_{\ell=0}^{L_b-1}\sum_{m=1}^{M_b} b_{k\ell m}x[n-\ell]\Big|x[k-\ell-m]\Big|^k + \\ &\sum_{k=0}^{K_c}\sum_{\ell=0}^{L_c-1}\sum_{m=1}^{M_c} c_{k\ell m}x[n-\ell]\Big|x[k-\ell+m]\Big|^k, \end{aligned} \tag{3.15}$$

where K_a, L_a are the number of coefficients for the diagonal terms, K_b, L_b, M_b and K_c, L_c, M_c determine the number of cross-terms with lagging envelope signal and with leading envelope signal, respectively.

3.2.2.6 Wiener and Hammerstein models

The Wiener and Hammerstein models depicted in Fig. 3.1 and Fig. 3.2, respectively, are special cases of the general Volterra series. The former consists of a linear dynamic system followed by a static nonlinear system and the latter has the sub-systems cascaded in reverse order. By separating

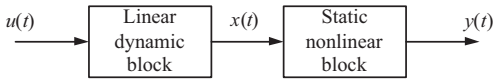

Figure 3.1. Wiener Model

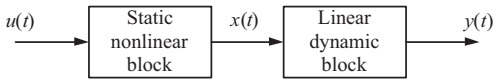

Figure 3.2. Hammerstein Model

the linear dynamics and static nonlinearities into two sub-systems, fewer parameters are needed to describe the nonlinear system with memory. In comparison with the Volterra series, these models are more suitable for practical application.

However, these models assume that the nonlinearity and the linear dynamics of the system are separable. The linear dynamic block is typically modeled using an finite impulse response (FIR) filter or infinite impulse response (IIR) filter and the nonlinear block is characterized by a static nonlinearity, see e.g., [13, 14, 16, 17]. The coefficients of the static nonlinear block are normally extracted using single-tone measurement. The shape of the nonlinearity of these systems is fixed. The linear filter at the input or output of the static nonlinear block is only shifting the fixed-shape static nonlinearity. The linear filter is normally identified using small-signal measurement, which leads to the possibility of ignoring memory effects that occur in the nonlinear region. Thus, these system can only capture linear memory effects.

The Wiener model does not have a linear-in-the-parameter expression. Thus, more tedious model parameter extraction procedure is required. Another drawback of block-oriented models in general, is associated with parameter identification. For example, the intermediate signal of the Wiener model is not measurable. A unique solution for the parameters of the sub-systems can only be found if the inverse of the static nonlinearity exists and the linear filter h is minimum phase [34, 87, 88]. The static gain of these models, which can be arbitrary distributed between the two subsystems, has to be fixed in either block to ease parameter identification.

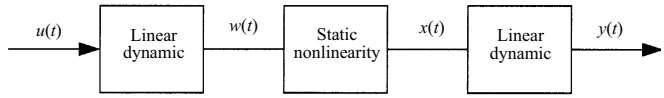

Figure 3.3. Wiener-Hammestein model

3.2.2.7 Wiener-Hammerstein model

The Wiener-Hammerstein model is a cascade of linear filter-static nonlinearity-linear filter, as show in Figure 3.3. Comparing to the two-box models, its additional linear filter offers an additional degree of freedom for characterizing the PA. The Poza-Sarkozy-Berger (PSB) model [89] is an example of using the Wiener-Hammerstein structure for modeling PA with memory. The static nonlinearity is obtained from single-tone measurement at the center frequency of the PA. Then the linear filters are identified using swept-tone measurement across the bandwidth of the PA. Similar to the two-box models, the nonlinearity of the Wiener-Hammerstein model is fixed. The input and output filters only cause a displacement of the static nonlinear curve (shifted vertically or horizontally), thus modeling only linear memory effects.

The Wiener-Hammerstein model poses similar disadvantages of block models discussed above.

3.2.2.8 Parallel Wiener model

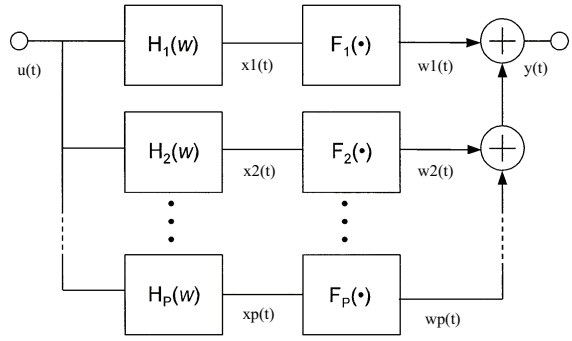

Figure 3.4. Parallel Wiener model

A limitation of the two-box and three-box models discussed above is their inability to capture nonlinear memory effects. Nonlinear PA with nonlinear memory cannot be characterised using swept-tone measurement. In this type of system, the shape of the nonlinearities are changing according to the frequency and bandwidth of the input signal level. In

order to capture the nonlinear memory effects, broadband input signal or two-tone input signal with varying tone spacing has to be employed for extracting the model coefficients.

The parallel Wiener model is proposed in [15] to overcome the limitation of the two-box and three-box models. The first branch is identified as a memoryless AM/AM and AM/PM model using single-tone measurements. The authors derived the AM/AM and AM/PM complex-envelope function that is expressed in terms of IMD products. Then, using two-tone measurement data obtained by sweeping the envelope frequency and power level, the AM/AM and AM/PM curves are extracted for each envelope frequency by measuring IMD products. Finally, the difference between the output of the first branch and the two-tone measurements is modeled by adding Wiener systems in parallel. This model topology provides the structure to support the dynamic interactions between different nonlinear processes. Thus, it is capable of modeling nonlinear memory and provides means for quantifying memory effects in a PA. Due to its structure, the model output may not be linear-in-the-parameter which makes model parameter extraction more tedious.

3.3 Modeling PA and PD using The SCPWL function

A piecewise linear (PWL) function is a function that divides the input space into a finite number of segments, each described by a linear affine function. Conventional PWL functions are expressed region by region and thus require a huge amount of coefficients. A compact form known as the canonical PWL function was first introduced in [90]. It is expressed as a global function with much less coefficients than the conventional PWL function. Later, the concept of simplicial partition is used in [32] to develop PWL functions in an even more compact form. This class of PWL functions known as the *simplicial canonical piecewise linear* (SCPWL) function. PWL functions have been used for modeling and analysis of nonlinear circuits [91, 92]. In this work, the SCPWL function is employed for modeling PA and PD nonlinearities.

3.3.1 The simplicial canonical piecewise linear function

The SCPWL function in $\mathbb{R}^1$ uses σ breakpoints, $\{\beta_i\}_{i=1}^{\sigma}$, where $(\beta_1 \leq \beta_2 \leq \cdots \leq \beta_\sigma)$, to divide the input domain into $(\sigma - 1)$ linear affine segments.

The SCPWL function with real-valued input x can be expressed as

$$f(x) = c_0 + \sum_{i=1}^{\sigma-1} c_i \lambda_i(x), \tag{3.16}$$

where $\lambda_i(x)$ is the i-th basis function and $\{c_i\}_{i=0}^{\sigma-1}$ are the real-valued coefficients of the SCPWL function. The basis function is given by

$$\lambda_i(x) = \begin{cases} \frac{1}{2}\big(x - \beta_i + |x - \beta_i|\big), & x \leq \beta_\sigma \\ \frac{1}{2}\big(\beta_\sigma - \beta_i + |\beta_\sigma - \beta_i|\big), & x > \beta_\sigma \end{cases}. \tag{3.17}$$

From the second line of (3.17), when the input value x exceeds the value of the last breakpoint β_σ, the basis function returns a fixed value for each $1 < i < \sigma - 1$. This results in the SCPWL function imposing a saturation when the input level exceeds the last breakpoint. When x falls within the defined input space, the first line of (3.17) is valid. The i-th basis is then equal the distance between the input value x and the i-th breakpoint β_i when $x > \beta_i$, and returns a null when $x \leq \beta_i$, for $1 < i < \sigma - 1$. Then these bases multiplied with the SCPWL coefficients as in (3.16) equal the total gain imposed on the input by each linear affine segment. For convenience, (3.16) can be expressed in matrix-vector form as

$$f(x) = \boldsymbol{\lambda}^T(x)\mathbf{c}, \tag{3.18}$$

where $\boldsymbol{\lambda}(x) = \begin{bmatrix} 1 & \lambda_1(x) & \cdots & \lambda_{\sigma-1}(x) \end{bmatrix}^T$ and $\mathbf{c} = \begin{bmatrix} c_0 & c_1 & \cdots & c_{\sigma-1} \end{bmatrix}^T$.

This function can be directly used for characterizing the AM/AM and AM/PM functions in (3.4), where x is now the input signal amplitude.

3.3.2 The proposed baseband SCPWL model with memory

In this work, a complex-valued SCPWL model suitable for modeling baseband nonlinearities is proposed. The original SCPWL function in (3.16) is modified to include phase information and complex-valued coefficients. Furthermore, the proposed model is formulated to include memory effects. The resulting complex-valued memory-SCPWL model, mapping $\mathbb{C} \to \mathbb{C}$, is formed by summing the output signals described by a baseband mapping $\mathbb{C} \to \mathbb{C}$ at the current and $L-1$ past time instants given by

$$\begin{aligned} f\big[\mathbf{r}(n)\big] &= \sum_{\ell=0}^{L-1} \Big\{ c_{\ell 0}^* + \sum_{i=1}^{\sigma_\ell - 1} c_{\ell i}^* \lambda_i\big(|r(n-\ell)|\big) \times \exp\big(j\varpi_r(n-\ell)\big) \Big\} \\ &= \sum_{\ell=0}^{L-1} \mathbf{c}_\ell^{\mathrm{H}} \boldsymbol{\lambda}[r(n-\ell)], \end{aligned} \tag{3.19}$$

where $\mathbf{r}(n) = [r(n) \;\; r(n-1) \;\; \cdots \;\; r(n-L+1)]^{\mathrm{T}}$ is the vector of input samples, $|r(n)|$ and $\varpi_r(n)$ are the respective amplitude and phase of the baseband

signal $r(n) \in \mathbb{C}$, and vectors $\mathbf{c}_\ell \in \mathbb{C}^{\sigma\times 1}$ and $\boldsymbol{\lambda}[r(n)] \in \mathbb{C}^{\sigma\times 1}$ are given by

$$\begin{aligned}\mathbf{c}_\ell &= \Big[c_{\ell 0} \;\; c_{\ell 1} \;\; \cdots \;\; c_{\ell(\sigma_\ell-1)}\Big]^{\mathrm{T}}, \;\; \ell = 0, \ldots, L-1,\\ \boldsymbol{\lambda}[r(n)] &= \Big[1 \;\; \lambda_1[|r(n)|]\exp\big(j\varpi_r(n)\big) \\ &\qquad \cdots \;\; \lambda_{\sigma-1}[|r(n)|]\exp\big(j\varpi_r(n)\big)\Big]^{\mathrm{T}}.\end{aligned} \tag{3.20}$$

The term in the curly bracket in (3.19) has a similar expression as the baseband equivalent of passband quasi-memoryless model (AM/AM and AM/PM conversion) discussed in [68, Sec. IV]. Equation (3.19) reduces to a memoryless (quasi-static) mapping when $L = 1$, and can be used to model $f\big(|x[n]|\big)$ in (3.5). When $L > 1$, the memory-SCPWL model can be used for modeling nonlinear PAs and PDs with memory.

The memory-SCPWL model has a similar form as the memory polynomial [5]. Both the functions have similar Volterra kernels pruning approach and have linear-in-the-parameter expression. The functions include only the equivalent of diagonal Volterra kernels. For instance, in both Equations (3.12) and (3.19), the nonlinearity in each memory branch is generated without any cross-term combinations, such as $r(n-\ell_1)r(n-\ell_2)$, of the input signal. The linear-in-the-parameter expression makes the model parameter estimation straightforward by using LS or LMS algorithms. The distinction between the memory-SCPWL function and memory polynomial is their different nonlinear functions, i.e., SCPWL function and polynomial, respectively, in each memory branch.

By using broadband excitation signal to obtain measurement data, nonlinear memory effect can be captured by the memory-SCPWL model.

3.4 Properties of the SCPWL function

The properties of the SCPWL function have been studied and exploited in this work for development of efficient PD identification and adaptation algorithms. The following summarizes the properties that are exploited to provide conveniences for PD implementation.

3.4.1 Saturation level

The SCPWL function imposes a saturation level after a given input level by using the second line of (3.17). It returns a fixed maximum value when the input level exceeds the last breakpoint and results in a saturation level. This feature makes the SCPWL suitable for modeling PA and PD

type nonlinearity. For instance, by placing the last breakpoint of the PD β_σ at the input saturation level of the PA, the maximum output level of the PD can be limited. This limitation provides control to avoid over-driving the PA and cause significant signal compression at the PA output when the input signal amplitude is large.

3.4.2 Linear affine segments and user-defined breakpoints

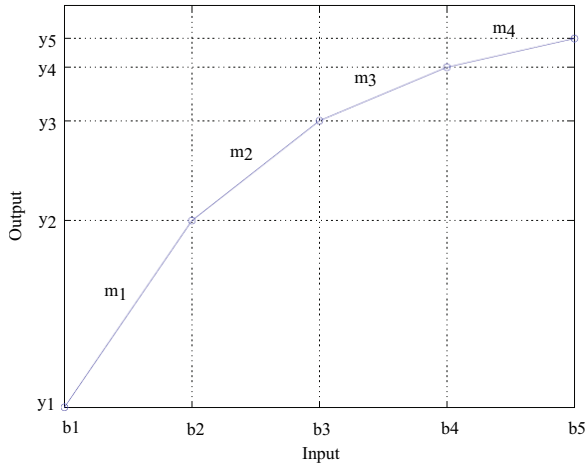

Figure 3.5. Piecewise linear representation of a static nonlinear behaviour

A piecewise linear function is composed of a set of non-overlapping linear functions, each defined within a segment as illustrated in Figure 3.5. Each segment is defined by two breakpoints. This linear affine structure of the SCPWL function has facilitated the development of the SCPWL PD identification and adaptive algorithms.

- As the breakpoints are defined by the user, the number of breakpoints and their distribution can be optimized to better fit the shape of the nonlinearity to be modeled. Simulation examples in [III] and [VII] shows that the performance of the SCPWL PDs improved as the number of breakpoints increases. In [VI], it is shown that the error in modeling the spectrum of a SCPWL nonlinearity decreases as the number of PWL segments is increased. A saturation in improvement is also observed.

- A static nonlinearity of a PA and its inverse nonlinearity resemble mirror images of each other. This indicates that the static nonlinear characteristic of the PD can be obtained by an appropriate projec-

tion of the PA characteristic. By exploiting this fact and the linear affine segments of the SCPWL function, two efficient vector projection based methods are developed for identifying static SCPWL PDs, i.e., the orthogonal image projection method and the inverse coordinate mapping (ICM) method, proposed in publications [I] and [III], respectively.

- Due to the linear affine property, the SCPWL function (3.16) can be fully defined by evaluating the function at all its breakpoints. This means that it is sufficient to collect the input-output data at the user-defined breakpoints in order to characterize a static nonlinearity using the SCPWL function. Furthermore, in [I], it is shown that the matrix inversion invoked in LS parameter extraction can be avoided. Instead, by exploiting the linear affine property and the known user-defined breakpoints, the inverse basis function matrix is constructed using the known breakpoints values as

$$\boldsymbol{\Lambda}^{-1}(\boldsymbol{\beta}) = \begin{bmatrix} 1 & 0 & 0 & 0 & 0 & \cdots & 0 \\ -\frac{1}{s_1} & \frac{1}{s_1} & 0 & 0 & 0 & \cdots & 0 \\ \frac{1}{s_1} & -\sum_1^2 \frac{1}{s_i} & -\frac{1}{s_2} & 0 & 0 & \cdots & 0 \\ 0 & \frac{1}{s_2} & -\sum_2^3 \frac{1}{s_i} & \frac{1}{s_3} & 0 & \cdots & 0 \\ 0 & 0 & \frac{1}{s_3} & \ddots & \ddots & \cdots & 0 \\ \vdots & \vdots & \vdots & \vdots & \ddots & \ddots & \vdots \\ 0 & 0 & \cdots & 0 & \frac{1}{s_{\sigma-2}} & -\sum_{\sigma-2}^{\sigma-1} \frac{1}{s_i} & \frac{1}{s_{\sigma-1}} \end{bmatrix}. \tag{3.21}$$

where $s_i = \beta_{i+1} - \beta_i$ is the length of ith segment. In [I]–[V], (3.21) is used for solving the static SCPWL model coefficients. The numerical instability problem associated with inversion of an ill-condition matrix can be totally avoided. Furthermore, only the elements of the main diagonal and two lower subdiagonals, i.e., $3(\sigma - 1)$ elements need to be computed.

3.4.3 SCPWL coefficients and the gradients of the linear affine segments

By evaluating the SCPWL function (3.16) at all the breakpoints $\boldsymbol{\beta}$, we get

$$\begin{aligned} f(\beta_1) &= c_0, \\ f(\beta_2) &= c_0 + c_1\lambda_1(\beta_2), \\ f(\beta_3) &= c_0 + c_1\lambda_1(\beta_3) + c_2\lambda_2(\beta_3), \\ &\vdots \\ f(\beta_\sigma) &= c_0 + c_1\lambda_1(\beta_\sigma) + \cdots + c_{\sigma-1}\lambda_{\sigma-1}(\beta_\sigma). \end{aligned} \tag{3.22}$$

Then, by substituting $f(\beta_1) = 0$ (this is the case for PA type nonlinearity) and rearranging the equations in (3.22), it can be shown that the SCPWL coefficients $\{c_i\}_{i=0}^{\sigma-1}$ are related to the gradients of its linear affine segments $\{m_i\}_{i=1}^{\sigma-1}$ as

$$\begin{aligned} c_1 &= m_1, \\ c_i &= m_i - m_{i-1}, \quad \forall\ 1 < i < \sigma \end{aligned} \tag{3.23}$$

Alternatively, the gradient of segment j is given by

$$m_j = \sum_{i=1}^{j} c_i, \tag{3.24}$$

for $j = 1, \cdots \sigma - 1$. This relationship is used in [VII] to estimate the value of the $\mathscr{G}(k) = \frac{d\mathbb{N}(v(k))}{dv(k)}$ in the direct-learning PD adaptation algorithm.[1]

3.4.4 Spectrum of the SCPWL model

It is well understood that the intermodulation distortion (IMD) components generated by a polynomial model is determined by the orders of the polynomial basis, e.g., x^5 produces the third and fifth order IMDs. For a PWL function such as the SCPWL model, the relationship between the basis functions and the order of IMD is not easily deducible. In [VI], an analysis is performed on how the SCPWL basis function introduces IMD. The results of the analysis found the following.

- The output spectrum of the SCPWL basis is given by

$$\boldsymbol{\lambda}_n(f) = \mathbf{R}(f) \otimes \boldsymbol{\Pi}_n(f) - \beta_n \boldsymbol{\Gamma}(f) \otimes \boldsymbol{\Pi}_n(f), \tag{3.25}$$

[1] The relationship in (3.24) is used for simplifying the direct learning algorithms in [VII]. This is presented here as it is not explained in [VII] due to space limitation.

where $\otimes$ denotes convolution, $\boldsymbol{\lambda}_n(f)$ and $\mathbf{R}(f)$ are the Fourier transform of $\lambda_n[r(t)]$ and the input signal $r(t)$, respectively. It is shown in [VI] that $\boldsymbol{\Pi}_n(f)$ and $\boldsymbol{\Gamma}(f)$ are sinc-like functions. Thus, the SCPWL basis operation causes spreading of the input signal spectrum, introducing frequency components that are not present in the input signal. The number of IMD components produced by the each basis function is theoretically infinite. Thus, IMD order of the SCPWL model is not determined by the highest order basis. The SCPWL function output spectrum given by

$$\hat{\mathbf{S}}(f) = \sum_{n=1}^{N-1} c_n \boldsymbol{\lambda}_n(f), \tag{3.26}$$

is a sum of scaled spectra of the basis functions. It can be deduced that the number of linear affine segments determines how accurately the function can model the IMD components.

- Simulation experiments are setup in [VI] to examine the influence of the number of breakpoints on modeling accuracy of the SCPWL function. The error in modeling the output spectral density (PSD) of a nonlinearity is used to gauge the modeling accuracy. It is shown that as the number of breakpoints increases, the modeling accuracy improves. The modeling capability saturates when the number of breakpoints increase above a certain number. In contrast, increasing the order of a polynomial above a certain order results in degradation of modeling capability.

3.5 Summary of contributions

The major contribution of this research concerning modeling of broadband PAs and PDs are as follows.

- A complex-valued memory-SCPWL model suitable for modeling baseband PAs and PDs with memory has been proposed. The model is linear-in-the-parameter. Thus, it can be conveniently identified using well-establish linear system identification methods such LMS algorithm. As compared to the polynomial model, it is more suitable for modeling strong nonlinearities.

- The properties of the SCPWL function have been studied in order to identified structures that can be exploited for development of simplified PD identification and adaptive algorithms. It is found that the

saturation behaviour of the function makes it suitable for modeling PA and PD type of nonlinearities. The linear affine structure (or piecewise linear structure) and the known user-defined breakpoints of the function are used for simplifying the implementation of the PD identification algorithms.

- An analysis on how the SCPWL function introduces IMD and the relationship between the basis function order and the order of IMD was carried out. A formula for predicting the output spectrum of the SCPWL function when excited by multi-tone signal is obtained. The analysis also show that each SCPWL basis function spreads the input signal spectrum to infinite order of IMD. Thus, the SCPWL function which consists of a superposition of scaled basis function output is capable of modeling infinite order of IMD. The accuracy of the model depends on the number of segments the function employs.

4. Predistorter identification algorithms

A PD identification algorithm typically consists of a training architecture designed for the PD function to learn the inverse characteristics of the PA, and a model parameter extraction algorithm derived based on an appropriate error objective function. The performance of a PD identification algorithm is commonly associated with the effectiveness of the identified PD and the efficiency of the algorithm. In other words, a good PD identification algorithm must be computationally efficient, able to extract the parameters of an effective PD and converges reasonably quickly. Another important aspect of PD identification algorithms is adaptivity, especially for linearizing PAs in modern communication systems such as LTE system. The PA characteristics in these systems may vary due to changes in the operating conditions such as carrier frequency, signal bandwidth, modulation format and operating temperature. With a varying PA behaviour, an adaptive PD algorithm is essential for ensuring satisfying linearization performance. In order to meet these objectives, a variety of PD identification algorithms have been proposed.

A straightforward method is one that identifies the PD in two steps. The PA model is first extracted by exciting the PA with a training signal. Then, the PD model is estimated by finding the inverse of the obtained PA model. An example of this 2-step PD identification approach can be found in [93], where the parameters of the memoryless polynomial PA is first extracted using the LS method. Then, the PA model parameters are used to derived the inverse memoryless polynomial function as the PD. When nonlinear PA with memory is involved, finding the inverse PA model becomes more challenging as the PA response is no longer a monotonic function. For instance, the Volterra series has been used by many authors for modeling nonlinear PA with memory. In order to find the inverse of a Volterra PA model, the p-th order inverse method [76, 94] can be employed. However, the p-th order inverse is computationally heavy, rendering it unsuitable for practical implementation. Thus, the above mentioned two-step PD

identification method is more suitable for identification of narrowband PD. In addition, to incorporate adaptivity in this method requires periodic training of the PD, which involves a two-step modeling procedure.

In the literature, the more popular solutions are algorithms that identify the PD parameters in one step, bypassing the explicit PA identification step. These more efficient PD identification algorithms employ learning architectures that allow the PD filter to directly learn the inverse characteristic of the PA. The two learning architectures that dominate the digital PD literature are the indirect learning [5, 10, 13, 95] and direct learning architectures [16, 22, 23]. In conjunction with these learning architectures, parameter extraction methods such as LS methods, LMS and RLS algorithms are proposed for tuning the PD filter parameters. Adaptivity is easy to incorporate into these methods as they identify the PD by learning the inverse of the PA in one step. The indirect learning and direct learning PDs found in the literature are reviewed in the later section of this chapter. More discussions on the advantages and drawbacks of these methods and techniques proposed in the literature to improve performance and efficiency of these algorithms are provided there.

In this work, the two-step method is developed for static SCPWL PD identification. For the SCPWL PDs with memory, indirect learning and direct learning algorithms are proposed. In [I] and [III], the two-step PD identification based on vector projection methods are proposed for static SCPWL PD. In these methods, the static nonlinearity of the PA is first modeled as the real-valued SCPWL function in (3.16). Then, a projection matrix is used to map the static nonlinear characteristics of the PA to its inverse to obtain the static SCPWL PD. The coefficients are extracted using LS method. Then, memory effects compensation is done by an adaptive linear filter cascaded after the static nonlinear block of the PD. In [VII], adaptive filtering methods adopting the indirect and direct learning architectures are proposed. The SCPWL PDs with memory, namely, the memory-SCPWL PD and Hammerstein-SCPWL PD, modeled using the proposed complex-valued SCPWL function in (3.19), are implemented as adaptive filters. Least mean square (LMS) algorithm is derived for adapting the coefficients of the PDs. In these PD identification algorithms, methods are developed for reducing the complexity of the identification algorithms.

Section 4.1, reviews the most referenced indirect learning and direct learning PDs found in the literature. The the advantages and drawbacks

of these algorithms, difference in implementation and methods proposed for improving effectiveness and efficiency of the algorithms are also discussed. Then, the SCPWL PD identification algorithms proposed in this thesis are presented in Section 4.2. The vector projection methods from [I] and [III] are first presented, followed by the adaptive filtering approach using both the indirect learning and direct learning architectures from [VII]. The modified Wiener model estimator employed to circumvent the non-convex cost function problem of Wiener/Hammerstein models identification is also discussed. In Section 4.3, analysis of measurement noise effects on the indirect learning SCPWL filter carried out in [VII] is summarized. Section 4.5 concludes the chapter by outlining the contribution of this work in the area of PD identification algorithms.

4.1 Review of indirect and direct learning PDs

The indirect learning and direct learning methods are the most adopted methods for PD identification in literature of the past two decades, see, e.g., [5, 10, 13, 16, 22, 23, 95–97]. These methods are more efficient and easier to implement as compared to the two-step approach discussed above. With these learning architectures, adaptivity is easier to incorporate into the PD identification algorithm as these methods employ a learning loop around the PA and identify the PD in one step. The major difference between the two learning architectures is in the way the learning loop around the PA is arranged. The indirect learning arrangement results in identification of the post-inverse model of the PA, which is then used as the PD. The direct learning method identifies the pre-inverse model as the PD. There are advantages and drawbacks associated with these learning architectures due to their learning loop arrangement. Besides the learning architecture, the method adopted for parameter extraction also affect the efficiency of the PD identification algorithm. In the more recent literature, efforts are focused on proposing techniques for improving efficiency and to overcome drawbacks associated with these methods. This section provides a review of the most referenced indirect learning and direct learning PDs in the literature.

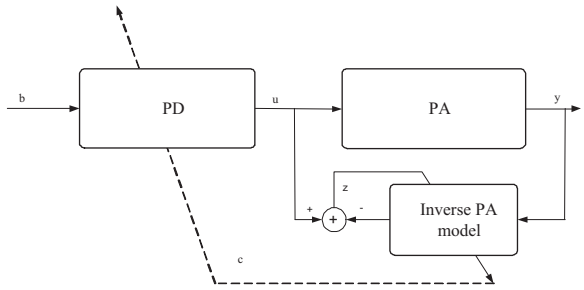

Figure 4.1. Indirect-learning architecture.

4.1.1 Indirect learning PDs

Figure 4.1 illustrates the indirect learning architecture employed for identifying a PD. A learning loop is formed around the PA where the PA output signal is fed back to the learning filter. The error signal is generated by comparing the output of the learning filter and the input signal to the PA. The error signal can then be used to form an appropriate objective function for the adapting the filter parameters. In the literature, the most common filter adaptation algorithms employed in conjunction with the indirect learning filter are LS, LMS and RLS. The indirect learning method identifies the post-inverse model of the PA. After the learning filter have converged to an optimum, they are directly copied to the PD filter.

The indirect learning architecture was first employed for PD identification in [10]. A truncated Volterra series is employed as the PD function. The indirect learning architecture is adopted and the recursive least squares (RLS) algorithm is formulated for extracting the Volterra PD parameters. As compared to the two-step method which employs the the p-th order inverse method [75] to identify a Volterra model PD [98], a significant reduction is complexity is seen. In [96], the authors proposed using V-vector algebra to expedite convergence and further reduce complexity of the indirect learning RLS algorithm for Volterra PD identification. In [5], memory polynomial, which is a special case of Volterra series, is used to characterize the PD function. The reduced number of coefficients and the linear-in-the-parameter input-output expression of the function ease the parameter extraction problem. The indirect learning memory polynomial PD coefficients are identified using LS method. In [95], the LS/Newton method is proposed for identifying indirect learning memory polynomial PD with envelope memory terms. The LS/Newton method provides improvement in convergence speed. The indirect learning architecture is

also employed for identifying a Hammerstein model PD in [13]. First, the the Narendra-Gallman method [99] is employed to iteratively identify the linear and nonlinear systems of the Hammerstein PD. Due to the non-convex cost function of the Hammerstein model, the Nadrendra-Gallman is prone to convergence problem. The authors proposed a two-step Least-Squares/Singular Value Decomposition (LS/SVD) method in order to avoid converging to a local minimum.

A drawback of the indirect learning architecture is due to noise at feedback path to the indirect learning filter. As shown in Figure 4.1, the input to the indirect learning filter is a feedback signal from the PA output. Thus, noise due to the imperfect transmission line, signal down-conversion and ADC is present at the filter input. It is shown in [25] that when polynomial function is employed as the indirect learning filter, input noise causes biased estimates of the PD coefficients, which compromises the performance of the PD. Instead of compensating the nonlinear effects, additional spectral regrowth at the PA output is observed, as reported in [23, 25, 86]. The negative impact of the noisy estimates of the PD coefficients is also known as the coefficient bias effects. It is shown in [95] that the in-band error and out-of-band noise caused by the bias estimates of the memory polynomial PD rise linearly with the level of noise at the feedback path of the indirect learning architecture. Two methods were proposed for reducing the noise effect in [25], namely, inverse modeling with block averaging of periodic training signal, and forward modeling followed by noiseless inverse modeling. These techniques increase the computational complexity of the PD algorithm considerably. More recently, a computationally more efficient modified LS method for parameter extraction is proposed in [27]. In this method, the feedback path is represented by a complex gain. A technique is proposed for measuring the gain and the information is incorporated in the input matrix for solving the LS equation, resulting in reduced bias in the estimates.

There is another concern for the indirect learning method of PD identification, which is the main reason researchers resort to direct learning method. As the post-inverse of the PA is employed as the PD in the indirect learning method, the concern is whether the post-inverse and the pre-inverse of the PA are commutable. However, a theory is established in [75] that if the p-th order post-inverse of a general Volterra system is obtained, then the p-th order pre-inverse is identical.

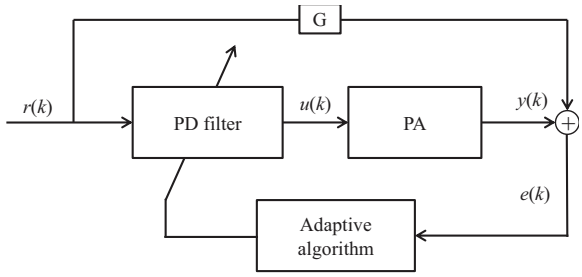

Figure 4.2. Direct-learning architecture.

4.1.2 Direct Learning PDs

The direct learning architecture is illustrated in Figure 4.2. Differing from the indirect learning architecture, the direct learning filter identifies the pre-inverse of the PA. The learning filter is the PD filter itself. The learning loop is closed around the PD-PA chain. The error signal that is used for deriving the PD parameter extraction algorithm is formed by comparing the output of the PA and the desired linearized PA output. As the PA appears at the output of the learning filter, i.e, the PD, the error function inevitably includes the PA function. Thus, the characteristics of the PA is required in the direct learning algorithms.

The direct learning method is employed in [16,22,23,97]. In [22], the direct learning architecture is employed for identifying a Volterra PD. The authors derived the LMS algorithm for updating the Volterra PD filter coefficients. The PA function appears as a nonlinear filter for the reference input signal in the update equation. Thus, the direct learning LMS algorithm is also known as nonlinear filtered-x LMS (NFxLMS) algorithm [22,28,29]. The authors characterized the PA as a Volterra filter. Instead of estimating the PA model in each iteration, the authors assumed that its parameters are known in order to simplify the implementation. The NFxLMS algorithm is also employed in [16] for adapting a Hammerstein model PD. The PA is modeled as a Wiener system and is estimated offline.

Besides the increased complexity due to the need to acquire the PA model and filtering of the reference input signal, another drawback of the NFxLMS algorithm is its extremely slow convergence speed. Nonlinear filtered-x Recursive Least-Squares (NFxRLS) algorithm is commonly employed in order to increase the convergence speed of direct learning PDs [23, 97], at a price of added computational complexity. In [97], the

static nonlinear block of the Wiener PA is modeled by PWL functions in order to simplify the direct learning Hammerstein model PD algorithm.

4.2 Identification algorithms for SCPWL PDs

This section summarizes the SCPWL PD identification algorithms proposed in this work, namely, the vector projection based methods and the adaptive filtering methods. The vector projection based methods are developed for identification of static SCPWL PD. The adaptive filtering methods adopt the indirect learning and direct learning architectures and the filters are adapted by the LMS algorithm. Issues associated with these algorithms and methods proposed to circumvent the issues and to simplify the algorithms are also discussed.

4.2.1 Vector projection methods

Two vector projection based methods are developed in this thesis, i.e., the image projection method [I] and the ICM method [III]. In these methods, the static nonlinearity of the PA is modeled as the static SCPWL function in (3.16) which composes of linear affine segments as shown in Figure 3.5. Each segment can be completely defined by the two coordinates $\mathbf{b}_k = [\beta_k, y_k]^{\mathrm{T}}$ and $\mathbf{b}_{k+1} = [\beta_{k+1}, y_{k+1}]^{\mathrm{T}}$ at the edges of the segment. The SCPWL nonlinearity of the PA can be written in vector-matrix form as

$$\mathbf{y} = \mathbf{f}(\boldsymbol{\beta}) = \boldsymbol{\Lambda}(\boldsymbol{\beta})\mathbf{c}. \tag{4.1}$$

Knowing that the static PD response is the inverse of the PA, the static SCPWL characteristics of the PD can be obtained by projecting the coordinates $(\mathbf{b}_1, \cdots, \mathbf{b}_{\sigma-1})$ using a suitable vector projection matrix [100]. Let the projection matrix be denoted by $\mathbf{Q}$. Then, the coordinates that define the SCPWL PD is $\mathbf{b}' = \mathbf{Q}\mathbf{b}$, where $b'_k = [\beta'_k,\ y'_k]$. Now, the SCPWL PD function can be written as

$$\mathbf{y}' = \mathbf{g}(\boldsymbol{\beta}') = \boldsymbol{\Lambda}'(\boldsymbol{\beta}')\mathbf{c}'. \tag{4.2}$$

The PD coefficients can then be extracted by solving the $\mathbf{c}' = \left[\boldsymbol{\Lambda}'(\beta')\right]^{-1}\mathbf{g}(\beta')$. Matrix inversion is computationally costly operation. Instead of computing $\left[\boldsymbol{\Lambda}'(\beta')\right]^{-1}$ directly, the inverse basis function matrix expressed in (3.21) is used, where $\boldsymbol{\Lambda}'_{\mathrm{I}}(\beta')$ can be constructed using the obtained PD breakpoints $\boldsymbol{\beta}'$. Then the static SCPWL coefficients of the PD is

$$\mathbf{c}' = \boldsymbol{\Lambda}'_{\mathrm{I}}(\boldsymbol{\beta}')\mathbf{g}(\boldsymbol{\beta}'). \tag{4.3}$$

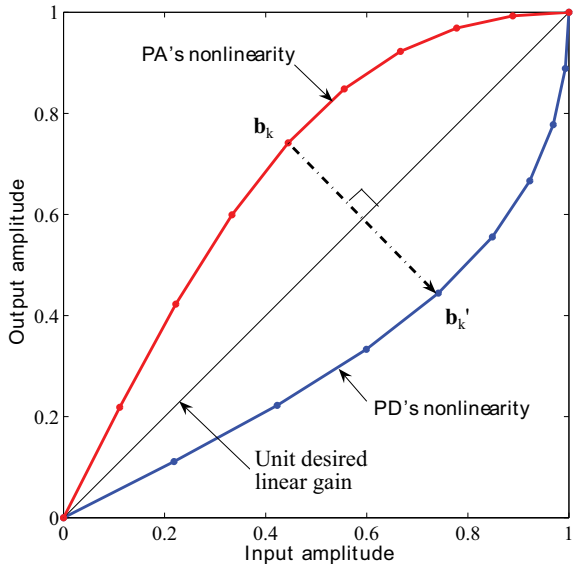

Figure 4.3. PD static nonlinear response resembles the mirror image of the PA static nonlinear response.

In this work, two projection matrices are derived, i.e., the image projection matrix and the ICM matrix.

4.2.1.1 Image projection matrix

The image projection method proposed in [I] is based on the idea that the normalized AM/AM response of the PD is the mirror image of the PA AM/AM response, as illustrated in Figure 4.3. The linearized gain of the PD-PA output is 1. Thus, the PA and PD characteristics are mirror images of each other. By modifying an orthogonal projection [100], the resulting image projection matrix derived in [I] is given by

$$\mathbf{Q} = \begin{bmatrix} 0 & 1 \\ 1 & 0 \end{bmatrix}. \tag{4.4}$$

However, the image projection method is limited to normalized PA and PD responses. In the following, the ICM method which allows mapping of PD that gives any arbitrary linearized gain is presented.

4.2.1.2 Inverse coordinate mapping matrix

In practice, the desired linearized gain of the PD-PA system is rarely unity. Instead, it is more likely to be the small signal gain of the PA or a gain that allows a maximum spanning of the PA input range up to the PA saturation point. When the desired linear gain $G \neq 1$, the static

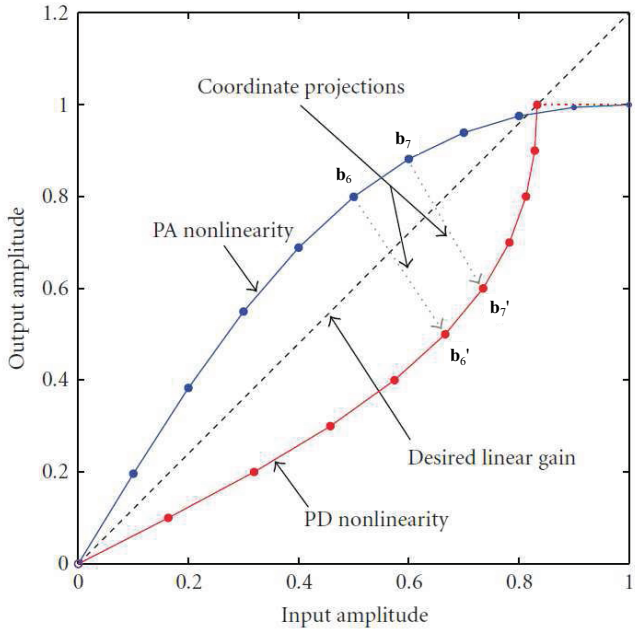

Figure 4.4. The inverse coordinate mapping method

nonlinear function of the PD is not an exact mirror image of the PA's, as illustrated in Fig. 4.4. In [III], the ICM method is developed, where a new projection matrix which allows mappings that give any arbitrary linearized gain $G \neq 1$ at the PD-PA output is derived. The ICM matrix is derived based on the following conditions.

C1 The output of the PD-PA cascade is a linear amplified version of the input signal with an arbitrary linearized gain G.

C2 The output space of the PD must coincide with the input space of the PA.

The ICM matrix that fulfils these conditions is given by

$$\mathbf{Q} = \begin{bmatrix} 0 & \frac{1}{G} \\ 1 & 0 \end{bmatrix}. \tag{4.5}$$

When $G = 1$, the ICM matrix reduces to the image projection matrix.

4.2.2 Adaptive filtering methods

In [VII], a Hammerstein-SCPWL PD and a memory-SCPWL PD are proposed for linearizing nonlinear PAs with memory. Both indirect and direct learning architectures are employed for identifying the SCPWL PDs with

memory. The LMS algorithm is derived for adapting the coefficients of the PDs.

The memory-SCPWL function is particularly suitable for adaptive filter implementation. Its adaptive algorithms are straightforward to derive due to its linear-in-the-parameter expression. The LMS algorithms for the Hammerstein-SCPWL PD are more tedious due to the non-convex cost function problem associated with block models [34–36]. A modified Wiener model estimator is employed in order to overcome the non-convex cost function problem.

In the following, the modified Wiener model estimator which is employed in the Hammerstein-SCPWL PD identification algorithms is first outlined. Then, the indirect learning and direct learning algorithms for the Hammerstein-SCPWL PD identification are summarized. Finally, the indirect learning and direct learning memory-SCPWL PD algorithms are presented.

4.2.2.1 Modified Wiener model estimator

In this thesis, the Hammerstein-SCPWL PD algorithms are designed by assuming that the PA can be modeled as a Wiener system. In the indirect learning algorithm, the linear subsystem of the Wiener model PA has to be estimated. In the direct learning algorithm, the Wiener PA model is required in the update equation. In order to avoid the non-convex cost function problem in block models identification, the modified Wiener model estimator shown in Figure 4.5 is employed. As a result, both the indirect learning and direct learning algorithms for the Hammerstein-SCPWL PD identification are simplified.

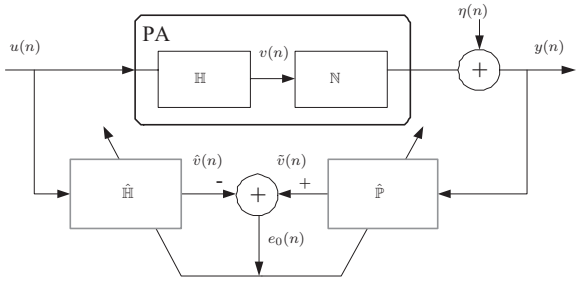

Figure 4.5. Modified Wiener model estimator.

Following from Figure 4.5, the estimator generates the error signal $e_0(n)$ by comparing the estimated intermediate signals of the Wiener system from the feed-forward and fed-back filters. The ambiguity of the total

static gain distribution in the two filters is resolved by anchoring $\hat{h}_0(n)$ to a fixed value $\hat{h}_0$, see [87]. The estimator configuration renders a linear-in-the-parameter error equation, leading to a convex cost function [101]. By minimizing the instantaneous squared error objective function $|e_0(n)|^2$, the LMS update equation for the modified Wiener model estimator is given by

$$\boldsymbol{\theta}(n+1) = \boldsymbol{\theta}(n) - \mu_0 \boldsymbol{\phi}(n) e_0^*(n), \tag{4.6}$$

where μ_0 is the adaptation step size that controls the convergence speed and final error. The vectors, $\boldsymbol{\theta}(n) \in \mathbb{C}^{(\sigma+N-1)\times 1}$ and $\boldsymbol{\phi}(n) \in \mathbb{C}^{(\sigma+N-1)\times 1}$ are the parameter vector and regression vector, respectively, given by

$$\boldsymbol{\theta}(n) = \left[\hat{c}_0(n) \ \cdots \ \hat{c}_{\sigma-1}(n), \ \hat{h}_1(n) \ \cdots \ \hat{h}_{N-1}(n)\right]^{\mathrm{T}} \tag{4.7}$$

$$\boldsymbol{\phi}(n) = \left[\boldsymbol{\lambda}^{\mathrm{T}}[y(n)], \ -u(n-1) \ \cdots \ -u(n-N+1)\right]^{\mathrm{T}}. \tag{4.8}$$

To ensure convergence for the algorithm in (4.6), the range of μ_0 is [102]

$$0 < \mu_0 < \frac{1}{\varrho_{\max}}, \tag{4.9}$$

where $\varrho_{\max}$ is the maximum eigenvalue of $\mathrm{E}\left[\boldsymbol{\phi}(n)\boldsymbol{\phi}^{\mathrm{H}}(n)\right]$. As shown in [VII], the upper bound for $\varrho_{\max}$ can be written as

$$\varrho_{\max} \leq 1 + \sum_{i=1}^{\sigma-1} (\beta_\sigma - \beta_i)^2 + (N-1)\sigma_u^2, \tag{4.10}$$

where σ_u^2 is the variance of the signal $u(n)$. Equation (4.10) indicates that the convergence speed of (4.6) is affected by the partition sizes of the static SCPWL function $\hat{\mathbb{P}}(\cdot)$, the linear filter length N and the input signal power. For example, for a given N and a fixed set of $\boldsymbol{\beta}$, increasing the input signal power renders a smaller upper bound for μ_0, leading to slower convergence.

The estimator yields the estimates of the PD static SCPWL nonlinearity $\hat{\mathbb{P}}$ and the linear filter of the PA $\hat{\mathbb{H}}$. The modified Wiener model estimator is employed in both the indirect and direct learning algorithms for the Hammerstein-SCPWL PD.

4.2.2.2 Indirect learning Hammerstein-SCPWL PD

Figure 4.6 illustrates the indirect learning Hammerstein-SCPWL PD. The indirect learning algorithm for the Hammerstein-SCPWL PD consists of two identification loops running simultaneously.

The first loop consists of the modified Wiener model estimator, which estimates the linear block $\hat{\mathbb{H}}(\cdot)$ and the inverse of the static nonlinear

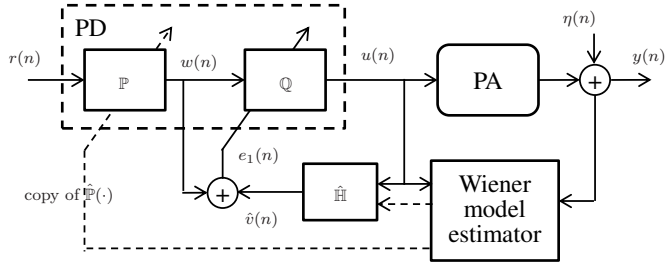

Figure 4.6. Indirect learning Hammerstein-SCPWL PD.

block $\hat{\mathbb{P}}(\cdot)$ of the Wiener model PA. The estimate $\hat{\mathbb{P}}(\cdot)$ is directly copied to the nonlinear block of the PD, and $\hat{\mathbb{H}}(\cdot)$ is fed to the second learning loop for adapting the PD linear filter $\mathbb{Q}(\cdot)$, see Figure 4.6.

The second loop uses the estimates of $\hat{\mathbb{H}}$ obtained from the modified Wiener model estimator to adapt the PD linear filter $\mathbb{Q}$, as illustrated in Figure 4.6. The LMS algorithm derived in [VII] for updating the PD filter $\mathbb{Q}(\cdot)$ is the given by

$$\mathbf{q}(n+1) \approx \mathbf{q}(n) - \mu_1 e_1^*(n) \sum_{i=1}^{N-1} \hat{h}_i^*(n)\mathbf{w}(n-i) \tag{4.11}$$

where $\mathbf{w}(n) = [w(n) \cdots \; w(n-M+1)]^{\mathrm{T}}$ and $\mathbf{q}(n) = \big[q_0(n) \cdots \; q_{M-1}(n)\big]^{\mathrm{T}}$. The approximation in (4.11) is valid for sufficiently small value of μ_1 so that $\mathbf{q}(n) \approx \mathbf{q}(n-i)$ for $i = 1, \cdots, N-1$.

Note that (4.11) is a filtered-x LMS algorithm. Thus, the stability of the recursion in (4.11) depends on the quality of the estimates $\{\hat{h}(n)\}_{i=0}^{N-1}$. To ensure stability, the phase response error between the estimate and the actual PA dynamics must be within the range $-\frac{\pi}{2}$ and $\frac{\pi}{2}$ [103, 104].

4.2.2.3 Direct learning Hammerstein-SCPWL PD

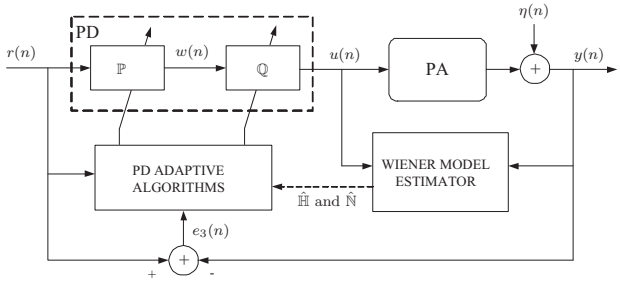

Figure 4.7. Direct learning Hammerstein model PD.

Figure 4.7 illustrates the direct learning Hammerstein-SCPWL PD proposed in [VII]. It is well-known that the estimate of the PA model is required in the direct learning algorithm, as the error signal is generated

at the output of the PA instead of the output of the PD filter. The modified Wiener model estimator is used for extracting the Wiener PA model, where the estimates $\hat{\mathbb{H}}(\cdot)$ and $\hat{\mathbb{P}}(\cdot)$ are obtained. The estimates are fed to the direct learning algorithm.

The direct learning LMS algorithm for the Hammerstein-SCPWL PD is derived in [VII]. The update equation for the linear and nonlinear filters parameter vectors, $\mathbf{q}(n)$ and $\mathbf{c}(n)$, are given by

$$\mathbf{q}(n+1) \approx \mathbf{q}(n) + \mu_3 e_3^*(n)\mathscr{G}(n) \sum_{i=0}^{N-1} \hat{h}_i^*(n)\mathbf{w}(n-i), \tag{4.12}$$

and

$$\mathbf{c}(n+1) \approx \mathbf{c}(n) + \mu_4 e_3^*(n)\mathscr{G}(n) \times \sum_{i=0}^{M+N-1} s_i^*(n)\boldsymbol{\lambda}[r(n-i)], \tag{4.13}$$

respectively. The signal $\mathbf{s}(n) = \{s_i(n)\}_{i=0}^{N+M-1}$ in (4.13) is the result of $\hat{\mathbf{h}}(n) \otimes \mathbf{q}(n)$, where $\otimes$ stands for convolution. The approximations in (4.12) and (4.13) are valid for sufficiently small step sizes such that $\mathbf{q}(n) \approx \mathbf{q}(n-i)$ for $i = 1, \cdots, N-1$ and $\mathbf{c}(n) \approx \mathbf{c}(n-i)$ for $i = 1, \cdots, M+N-1$, respectively. Equations (4.12) and (4.13) resemble the nonlinear filtered-x algorithms as in [105] and constitute the direct learning algorithm for the Hammerstein-SCPWL PD.

Notice that the signal $\mathscr{G}(n) = \frac{\partial \hat{\mathbb{N}}\left(\hat{v}(n)\right)}{\partial \hat{v}(n)}$ appears in both (4.12) and (4.13). The expression is the derivative of the PA static nonlinearity w.r.t. its input signal. The computation of $\mathscr{G}(n)$ requires the estimate $\hat{\mathbb{N}}(\cdot)$.

As the modified Wiener model estimator is employed for PA model estimation the estimate of $\hat{\mathbb{N}}(\cdot)$ is not explicitly available. Instead, the estimator provides its inverse $\hat{\mathbb{P}}(\cdot)$. To avoid identifying $\hat{\mathbb{N}}(\cdot)$ explicitly, a solution for estimating $\mathscr{G}(n)$ is proposed in [VII]. We recognize that $\hat{\mathbb{P}}(\cdot)$ approximates the inverse of $\hat{\mathbb{N}}(\cdot)$. Then, using the fact that the derivative of inverse functions are reciprocals of each other, the derivative of $\hat{\mathbb{N}}(\cdot)$, denoted by $\mathscr{G}(n)$, can be estimated using the parameters of $\hat{\mathbb{P}}(\cdot)$ as (see Appendix in [VII] for details),

$$\hat{\mathscr{G}}(n) = \begin{cases} \left[\frac{\hat{v}(n)}{y(n)} + \sum_{i=1}^{N_s} c_i^*(n)\right]^{-1} & , \left|y(n)\right| \leq \beta_\sigma \\ \frac{y(n)}{\hat{v}(n)} & , \left|y(n)\right| > \beta_\sigma \end{cases}. \tag{4.14}$$

In (4.14), N_s specifies the PWL segment number that $|\hat{v}(n)|$ falls into and c_i are the parameters of the PD static nonlinearity $\mathbb{P}(\cdot)$.

To further reduce computational complexity, the complex-valued gain $\mathscr{G}(n)$ can be dropped at the expense of a decrease in convergence speed [105].

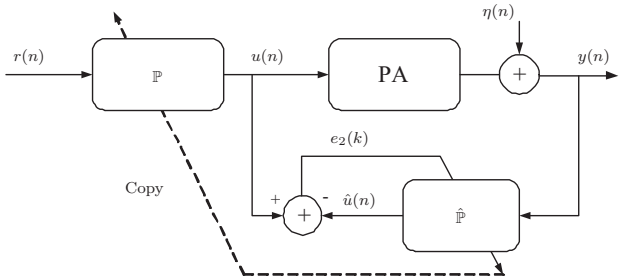

Figure 4.8. Indirect learning memory SCPWL PD

4.2.2.4 Indirect learning Memory-SCPWL PD

In [VII], the proposed memory-SCPWL (3.19) is also employed for PD designed. The SCPWL function with memory has a linear-in-the-parameter input-output expression. This property lends a hand to simplifying identification algorithms for PD with memory. Figure 4.8 illustrates the indirect learning memory-SCPWL PD algorithm. The indirect learning filter $\hat{\mathbb{P}}$ at the feedback path is characterized by a memory-SCPWL model, with memory length $L > 1$. Due to its linear-in-the-parameter expression, the formulation of the PD adaptation algorithm is greatly simplified compared to that of the Hammerstein model PD.

By minimizing the instantaneous squared error $|e_2(n)|^2$ with respect to $\hat{\mathbf{c}}_\ell(n)$, the LMS algorithm for adapting the filter coefficients is given by

$$\hat{\mathbf{c}}_\ell(n+1) = \hat{\mathbf{c}}_\ell(n) + \mu_2 e_2^*(n)\boldsymbol{\lambda}[y(n-\ell)], \tag{4.15}$$

where $\ell = 0, \ldots, L-1$. The memory-SCPWL PD $\mathbb{P}(\cdot)$ is updated by directly copying the adaptive filter coefficients, i.e., $\mathbf{c}_\ell(n) = \hat{\mathbf{c}}_\ell(n-1)$ for $\ell = 0, \ldots, L-1$.

4.2.2.5 Direct learning Memory-SCPWL PD

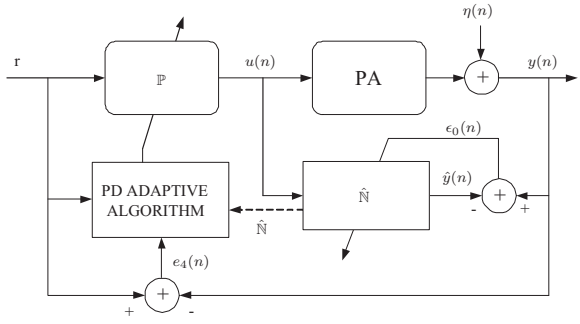

Figure 4.9. Direct learning memory SCPWL PD

Figure 4.9 illustrates the direct learning memory-SCPWL PD. Since the

PA model is required for formulating the direct learning algorithm, two learning loops are formed. One for estimating the PA model and another for updating the PD coefficients. The PA learning filter $\hat{\mathbb{N}}$ is modeled using a memory-SCPWL model with memory length L_1 with coefficient vectors in each memory branch denoted by $\{\mathbf{a}_{\ell_1}\}_{\ell_1=0}^{L_1-1}$. Then, by minimizing the instantaneous squared error $|\epsilon_0|^2$, the LMS algorithm for updating the coefficients of $\hat{\mathbb{N}}$ is given by

$$\mathbf{a}_{\ell_1}(n+1) = \mathbf{a}_{\ell_1}(n) + \mu_5 \epsilon_0^*(n) \boldsymbol{\lambda}\big[u(n-\ell_1)\big], \tag{4.16}$$

The PA model estimates $\mathbf{a}_{\ell_1}(n)$ are then fed to the direct learning algorithm for adapting the PD coefficients.

Let the memory length of the memory-SCPWL PD be L_2, and PD coefficients vector of each memory branch be denoted as $\{\mathbf{c}_{\ell_2}\}_{\ell_2=0}^{L_2-1}$. Then, by minimizing the instantaneous squared error $|e_4(n)|^2$ with respect to $\mathbf{c}_{\ell_2}(n)$, the LMS algorithm for the memory-SCPWL PD filter is given by

$$\hat{\mathbf{c}}_{\ell_2}(n+1) = \hat{\mathbf{c}}_{\ell_2}(n) + \mu_6 e_4^*(n) \sum_{\ell_1=0}^{L_1-1} \mathscr{G}_{\ell_1}(n) \boldsymbol{\lambda}[r(n-\ell_1-\ell_2)], \tag{4.17}$$

where $\mathscr{G}_{\ell_1}(n)$ is the derivative of the PA model. Equation (4.17) is valid for sufficiently small μ_6 such that $\mathbf{c}_{\ell_2}(n) \approx \mathbf{c}_{\ell_2}(n-\ell_1-\ell_2)$ for $(\ell_1+\ell_2) = 0, \cdots, (L_1+L_2-1)$.

In order to estimate $\mathscr{G}_{\ell_1}(n)$, the estimates of the PA coefficients $\{\mathbf{a}_{\ell_1}\}_{\ell_1=0}^{L_1-1}$ and Equation (36) in the Appendix of [VII] are needed. The estimate of $\mathscr{G}_{\ell_1}(n)$ is expressed as

$$\hat{\mathscr{G}}_{\ell_1}(n) = \begin{cases} \frac{\mathbf{a}_{\ell_1}^{\mathrm{H}}(n)\boldsymbol{\lambda}[u(n-\ell_1)]}{u(n-\ell_1)} + \sum_{p=1}^{N_{\ell_1}} a_{\ell_1,p}^*(n), & \big|u(n-\ell_1)\big| \le \beta_\sigma \\ \frac{\mathbf{a}_{\ell_1}^{\mathrm{H}}(n)\boldsymbol{\lambda}[u(n-\ell_1)]}{u(n-\ell_1)}, & \big|u(n-\ell_1)\big| > \beta_\sigma \end{cases}, \tag{4.18}$$

where N_{ℓ_1} is the segment number that $|u(n-\ell_1)|$ falls into.

Remark: Unlike the case of a static nonlinearity, $\{\mathscr{G}_{\ell_1}(n)\}_{\ell_1=0}^{L_1-1}$ cannot be omitted from (4.17). It contains the coefficients filtering $\boldsymbol{\lambda}[r(n-\ell_1-\ell_2)]$ as well as the phase response information of the PA which is crucial for the algorithm stability.

4.3 Measurement noise effects on indirect learning filters

Measurement noise at the feedback path of the indirect learning filter, which constitutes for example the perturbations due to down-conversion

and ADC, is known to cause coefficient bias effect [25] on polynomial or Volterra PDs. The bias estimates are shown to have an impact on the performance of the PD in terms of NMSE of the PA output spectrum estimates and the ACPR of the linearized output [25, 26].

In [VII], analysis of measurement noise effects on the indirect learning SCPWL filter is performed. In order to examine the impact of noise on the identified coefficients, the error in the mean amplitude of each noise corrupted basis of a static SCPWL function is derived. In the context of predistortion, the derivation is done with the following assumptions:

- The algorithm has converged
- The step size for the algorithm is assumed sufficiently small so that effects due to parameter copying (associated with indirect learning) can be neglected
- The input signal is backed off sufficiently so that no signal is clipped by the PD nor PA.

Then, $y(n)$ is Gaussian distributed with zero mean and variance σ_y^2. Its amplitude $|y(n)|$, denoted by $x(n)$ follows the Rayleigh distribution with parameter $\sigma_x = \sqrt{\frac{\sigma_y^2}{2}}$.

Impact of noise on estimates of SCPWL coefficients The mean amplitude of the ith SCPWL basis derived in the Appendix of [VII] is given by

$$E\Big[\lambda_i[a(n)]\Big] = \sigma_y\sqrt{\pi} \times \Big\{\Pr\Big(\beta_i < x(n) < \beta_\sigma\Big)\Big\}. \tag{4.19}$$

The expression between the curly bracket is the probability that the signal amplitude $a(n)$ falls between β_i and β_σ. For sufficiently high SNR,[1] $\Pr(\beta_i < \tilde{x}(n) < \beta_\sigma) \approx \Pr(\beta_i < x(n) < \beta_\sigma)$. Using (4.19), and assuming that the SNR is sufficiently high, i.e., $\gamma \gg 1$, the error in the SCPWL basis caused by input noise is derived and is given by

$$E\Big[\lambda_i[\tilde{x}(n)]\Big] - E\big[\lambda_i[x(n)]\Big] = \frac{1}{2\gamma} E\Big[\lambda_i[x(n)]\Big]. \tag{4.20}$$

From (4.20), it follows that the noise-induced bias is proportional to the unperturbed basis $\lambda_i[x(n)]$, but not the basis number i. In effect, each SCPWL basis is scaled by the factor $(1 + \frac{1}{2\gamma})$, which also leads to uniform scaling of the coefficients when a stochastic gradient algorithm as in (4.15) is employed. Thus, the spectral profile of the identified SCPWL PD is not affected by the measurement noise.

[1] Simulations verify that $\gamma \geq 20$ dB is sufficient.

Impact of noise on estimates of polynomial coefficients For comparison, the error in the expected amplitude of a polynomial basis is also derived in [VII].

The mean amplitude of the kth polynomial basis $\psi_k[x(n)] = x^k(n)$ given in [19] is

$$E\Big[\psi_k[x(n)]\Big] = \begin{cases} \frac{k}{2}!\Big(\sigma_x\Big)^k, & k \text{ is even} \\ \Big(\sqrt{\frac{\pi}{2^{k+1}}}\Big)k!!\Big(\sigma_x\Big)^k, & k \text{ is odd} \end{cases}, \tag{4.21}$$

where $k!! = (1 \cdot 3 \cdot \cdots \cdot k)$. Then, denoting the noisy input signal amplitude as $\tilde{x}(n) = |y(n) + \eta(n)|$, where $\eta(n)$ is a zero-mean Gaussian noise process with variance σ_η^2, the error caused by noise in the mean amplitude of the k-th polynomial basis is derived and is given by

$$E\Big[\psi_k[\tilde{x}(n)]\Big] - E\Big[\psi_k[x(n)]\Big] = \frac{(k-1)}{2\gamma} E\Big[\psi_k[x(n)]\Big], \tag{4.22}$$

where $\gamma = \frac{\sigma_y^2}{\sigma_\eta^2}$ denotes signal-to-noise-ratio (SNR). Equation (4.22) shows that the effect of noise on the polynomial basis is a bias that is proportional to the mean of the unperturbed basis and increases with the order of the basis k. Consequently, the identified polynomial coefficients are biased by different factors, with larger bias for higher order coefficients. In effect, this alters the spectral shape of the PD, which may cause increased out-of-band power at the PA output.

4.4 Convergence of direct learning filters

Although the direct learning method circumvents the problem of measurement noise at the PA output, a major concern for the NFxLMS algorithm is its slow convergence [23]. The convergence speed of the NFxLMS algorithm for the memory polynomial PD reduces drastically as the memory length is increased. The convergence speed of the direct learning memory-SCPWL PD and memory polynomial PDs are compared by simulations. The memory-SCPWL PD algorithm is shown to converge significantly faster than that of the memory polynomial PDs. More details of the simulation results are presented in the next chapter.

4.5 Summary of contributions

The contributions of this work in terms of SCPWL PD parameter identification algorithms are as follows.

- Development of the vector projection based methods, namely the image projection and ICM methods for static SCPWL PD identification. The simplicity of the methods is due to the linear affine structure and the known user-defined breakpoints of the SCPWL function. The extraction of the coefficients is simplified by using the inverse basis function matrix which can be constructed using the user-defined breakpoints as in (3.21).

- Derivation of the indirect and direct learning adaptive algorithms for the memory-SCPWL PD and Hammerstein-SCPWL PD.

- In the adaptive Hammerstein-SCPWL PD algorithms, a modified Wiener model estimator is employed in order to avoid the non-convex cost function problem.

- The derivative of the SCPWL PA models w.r.t. to their respective input, $\mathscr{G}(n) = \frac{\partial \hat{\mathbb{N}}\left(\hat{v}(n)\right)}{\partial \hat{v}(n)}$, is required in the direct learning algorithms in order to gain convergence speed and ensure stability. In order to avoid estimation of $\hat{\mathbb{N}}(\cdot)$, an expression is derived to approximate $\mathscr{G}(n)$, thus reducing the complexity of the algorithm.

- Analysis of the effects of measurement noise on the indirect learning SCPWL filter. It is found that due to its linear basis functions, the SCPWL filter coefficients are not affected by noise-induced coefficient bias effect which affects polynomial filters

5. Performance evaluation of the SCPWL PDs

This chapter summarizes the results of performance evaluation and comparison of the proposed SCPWL PDs with well-referenced polynomial PDs obtained by simulations and measurements.

Simulations were performed in MATLAB® environment [I, III, IV, VII] and MATLAB-Agilent Advanced Design System (ADS)-Ptolemy co-simulator environment [VII]. In the MATLAB simulations, baseband system level models of the PA and PD are simulated, in which, various PA models were simulated. In the MATLAB-ADS-Ptolemy co-simulations, a circuit level simulator is used to design a WiMAX base station PA. The PA model is based on the Freescale MRF6S23100H LDMOS device model provided in the ADS component library [106]. The PD model is extratced and implemented as a baseband system level model in MATLAB®. Signal predistortion is also performed in MATLAB®. A memoryless SCPWL PD is also evaluated by measurement on a real PA in a testbed [II, V]. The PA under test is the MC-ZVE8G PA from Minicircuits. The testbed consists of an RF transceiver, a digital signal processing (DSP) part and MATLAB® environment. Input-output measurement data are converted to discrete baseband signal samples and fed back to MATLAB®. The SCPWL PD model extraction and signal predistortion are performed in MATLAB®.

The simulation and measurement experiments in this thesis study the following topics, see Figure 5.4 for summary. Firstly, it is well-known that polynomial model poses numerical problems when high order model are used to model strong nonlinearity. Increasing the order of the polynomial PD to a certain extend will lead to performance degradation. Thus, the effect of increasing the model order (number of breakpoints) of the SCPWL function on the PD performance is studied. The performance of the SCPWL PD and polynomial PD are also compared for linearizing a PA driven closer to its saturation point (strong nonlinearity). When im-

plementing adaptive PD algorithm using the indirect learning and direct learning architectures, the former is faced with the issues of measurement noise at the feedback path and the latter is often observed to have slow convergence rate. Investigation on these issues are performed on the proposed adaptive SCPWL PDs and comparison are made with polynomial PDs. In terms of linearization performance, the adaptive SCPWL PDs are evaluated on various broadband PA models in OFDM system by simulations. In addition, the SCPWL PD is also evaluated on a WiMAX base station PA based on a circuit-level model. The results are grouped into linearization of different PA models and different PD adaptation approaches. In addition to linearization performance, simulations are also carried out to gauge the efficiency gain by combining PD and PAPR reduction schemes.

The chapter is organized as follows. The detailed setup of the simulation environments and measurement testbed are presented in Section 5.1. Section 5.2 summarizes the performance evaluation and comparison results of the SCPWL PDs with well-referenced polynomial PDs. The summary are organized into topics outlined in the previous paragraph. The chapter ends with a discussion on the overall results of the performance evaluation and comparison in Section 5.3

5.1 Setup of simulation environments and measurment testbed

5.1.1 System level simulations in MATLAB®

In [I – III] and [V], the excitation signals used for the PD identification and performance evaluation include power-swept single-tone signal and random-phase multi-sine signal expressed in (5.1). The former is used for extracting the memoryless AM/AM and AM/PM characteristics of the PA. The latter is employed as excitation for extracting the memory part of the PA or PD models. It also emulates a broadband multicarrier signal in performance evaluation experiments.

In [IV] and [VII], a generic baseband OFDM system is considered. Various broadband PA models are considered, including Wiener model PA and Wiener-Hammerstein PA. Figure 5.1 illustrates the baseband OFDM system model used in the system level simulations. The transmitted binary digits b_i, are generated and fed to a QAM modulator. The M-QAM

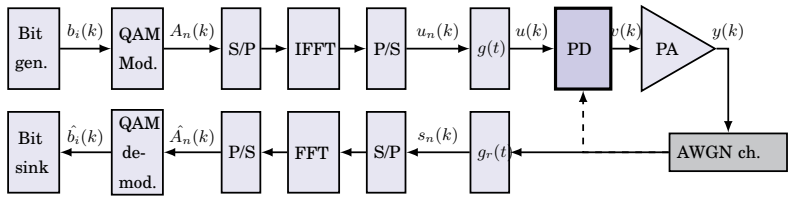

Figure 5.1. System model used in the MATLAB® system level simulations

symbols $A_n(k)$ are then serial-to-parallel converted and fed to the IFFT block for generation of OFDM symbols. The index variables are defined as $i = [1, 2, \cdots, N \log_2 M]$, $n = [1, 2, \cdots, N]$ and N is the number of sub-carriers in an OFDM symbol. Then, the OFDM symbol samples $u_n(k)$ is pulse-shaped using a root-raised cosine filter $g(t)$ with a roll-off factor of 0.22 and an oversampling factor $R = 8$. The PAPR of the pulse-shaped OFDM signal $u(t)$ is approximately 12 dB. Thus, an IBO of 12 dB is applied and the signal samples $u(t)$ are fed to the PD-PA chain.

The output of the PD-PA chain is then transmitted through an additive white Gaussian noise (AWGN) channel. For PD parameter identification, the PD input signal $u(t)$ and the PA output signal $y(t)$, which is corrupted by noise, are fed to PD identification algorithm. In the case where the PA model needs to be identified explicitly (e.g., in direct learning method), the signals $v(t)$ and $y(t)$ are fed to the PA identification algorithm.

At the output of the PA, the power spectral density (PSD) of $y(t)$ is calculated. The linearization performance of the PD measured by the ACPR is then observed from the PSD. At the receiver, the received baseband signal is filtered and down-sampled using a root-raised cosine filter $g_r(t)$ that matches the transmitter baseband filter $g(t)$. The discrete-time OFDM symbol samples $s_n(k)$ are then serial-to-parallel converted and demodulated using the FFT operation to obtain the M-QAM digital symbols $\hat{A}_n(k)$. Finally, $\hat{A}_n(k)$ is fed to the M-QAM detector and received bit sequence $\hat{b}_i(k)$ is obtained. The received symbols and bit sequence are used for calculating the EVM and BER, respectively.

5.1.2 MATLAB and ADS-Ptolemy co-simulation setup

The circuit level simulations in this work are run on MATLAB® and ADS-Ptolemy co-simulation environment. The performance of the indirect learning memory-SCPWL PD is evaluated on a PA in a the WiMAX 802.16d downlink transmitter by circuit level simulations. The Freescale

MRF6S23100H LDMOS device model provided in the ADS component library for a WiMAX base station is used for designing the PA [106]. The resultant circuit level simulated PA exhibits short term memory effect and includes up to the seventh order harmonic of the fundamental frequency. The PA is biased at class-AB. The final circuit level PA design has been prototyped and validated in a laboratory by IMD test [106].

In the ADS-Ptolemy simulator, the WiMAX system operates at carrier frequency 2.4 GHz and channel bandwidth of 14 MHz. The OFDM signal is generated with 256 subcarriers. Each symbol is composed of 192 data subcarriers, 1 zero DC subcarrier, 8 pilot subcarriers and 55 guard carriers. A cyclic prefix ratio of 1/4 is used. The OFDM subcarriers are modulated with 64-QAM symbols encoded with code rate 3/4. The baseband OFDM signal is oversampled by 8 times and filtered using a raised cosine filter with roll-off factor 0.2. In the simulations, the SNR at the PA output is 40 dB, unless otherwise indicated.

A block of the downconverted PA input-output (IO) baseband signal (384 639 samples) from the ADS-Ptolemy simulator is then exported to MATLAB for PD identification and signal predistortion. After each adaptation, the PD coefficients obtained are used to predistort the next block of signal and then parsed to the PA in the ADS-Ptolemy simulator. Then, the IO data obtained with the predistorted input is fed to PD identification algorithm for the next iteration. The loop repeats until the PD has converged. The signal feed between MATLAB and ADS-Ptolemy simulators during the PD adaptation is summarized in Figure 5.2.

5.1.3 Measurement testbed setup

The setup of the measurement testbed is illustrated in Figure 5.3. The system consists of a digital baseband processing part and an RF processing part. The device under test (DUT) is a broadband power amplifier from Minicircuits, type ZVE-8G. In the digital baseband processing part, a random phase multitone excitation signal $u[n]$, covering a bandwidth of 5 MHz is generated using MATLAB as

$$u[n] = \sum_{k=0}^{K-1} A_k[n] \cos\big(2\pi \Delta f k n + \phi_k\big), \tag{5.1}$$

where k is the tone number, K is the total number of tones used to generating the signal and Δf is the tone spacing. The tone amplitude, $A_k[n] = 1$ is used for all k and all n. The signal is then transferred to the memory of the digital-to-analog converter (DAC) module SMT 370 from Sun-

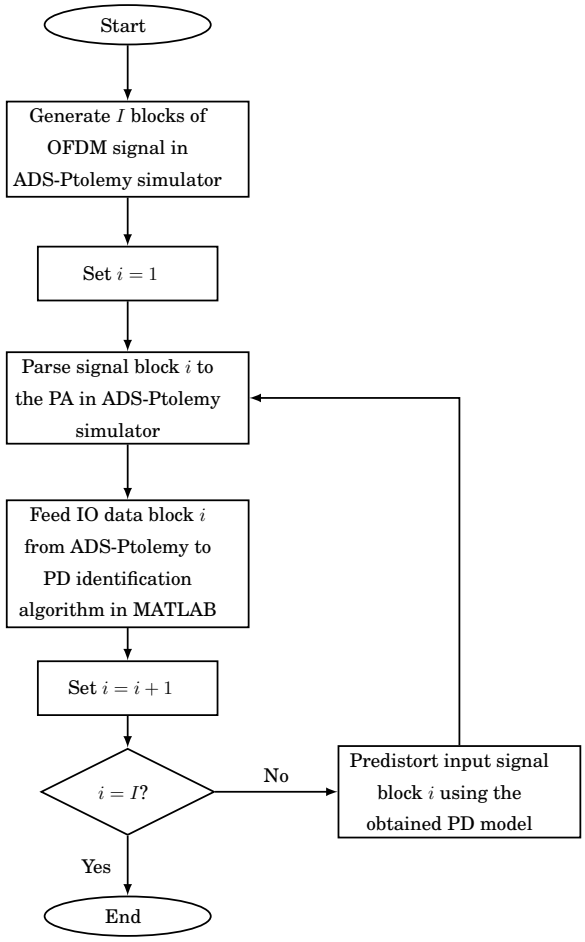

Figure 5.2. Signal feed between MATLAB and ADS-Ptolemy simulators during the PD adaptation phase

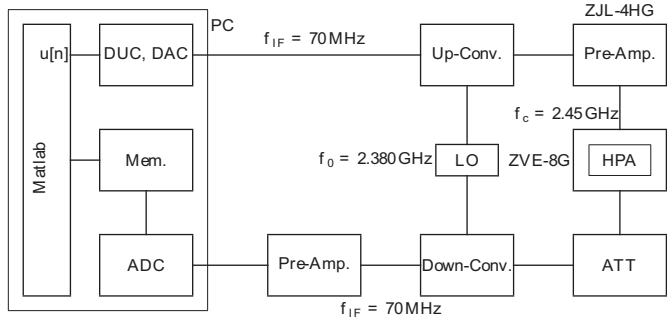

Figure 5.3. Measurement system setup

dance [107], carried by a PCI board (SMT 310Q) in the host PC. This excitation signal is digitally modulated ($f_IF = 70$ MHz) and converted to analog signal before being fed to the RF part. The up-converter mixes the signal to a center frequency $f_c = 2.45$ GHz and filters the signal. A pre-amplifier (Minicircuits ZJL-4HG) and an adjustable attenuator are used to boost the signal before the DUT and to control the input backoff (IBO) of the DUT, respectively. Then the output signal of the DUT is attenuated, down-converted to $f_{IF} = 70$ MHz and filtered. The filters of both the up- and down-converter are bandlimited to 20 MHz. A common local oscillator is used for the up-conversion and down-conversion to avoid phase imbalance. The analog-to-digital converter (ADC) samples the IF signal at a rate of fs = 100MHz and a resolution of 14 bit. The output signal is then stored in a memory module (SMT 351G) and is accessible for model identification.

The measurement system poses a few limitations, such as the limited dynamic range of the ADC, noise introduced by pre-amplification and bandwidth limitation of the up- and down-converters. The details of these limitations are discussed in detail in [V].

5.2 Simulation and measurement results

This section summarizes the performance evaluation and comparison results of the proposed SCPWL PDs obtained by computer simulations, circuit level simulations and by measurement on a microwave PA. As discussed in the beginning of the chapter, the simulation and measurement experiments in this thesis are setup for studying various topics concerning performance of a PD. The evaluation topics and their corresponding experiment setup are summarized in Figure 5.4. The first topic is evaluated in the measurement testbed and the following five topics are evaluated by simulations. The simulation environment in which each topic is evaluated is indicated by the lines connecting the boxes in Figure 5.4. The results of each study are summarized in the following subsections.

5.2.1 Linearization of PA driven to nonlinear region

In [II] and [V], the performance of the static SCPWL PD is evaluated on the Mini Circuit (MC) ZVE-8G PA in the measurement testbed described in Section 5.1.3. The PA is first excited by a random phase multitone

Measurements on RF PA in testbed

1. Effectiveness of linearizing highly nonlinear PA
The performances of the static SCPWL PD and memoryless polynomial PD in linearizing the MC-ZVE-8G RF PA when driven to weak and strong nonlinear regions are compared. The results are reported in [II, V], and are summarized in Sec. 5.2.1

Matlab®
System level simulations

Matlab® & ADS-Ptolemy system and circuit level co-simulations

2. Effect of SCPWL model order on PD performance
In various Matlab simulations, the number of segments of the SCPWL PD is increased over the optimum number to examine whether degradation is observed in PD performance, as in the case of high order polynomial PDs. The results are reported in [I, III, VII] and summarized in Sec. 5.2.2

3. Comparison of adaptive SCPWL and polynomial PDs
In [VII], Hammerstein-SCPWL & memory-SCPWL PDs are compared with Hammerstein-polynomial & memory polynomial PDs, respectively. Various broadband PAs are considered. Indirect and direct learning algorithms are developed for adapting the PDs. The following comparisons are carried out.

- Hammerstein-SCPWL PD vs. Hammerstein polynomial PD
  - Indirect learning PDs for Wiener PA (MATLAB)
  - Direct learning PDs for Wiener PA (MATLAB)
- Memory-SCPWL PD vs. memory polynomial & GMP PDs
  - indirect learning PDs for Wiener-Hammerstein PA (MATLAB)
  - Indirect learning PDs for a LDMOS WiMAX PA (Matlab®-ADS-Ptolemy)
  - direct learning PDs for Wiener PA (Matlab®)

The results are summarized in Sec. 5.2.3

4. Impact of noise on indirect learning PD
Noise at the feedback path of the indirect learning filter is known to cause coefficient bias effects which degrade the performance of polynomial PDs. In [VII], the influence of noise on the performance of indirect learning SCPWL PDs is investigated. The results are summarized in Sec. 5.2.4.

5. Convergence speed of direct learning PDs
The direct learning method is known to be hindered by slow convergence rate when LMS algorithm is employed. In [VII], the convergence rate of direct learning SCPWL PDs and polynomial PDs are compared. The results are summarized in Sec. 5.2.5.

6. Combining PD and PAPR reduction scheme
In [IV], the improvement in linearity and power efficiency of nonlinear PA is studied when PD and PAPR reduction schemes are combined or applied alone. The results are summarized in Sec. 5.2.6.

Figure 5.4. Summary of measurement and simulation experiments

signal, spanning a bandwidth of 5 MHz, in order to obtain a set of input-output (IO) data. The IO data is subsequently used to identify the static SCPWL PD (AM/AM characteristic) using the ICM method in MATLAB®. The identified PD is used to predistort the multi-tone signal and then send back out to the measurement testbed. A spectrum analyser is used for measuring the signal spectrum at the PA output. The performance of the SCPWL PD is compared with that of a static polynomial PD identified using the secant method.

Figure 5.5 shows the results of linearizing the MC ZVE-8G PA driven to a weakly nonlinear region. The spectrum is measured after the down-converter at 70 MHz center frequency. For comparison, an appropriate IBO was imposed on the uncompensated PA so that the inband power of the signal is leveled to that of the compensated output. Both the SCPWL PD and the polynomial PD were able to reduce the adjacent channel power by approximately 12 dB to 15 dB.

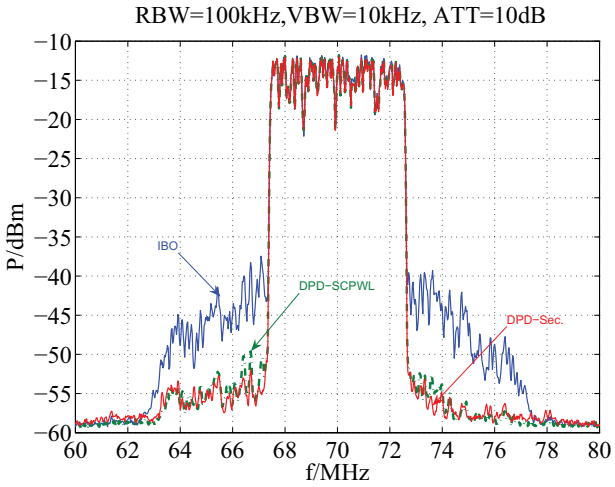

Figure 5.5. Measured power spectra of a PA driven into a weakly nonlinear region – comparison of a PA with IBO, secant Volterra PD and SCPWL PD

Then the performance of the PDs are measured again with the MC ZVE-8G PA driven a bit further into its nonlinear region. In this case, the spectrum analyzer is placed before the down-converter in order to observe a larger dynamic range (see [V] for more details). The results are shown in Fig. 5.6. The polynomial PD performs approximately 2 dB worse than in the case of the weakly nonlinear PA case. Whereas, the SCPWL PD outperforms the polynomial PD by approximately 5 dB at the best case, resulting in an ACPR reduction of 15 dB.

The results showed that the SCPWL PD is more effective in linearizing

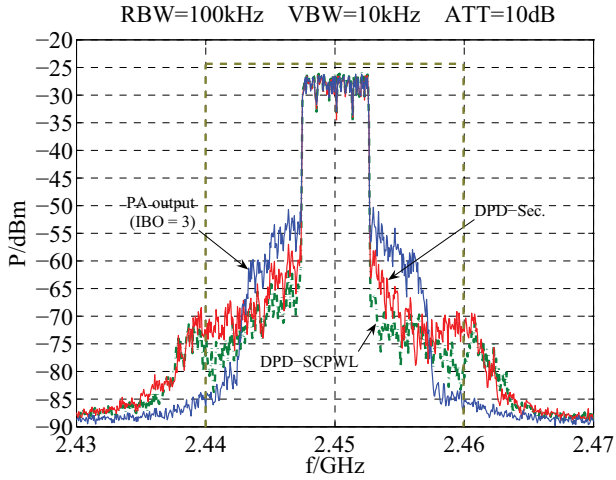

Figure 5.6. Measured power spectra of a PA driven into stronger nonlinear region – comparison of a PA with IBO, polynomial PD and SCPWL PD

strongly nonlinear PA.

5.2.2 Effect of model order on SCPWL PD performance

In [I], [III] and [VII], the performances of the SCPWL PDs are examined as the model order (number of PWL segments) increases. The ACPR performance of the PDs are shown to improve as the number of PWL segment increases, see e.g., Figure 5.13. It is also found in our experiments that the performance improvement of the PDs saturates after a given number of segments. Increasing the number of breakpoints further does not provide performance improvement nor degradation. In contrast, it is well-known that increasing the order of polynomial PDs above an optimum number causes performance degradation.

In [III], the modeling error of identifying a Hammerstein-SCPWL PD, in terms of MSE, is examined with increasing number of breakpoints employed by the SCPWL block. A Hammerstein-SCPWL PD with its nonlinear block modeled with two parallel static SCPWL functions (AM/AM and AM/PM conversions) is identified for a Wiener model PA. The linear and nonlinear blocks of the PA are first estimated, and the ICM method is used to identify the quasi-static SCPWL nonlinear block of the PD. Then, the linear filter of the PD is adaptively identified using the indirect learning architecture employing LMS algorithm (see Figure 5 in [III]). Figure 5.7 shows the output MSE of the adaptive linear filter. The MSE decreases as the number of breakpoints increases. Once again, it is found that in-

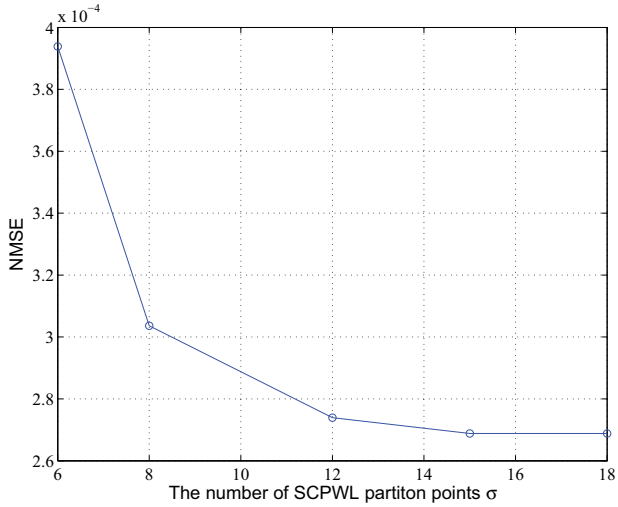

Figure 5.7. Influence of model order (number of segments) on model accuracy .

creasing the number of breakpoints beyond a given number, no significant improvement is observed in the MSE, nor does it degrade.

This illustrates the robust modeling capability of the SCPWL function, especially when strong nonlinearities are characterized.

5.2.3 Comparison of SCPWL PDs with polynomial PDs

In the literature, the most well-referenced digital PDs are dominantly polynomial or simplified Volterra model based PDs. For instance, the memory polynomial [5], generalized memory polynomial (GMP) [86] and dynamic deviation reduction (DDR) Volterra [85] PDs exemplify the state-of-the-art digital PDs with memory. Hammerstein model PDs with polynomial nonlinearity [13,14,16,17] are also popular solution for linearizing nonlinear PAs with memory. Adaptive algorithm employing the indirect and direct learning architectures are most widely adopted for identification of the PD parameters.

The linearization performance of the Hammerstein-SCPWL PD and memory-SCPWL PD proposed in this thesis are compared with polynomial PDs with similar model structure in [VII]. The results are summarized in the following.

5.2.3.1 Hammerstein-SCPWL PD

The performance of the Hammerstein-SCPWL PDs is compared with that of polynomial PDs with Hammerstein model structure by system level

simulations. The indirect learning PDs are evaluated on a Wiener-Hammerstein (W-H) PA given by Equation (32) in [VII], and the direct learning PDs are evaluated on a Wiener model PA described in Equation (31) in [VII].

Indirect learning The indirect learning Hammerstein-SCPWL PD is identified using the algorithm described in Section 4.2.2. The Hammerstein-polynomial PD is identified using the Narrendra-Gallman (NG) method [13, 108], employing blocks of data with 5 OFDM symbols in each iteration for 15 iteration.

The SCPWL PD with $\sigma = 11$ breakpoints for the nonlinear block and linear filter of length $M = 7$ is compared with a Hammerstein polynomial PD with a fifth order polynomial and a linear filter of length $M = 7$. Polynomials of odd-order terms only and of odd-and-even-order terms are employed. Figure 5.8 shows the ACPR performances of the indirect learning PDs. The Hammerstein-SCPWL PD is shown to outperforming the odd-order Hammerstein-polynomial PD of 5th order by approximately 10 dB. The results show that including even order terms in the polynomial model does not show significant improvement in the polynomial PD performance.

As shown in Table 5.1, the Hammerstein-SCPWL PD was able to reduce the inband distortion, in terms of EVM, by approximately 16.8 dB, outperforming the Hammerstein-polynomial PD by approximately 4 dB.

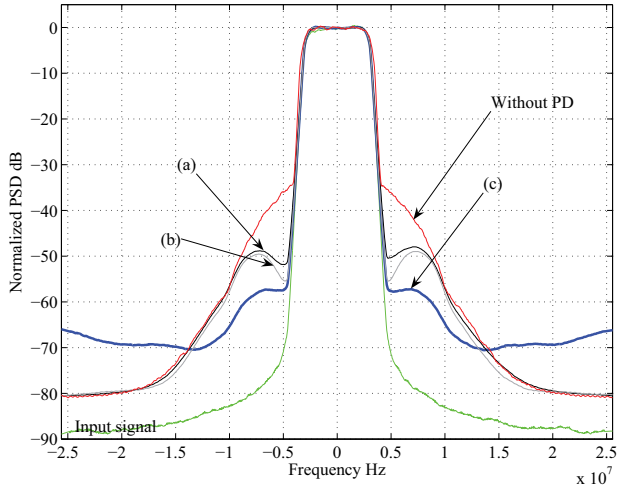

Figure 5.8. ACPR performance of the indirect learning Hammerstein-SCPWL PD and various polynomial based PDs in linearizing a Wiener-Hammerstein PA. (a) Hammerstein-polynomial PD, $K = 5$, odd orders only, $M = 7$. (b) Hammerstein-polynomial PD, $K = 5$, even and odd orders, $M = 7$. (c) The proposed Hammerstein-SCPWL PD, $\sigma = 11$, $N = 5$, $M = 7$.

Direct learning The direct learning Hammerstein-SCPWL PD is adaptively identified using the algorithm summarized in 4.2.2, where the PA model is identified simultaneously with the PD algorithm. The Hammerstein-polynomial PD is identified using the NFxLMS algorithm as in [23], which assumes the Wiener PA model is known. Thus, for fair comparison, the direct learning PDs are evaluated on a Wiener model PA described in Equation (31) in [VII].

The Hammerstein-SCPWL PD employs a linear filter of length $M = 5$ and $\sigma = 11$ breakpoints for the nonlinear block is compared with Hammerstein-polynomial PDs of a fifth order (with odd-order terms and odd-and-even-order terms) and memory length $M = 5$. Figure 5.9 shows the ACPR

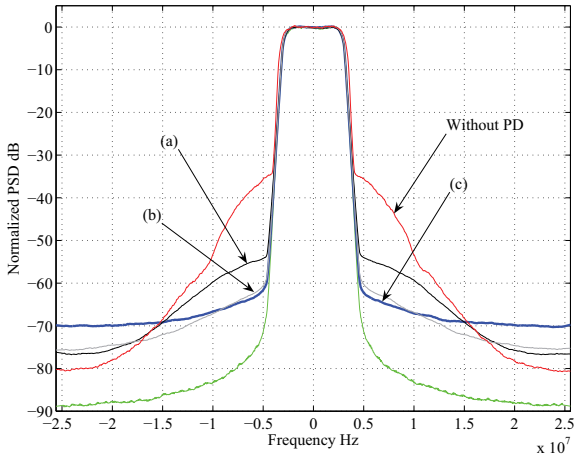

Figure 5.9. Comparison of the direct learning Hammerstein-SCPWL PD with the Hammerstein-polynomial PDs for a Wiener model PA. (a) Hammerstein-polynomial PD, $K = 5$, odd orders only, $M = 5$. (b) Hammerstein-polynomial PD, $K = 5$, even and odd orders, $M = 5$. (c) The proposed Hammerstein-SCPWL PD, $\sigma = 11$, $N = 3$, $M = 5$.

performances of the Hammerstein model PDs. The Hammerstein-SCPWL PD attains an ACPR of approximately 63 dB. The odd-order-only Hammerstein-polynomial PD attained an ACPR of approximately 55 dB, 8 dB worse than that of the Hammerstein-SCPWL PD. By including the even order terms, the ACPR performance of the Hammerstein-polynomial PD is leveled close to that of the Hammerstein-SCPWL PD.

Both the Hammerstein-SCPWL PD and Hammerstein-polynomial PD show similar EVM performance of approximately 24 dB, see Table 5.1.

5.2.3.2 *Memory-SCPWL PD*

The indirect learning memory-SCPWL PD is first evaluated on the Wiener-Hammerstein PA by system level simulations. Its performance is compared with that of the memory polynomial PD [5] and the generalized memory polynomial (GMP) PD [86]. The indirect learning memory-SCPWL PD is also evaluated on an LDMOS PA in a WiMAX downlink transmitter and compared with an indirect learning memory polynomial PD [5] by circuit level simulations in MATLAB-ADS-Ptolemy co-simulator environment described in Section 5.1.2.

The direct learning memory-SCPWL PD is evaluated on the Wiener model PA as described above by system level simulations in MATLAB®. Its performance is compared with that of a polynomial PDs of similar model structure which are identified using the NFxLMS algorithm, assuming the PA model is known [23].

Indirect learning The indirect learning memory-SCPWL PD employs $\sigma = 11$ breakpoints and memory lengths are $L = 3$ and is adapted using (4.15). The memory polynomial PD employs nonlinear term of order $K = 5$ and memory length $L = 4$. The GMP PD employs 5th order aligned terms, i.e., $\mathcal{K}_a = [0\ 1\ 2\ 3\ 4]$ and memory length 4, i.e., $\mathcal{L}_a = [0\ 1\ 2\ 3]$. The cross-terms parameters $\mathcal{K}_b = [2\ 4]$, $\mathcal{L}_b = [0\ 1\ 2\ 3]$ and $\mathcal{M}_b = [1\ 2\ 3]$ are employed.[1] The polynomial PDs are identified using the indirect learning architecture and the "damped" Newton algorithm is used for extracting the PD parameters.

The ACPR performance of the PDs are shown in Figure 5.10. The memory-SCPWL PD attained an ACPR of 60 dB, outperforming both the polynomial PDs when the SNR at the feedback path is 40 dB. As discussed in the previous chapter, the polynomial PDs are prone to coefficient bias effect [25] caused by measurement noise at the feedback path of the indirect learning filter. When the measurement noise is reduced, at SNR 60 dB, the GMP PD is able to attain a similar performance as the memory-SCPWL PD. Whereas, the memory polynomial PD performance is only improved by 5 dB, lacking behind by 5 dB compared to the memory-SCPWL PD.

In terms of inband distortion compensation, the EVM of the linearized received signal is tabulated in Table 5.1. The improvement in EVM provided by the memory-SCPWL PD with 11 breakpoints and memory length 3 is approximately 12 dB. The polynomial PDs with the above mentioned

[1] Please refer to [86] for detailed description of $\mathcal{K}_a$, $\mathcal{L}_a$, $\mathcal{K}_b$, $\mathcal{L}_b$ and $\mathcal{M}_b$.

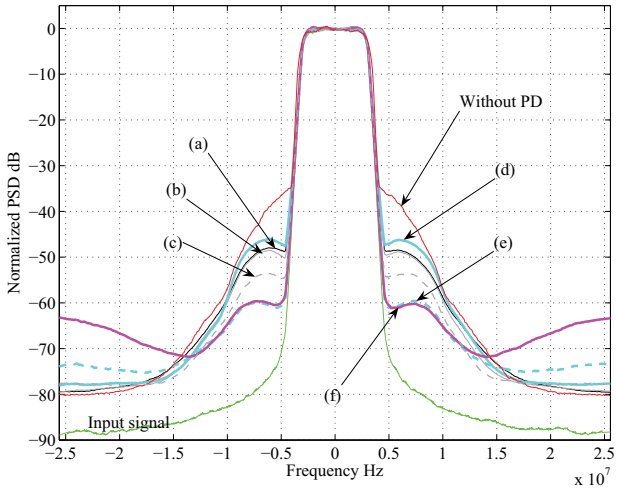

Figure 5.10. ACPR performance of the indirect learning memory-SCPWL PD and various memory polynomial based PDs in linearizing a Wiener-Hammerstein PA. (a) Memory polynomial PD, $K = 5$, odd orders only, $L = 4$. (b) Memory polynomial PD $K = 5$, even and odd orders, $L = 4$. (c) Memory polynomial PD $K = 5$, even and odd orders, SNR = 60 dB. (d) GMP PD, $\mathcal{K}_a = [0 : 4]$, $\mathcal{L}_a = [0 : 3]$, $\mathcal{K}_b = [2\ 4]$, $\mathcal{L}_b = [0 : 3]$, $\mathcal{M}_b = [1 : 3]$. (e) GMP PD at SNR = 60 dB (dashed plot). (f) The proposed indirect learning memory-SCPWL PD, $\sigma = 11$, $L = 3$.

model parameters give slightly better EVM values, i.e., slightly over 1 dB better than the memory-SCPWL PD. Through simulations, the EVM performance of the memory-SCPWL PD is improved by 2 dB when the memory length of the PD is increased to 4 (not shown in the table).

Figure 5.11 shows the ACPR performances of the PDs in linearizing a LDMOS PA in a WiMAX system. The results are obtained by circuit level simulations in MATLAB ADS-Ptolemy co-simulator. The SCPWL PD with memory length 2 and 10 segments is able to keep the PA output under the spectrum mask defined for WiMAX downlink signal (the mask is indicated by the dotted-line plot), as shown in Figure 5.11. Increasing the number of segments to 14 further improves the ACPR performance of the memory-SCPWL PD by approximately 6 dB, reducing the adjacent channel power (ACP) by more than 25 dB. The 5th order polynomial PD with memory length 3 is required to keep the PA output spectrum under the mask. The memory-SCPWL PD with 10 segments outperforms the 5th order memory polynomial PD by approximately 3 dB. The 7th order memory polynomial PD gives slightly better performance than the 5th order PD. However, the 14-segment memory-SCPWL PD outperforms the 7th order memory polynomial PD by 5 dB. The performance of the memory

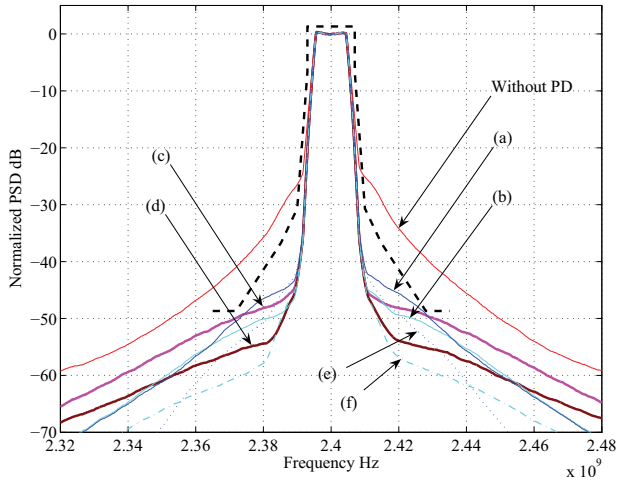

Figure 5.11. Linearization of the Freescale MRF6S23100HPA by the indirect learning PDs. (a) Memory polynomial PD, $K = 5$, odd and even orders, $L = 3$ (b) Memory polynomial PD, $K = 7$, odd and even orders, $L = 3$ (c) Memory-SCPWL PD, $\sigma = 11$, $L = 2$ (d) Memory-SCPWL PD, $\sigma = 15$, $L = 2$. (e) Memory polynomial PD, $K = 5$, $L = 3$, noiseless (f) Memory polynomial PD, $K = 7$, $L = 3$, noiseless.

polynomial PDs are affected by noise at the feedback path. This can be seen from plots (e) and (f), showing the performances of the 5th and 7th order memory polynomial PDs, respectively, when there is no noise at the feedback path.

Direct learning The direct learning memory-SCPWL PD employs $\sigma = 11$ breakpoints and memory length $L_2 = 3$. Its online PA model estimator identifies the PA as a memory-SCPWL model with $\sigma = 11$ and $L_1 = 3$. The NFxLMS algorithm [23] that adapts the memory polynomial PD is shown to have slow convergence rate. The convergence rate decreases greatly when the number of coefficients is increased as shown in Figure 5.17. Thus, in the simulations, the memory polynomial PDs are limited to non-linearity of third and fifth order and memory length of 4 and 5.

Figure 5.12 shows the ACPR performance of the direct learning memory-SCPWL PD and memory polynomial PDs. The memory-SCPWL PD attained an ACPR of 65 dB, i.e., reducing the ACP by approximately 30 dB. The 5th order memory polynomial PD with memory length 5 is also able to attained an ACPR of 65 dB. However this performance is only achieved after adapting the NFXLMS algorithm with 100 000 OFDM symbols, as compared to only a few thousand symbols required by the SCPWL PD. The memory-SCPWL PD outperforms the polynomial PDs with lower order and shorter memory length.

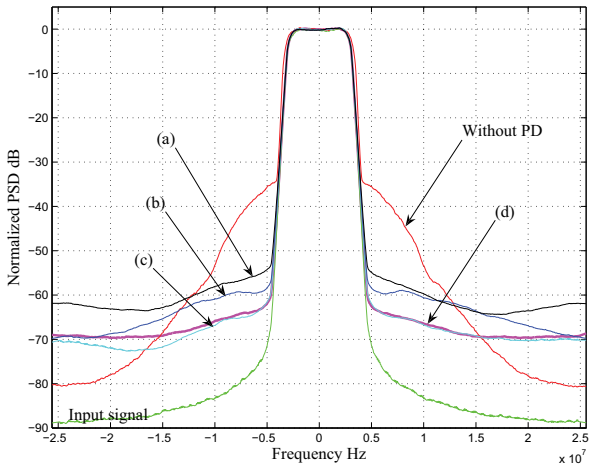

Figure 5.12. Comparison of the ACPR performance of the direct learning memory-SCPWL PD with memory polynomial PDs for a Wiener model PA. (a) Memory polynomial PD, $K = 3$, $L_2 = 5$. (b) Memory polynomial PD $K = 5$, $L_2 = 4$. (c) Memory polynomial PD $K = 5$, $L_2 = 5$. (d) The proposed direct learning memory-SCPWL PD, $\sigma = 11$, $L_1 = L_2 = 3$.

As tabulated in Table 5.1, the memory-SCPWL PD with memory length 3 and the memory-polynomial PDs with memory length 5 attained similar EVM performance of approximately -24 dB. Whereas, when the memory length of the 5th order memory polynomial PD is decreased to 4, the EVM performance dropped by 2 dB.

5.2.4 Impact of noise on indirect learning PDs

Simulations were performed in [VII] to verify the indication of the results in (4.20) and (4.22). Figure 5.13 shows that the indirect learning memory-SCPWL PDs (each with different number of segments) perform equally well when the SNR at the feedback path is set to 40 dB and 50 dB. On the other hand, the ACPR performance of the memory-polynomial PDs degrades as the SNR decreases from 50 dB to 40 dB, as shown in Figure 5.14.

Figure 5.15 summarizes the comparison of noise effects on the performance of polynomial and SCPWL PDs. The normalized adjacent channel power (ACP) at the output of the SCPWL PDs remains almost the same as the SNR decreases. Whereas, a significant increase in normalized ACP is observed at the output of the polynomial PD. (The adjacent channels are indicated in Figure 5.13 by the double arrows)

Table 5.1. Linearized output EVM.

Indirect learning PDs for W-H PA	
Without PD	-5.93 dB
M-SCPWL PD, $\sigma = 11$, $L = 3$	-18.31 dB
GMP PD, 5th order	-19.21 dB
M-Poly. PD, $K = 5$ odd, $L = 4$	-19.94 dB
M-Poly. PD, $K = 5$, even & odd orders, $L = 4$	-20.06 dB
Hammerstein-SCPWL PD, $\sigma = 11$, $N = 5$, $M = 7$	-22.76 dB
Hammerstein-poly. PD, $K = 5$ odd, $M = 7$	-18.55 dB
Hammerstein-poly. PD, $K = 5$ odd & even, $M = 7$	-18.50 dB
Direct learning PDs for Wiener PA	
Without PD	-10.64 dB
M-SCPWL PD $\sigma = 11$, $L_1 = L_2 = 3$	-24.01 dB
M-Poly. PD, $K = 3$, $L_2 = 5$	-23.70 dB
M-Poly. PD, $K = 5$, $L_2 = 4$	-21.81 dB
M-Poly. PD, $K = 5$, $L_2 = 5$	-23.81 dB
Hammerstein-SCPWL PD	-24.02 dB
Hammerstein-poly. PD, 5th odd order	-23.66 dB
Hammerstein-poly. PD, 5th odd & even orders	-24.18 dB

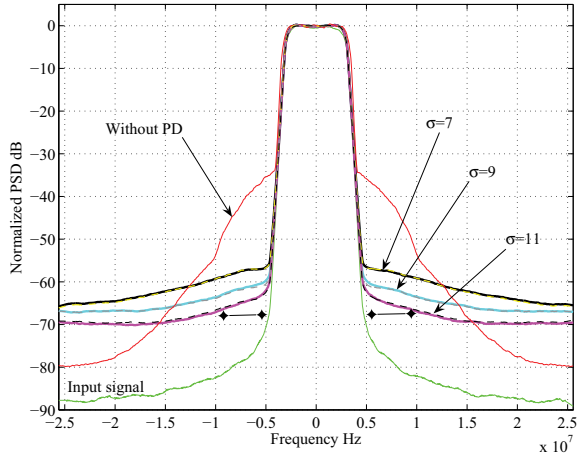

Figure 5.13. ACPR performance of the indirect learning memory-SCPWL PDs with $\sigma = 7, 9, 11$. The solid plots indicate SNR = 40 dB and dotted plots indicate SNR = 50 dB. As the number of breakpoints increases, the performance of the PD improves. The effect of measurement noise is insignificant on the memory-SCPWL PD.

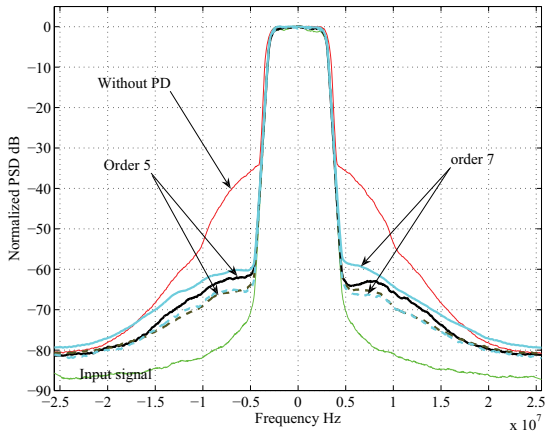

Figure 5.14. ACPR performance of the indirect learning memory polynomial PDs of order 5 and 7. The solid plots indicate SNR = 40 dB and dotted plots indicate SNR = 50 dB. The noise effects are more pronounced on the higher order memory-polynomial PD, as can be seen in the performance degradation of the 7th order PD at SNR 40 dB.

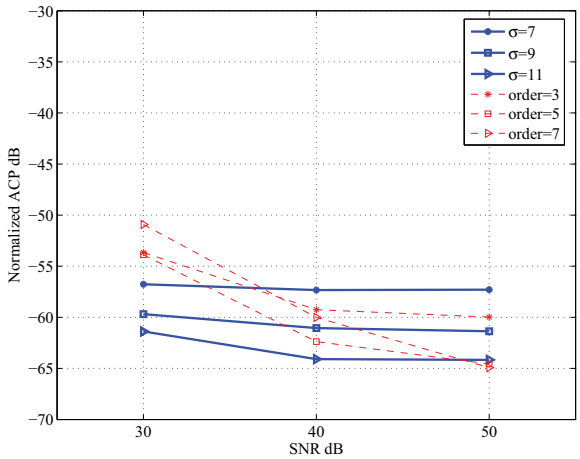

Figure 5.15. Normalized ACP of linearized PA output vs. SNR at the PA output. Solid lines and dashed lines represent the performance of the memory-SCPWL PD and memory polynomial PD, respectively.

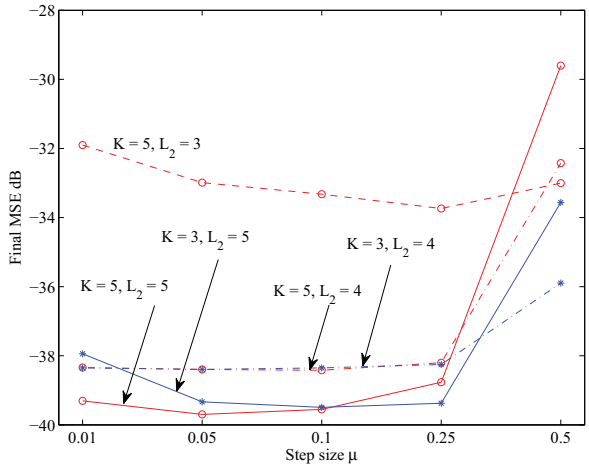

Figure 5.16. MSE after convergence with different step sizes for the direct learning memory polynomial PDs. Lines with '*' markers indicate third order polynomial and 'o' markers indicate fifth order polynomial. Dashed line indicates memory length $L_2 = 3$, dash-dotted line indicates $L_2 = 4$ and solid line indicates $L_2 = 5$.

5.2.5 Convergence speed of direct learning PDs

In [VII], the adaptation of the direct learning memory polynomial PD using the NFxLMS algorithm is found to be hindered by slow convergence, especially when the memory length is increased. Figure 5.16 shows the mean-squared error (MSE) achieved after convergence for the third and fifth order PDs with different memory lengths, adapted using different step sizes. The curves indicate the best step sizes for adapting the polynomial PDs of different orders and memory length. The memory polynomial PD with memory length $L_2 < 5$, both the third and fifth order polynomial PDs could not converge to the SNR level of the PA output. With $L_2 = 4$, the NFxLMS memory polynomial PDs can only attain an MSE of approximately 38.5 dB, after 2000 OFDM symbols. For $L_2 = 5$, a minimum MSE close to noise floor, i.e., SNR $= 40$ dB can be attained. However, the algorithm converged approximately after 80000 OFDM symbols.

On the other hand, only to few hundred symbols is needed for the direct learning memory-SCPWL PD to converge, as seen in Figure 5.17.

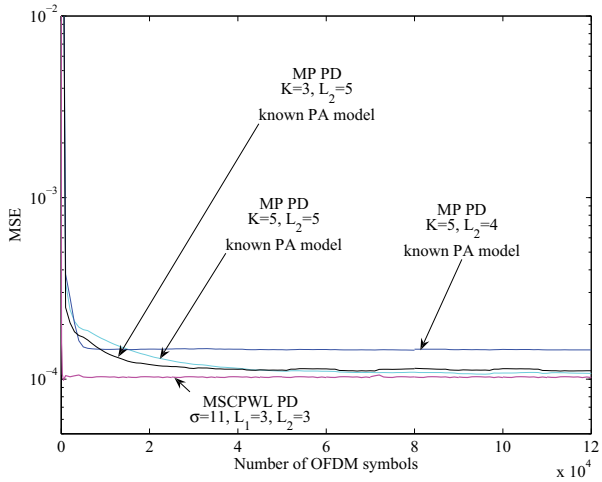

Figure 5.17. Learning curves of the direct learning memory-SCPWL PD ($\sigma = 11$, $L_1 = L_2 = 3$) and the memory-polynomial PDs (3rd and 5th order, $L_2 = 3, 4, 5$, known Wiener PA model).

5.2.6 Combining PD and PAPR reduction schemes

Power efficiency and linearity are two well-known contradicting requirements for the PAs is modern communication systems. In [IV], the result of combining PD and PAPR reduction schemes is compared with the results of the two schemes applied separately. A static nonlinear PA described by the TWTA model [40] which imposes only AM/AM distortion, given by

$$\mathbb{N}\big(\rho(t)\big) = \frac{2\rho(t)}{1+\rho^2(t)}, \tag{5.2}$$

is simulated in the MATLAB environment. The transmitted OFDM signal is generated as described in Section 5.1.1, except that the root-raised cosine filter has a rolloff factor of 0.5. A static SCPWL PD with 12 breakpoints identified using the ICM method is used as the linearizer. For PAPR reduction, the selective mapping (SLM) method [53] using six phase sequences is employed. The PAPR of the OFDM signal, calculated using (2.13), is reduced by approximately 3 dB when the SLM method is applied.

Figure 5.18 shows the normalized PSD of the PA-PD output signal. By reducing the PAPR of the signal alone shows no significant improvement in the ACPR performance. On the other hand, the PD scheme gives an improvement of approximately 20 dB at 8 dB input backoff (IBO). This indicates that the compressive gain distortion is causing more spectral spreading than signal clipping distortion. However, by combining the two schemes, a significant 40 dB improvement is achieved, i.e., twice the

ACPR improvement obtained by the PD scheme alone.

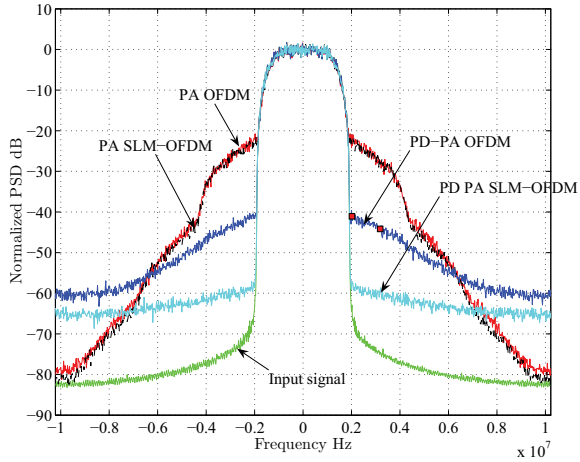

Figure 5.18. ACPR improvement when combining PD and PAPR reduction

The gain in power efficiency by combining the two schemes is measured using the TD defined in (2.8). Figure 5.19 shows the TD at targeted BER of 10^{-4} for the PA with and without any linearization or PAPR reduction schemes, and when the two schemes are combined. It is shown that the minimum TD improves by 1 dB and 2 dB when the PAPR reduction or PD is applied, respectively. When the PAPR reduction and PD are combined, a significant reduction of 3 dB in minimum TD is observed. Notice also that the minimum TD is achieved at a lower OBO when compensation schemes are applied. When the two schemes are combined, the OBO required to achieve the minimum TD is reduced by 5 dB, which is 2.5 dB better than the uncompensated system and more than 1 dB than either of the schemes applied alone. By combining PAPR reduction with PD linearizer effectively reduces the power loss due to the nonlinear distortion, and thus improves the power efficiency of the transmitter.

These results show that combining PAPR reduction with PD is an effective mean to improve ACPR and power efficiency performances.

5.3 Summary of results

The SCPWL PDs proposed in this thesis have been compared with well-referenced polynomial based PDs. The linearization performance of the SCPWL PDs are shown to be in par with and, in some cases, out performed the state-of-the-art polynomial PDs.

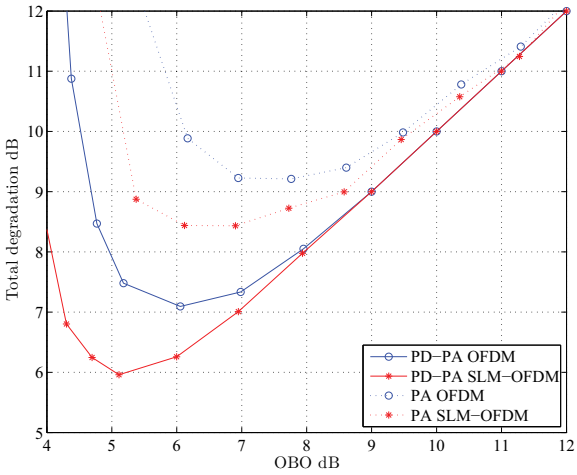

Figure 5.19. Total degradation of the system at targeted BER of 10^{-4}

The results show that the SCPWL PD is more robust for PA driven to nonlinear region compared to a polynomial PD. The SCPWL PD performance can be improved by increasing the number of breakpoints that define the SCPWL function. Its performance does not degrade but saturates when the model order increases beyond an optimal number.

The indirect learning memory-SCPWL PD is shown to have immunity to the effects of noise at the feedback path. Due to the linear basis function of the SCPWL model, it is not affected by the noise induced coefficient bias effects experienced by polynomial PDs. In contrast, memory polynomial and GMP PDs show performance degradation when the SNR at the feedback is low, especially when higher order model parameters (nonlinearity and dynamics) are included.

Comparing the convergence rate of direct learning adaptation, our results show that the direct learning memory-SCPWL PD employing the LMS algorithm converges at a significantly higher rate than the direct learning memory polynomial PD.

It is also shown that in system with high PAPR signal such as OFDM signal, combining PD linearizer with PAPR reduction scheme gives significant gain in power efficiency. By applying PD alone in these systems, the PA has to be backed off to a level where most of the clipping distortion is avoided. By combining PAPR reduction scheme, the PA can be driven further into its nonlinear region which imposes mainly compressive gain distortion. The compressive gain can then be linearized by a PD, thus avoiding the efficiency loss due to the large power backoff.

6. Conclusions

This thesis focuses on digital PD design for broadband PAs in OFDM system, using the SCPWL function. The SCPWL function imposes a saturation level after a maximum input level, which is defined by the last breakpoint, makes the function suitable for modelling PA and PD type of nonlinearities. The original real-valued SCPWL function was employed for modeling the static nonlinearities, i.e., the AM/AM and AM/PM characteristics of the proposed PDs. An analysis on the spectral property of the SCPWL function shows that its basis functions introduce nonlinearity by spreading the spectrum of the input signal to infinite IMD components. Thus, it is suitable for modeling strong nonlinearity, theoretically PA with infinite IMD order. The modeling capability of the function can be improved by increasing the number of segments/breakpoints of the function. It is shown that the model accuracy saturates after a maximum number of breakpoints. Whereas, increasing the order of a polynomial to a high level may significantly degrade the model accuracy.

Given the static nonlinearities of the PA, the image projection method and inverse coordinate mapping method were developed for identifying the corresponding static nonlinear characteristics of the PD. The simplicity of these methods is facilitated by the linear affine structure and the known user-defined breakpoints of the SCPWL function.

A novel complex-valued SCPWL function with memory, suitable for modelling baseband PAs and PDs with memory was proposed. When, the memory length parameter of the model is set to zero, the function reduces to a quasi-static model. The model has a linear-in-the-parameter structure. Thus, well-established linear system identification methods such as least squares (LS) method and the least mean square (LMS) algorithm can be employed for extracting the model coefficients. The function is used for implementing the memory-SCPWL PD and Hammerstein-SCPWL PD.

Indirect and direct learning architectures were employed for training the proposed SCPWL PDs and LMS-based algorithms are derived for updating the coefficients of the proposed PDs. For the identification of the Hammerstein-SCPWL PDs, the non-convex cost function problem is circumvented by employing a modified Wiener model estimator. In the direct learning PD algorithms, computational complexity is mainly attributed to the requirement for PA model estimation, filtering of the input signal with the PA function and computing the derivative of the PA model. Methods are proposed where the properties of the SCPWL function are exploited in order to reduce the complexity of the direct learning algorithms. An analysis on measurement noise effects on the indirect learning SCPWL filter is performed. Results shows that the SCPWL model is not affected by noise-induced coefficient bias effects, which is known to affect polynomial PDs when the indirect learning architecture is employed.

The performance of the proposed SCPWL PDs are evaluated and compared against polynomial PDs. The performance of the static SCPWL PD is evaluated on the MC-ZVE8G PA in a measurement test bed. The SCPWL PD is shown to outperform a polynomial PD when the PA is driven to its nonlinear region. A simulation in MATLAB is also carried out to examine the gain in linearization performance and power efficiency of a PA in OFDM system when combining PAPR reduction method and PD. The ACPR performance of the combined scheme is twice as good as only employing a PD. The total degradation improved by 1 dB compared to either of the schemes applied alone. The indirect and direct learning memory-SCPWL PD and Hammerstein-SCPWL PD are evaluated by simulations in MATLAB. The indirect learning memory-SCPWL PD is found to outperform the memory polynomial PD and generalized memory polynomial PD when measurement noise is present at the feedback path of the indirect learning filter. The direct learning SCPWL PDs are shown to converge significantly faster and perform better than the direct learning polynomial PDs. The indirect learning memory-SCPWL PD was also evaluated on the Freescale MRF6S23100 PA for WiMAX base station by circuit level simulations. The memory-SCPWL PD is found to outperform the memory polynomial PD when measurement noise is present at the feedback path.

Bibliography

[1] P. B. Kenington, *High-Linearity RF Amplifier Design*. Artech House, 2000. 1Cited on pages 1, 11, 12, 13, 14, 16, and 34.

[2] S. C. Cripps, *RF Power Amplifiers for Wireless Communications*. Artech House, 1999. 1Cited on pages 1 and 13.

[3] C. Han, T. Harrold, S. Armour, I. Krikidis, S. Videv, P. M. Grant, H. Haas, J. Thompson, I. Ku, C.-X. Wang, T. A. Le, M. Nakhai, J. Zhang, and L. Hanzo, "Green radio: radio techniques to enable energy-efficient wireless networks," *IEEE Communications Magazine*, vol. 49, no. 6, pp. 46–54, 2011. 1Cited on page 1.

[4] L. Correia, D. Zeller, O. Blume, D. Ferling, Y. Jading, I. GoÌdor, G. Auer, and L. Van der Perre, "Challenges and enabling technologies for energy aware mobile radio networks," *IEEE Communications Magazine*, vol. 48, no. 11, pp. 66–72, 2010. 1Cited on page 1.

[5] L. Ding, G. T. Zhou, D. R. Morgan, Z. Ma, J. S. Kenney, J. Kim, and C. R. Giardina, "A robust digital baseband predistorter constructed using memory polynomials," *IEEE Trans. Commun.*, vol. 52, no. 1, pp. 159–165, Jan. 2004. 1Cited on pages 2, 3, 35, 42, 50, 51, 52, 76, and 79.

[6] A. Zhu, P. Draxler, J. Yan, T. Brazil, D. Kimball, and P. Asbeck, "Open-loop digital predistorter for RF power amplifiers using dynamic deviation reduction-based Volterra series," *IEEE Trans. Microwave Theory Tech.*, vol. 56, no. 7, pp. 1524–1534, 2008. 1Cited on page 2.

[7] M. Ebrahimi, S. Bassam, M. Helaoui, and F. Ghannouchi, "Feedback-based digital predistorter for multi-bit delta-sigma transmitter," in *2011 IEEE 54th International Midwest Symposium on Circuits and Systems (MWSCAS)*, 2011, pp. 1–4. 1Cited on page 2.

[8] S. Bassam, M. Helaoui, and F. Ghannouchi, "2-D digital predistortion 2-D-DPD architecture for concurrent dual-band transmitters," *IEEE Trans. Microwave Theory Tech.*, vol. 59, no. 10, pp. 2547–2553, 2011. 1Cited on page 2.

[9] A. Kwan, F. Ghannouchi, O. Hammi, M. Helaoui, and M. Smith, "Look-up table-based digital predistorter implementation for field programmable gate arrays using long-term evolution signals with 60 MHz bandwidth," *IET Science, Measurement Technology*, vol. 6, no. 3, pp. 181–188, 2012. 1Cited on page 2.

[10] C. Eun and E. J. Powers, "A new Volterra predistorter based on the indirect learning architecture," *IEEE Trans. Signal Processing*, vol. 45, no. 1, pp. 223–227, Jan. 1997. 1Cited on pages 2, 3, 50, 51, and 52.

[11] A. Zhu, M. Wren, and T. Brazil, "An efficient Volterra-based behavioral model for wideband RF power amplifiers," *IEEE Int. Microwave Symposium Digest, 2003 IEEE MTT-S International*, vol. 2, pp. 787–790, Jun. 2003. 1Cited on page 2.

[12] L. Aladrén, P. García-Dúcar, P. Carro, J. De Mingo, and C. Sánchez-Pérez, "High power amplifier linearization using Zernike polynomials in a LTE transmission," in *2012 IEEE Vehicular Technology Conference (VTC Fall),*, 2012, pp. 1–5. 1Cited on pages 2 and 3.

[13] L. Ding, R. Raich, and G. T. Zhou, "A Hammerstein predistortion linearization design based on the indirect learning architecture," in *Proc. IEEE Conference on Acoustic, Speech and Signal Processing (ICASSP'02)*, vol. 3, May 2002, pp. 2689–2692. 1Cited on pages 2, 38, 50, 51, 53, 76, and 77.

[14] Y. Ding, L. Sun, and A. Sano, "Adaptive nonlinear predistortion schemes with application to OFDM system," in *Proc. of IEEE 2003 Conference on Control Applications*, vol. 1, Istanbul, Turkey, June 2003, pp. 1130–1135. 1Cited on pages 2, 38, and 76.

[15] H. Ku, M. D. McKinley, and J. S. Kenney, "Quantifying memory effects in RF power amplifiers," *IEEE Trans. on Microwave Theory Tech.*, vol. 50, no. 12, pp. 2843–2849, Dec. 2002. 1Cited on pages 2, 20, and 40.

[16] H. W. Kang, Y. S. Cho, and D. H. Youn, "On compensating nonlinear distortions of an OFDM system using an efficient adaptive predistorter," *IEEE Trans. Commun.*, vol. 47, no. 4, pp. 522–526, Apr. 1999. 1Cited on pages 2, 3, 38, 50, 51, 54, and 76.

[17] C. Eun and E. J. Powers, "A predistorter design for a memory-less nonlinearity preceded by a dynamic linear system," in *Proc. IEEE Global Telecommunication Conf. (GLOBECOM '95)*, vol. 1, 1995, pp. 152–156. 1Cited on pages 2, 38, and 76.

[18] G. Dahlquist and A. Bjorck, *Numerical methods*. Englewood Cliffs, N.J., Prentice Hall Inc., 1974. 1Cited on page 3.

[19] R. Raich, H. Qian, and G. T. Zhou, "Orthogonal polynomials for power amplifier modeling and predistorter design," *IEEE Trans. Veh. Technol.*, vol. 53, no. 5, pp. 1468–1479, Sep. 2004. 1Cited on pages 3, 8, 33, and 65.

[20] 3GPP, "TR 25.814 - Physical Layer Aspects for Evolved Universal Terrestrial Radio Access (UTRA)," Specifications, 2006. 1Cited on page 3.

[21] "Requirements related to technical performance for IMT-Advanced radio interface(s)," ITU-R, Tech. Rep., 2008. 1Cited on page 3.

[22] Y. H. Lim, Y. S. Cho, I. W. Cha, and D. H. Youn, "An adaptive nonlinear prefilter for compensation of distortion in nonlinear systems," *IEEE Trans. Signal Processing*, vol. 46, no. 6, pp. 1726–1730, June 1998. 1Cited on pages 3, 50, 51, and 54.

[23] D. Zhou and V. E. DeBrunner, "Novel adaptive nonlinear predistorters based on the direct learning algorithm," *Signal Processing, IEEE Transactions on [see also Acoustics, Speech, and Signal Processing, IEEE Transactions on]*, vol. 55, no. 1, pp. 120–133, Jan. 2007. 1Cited on pages 3, 50, 51, 53, 54, 65, 78, 79, and 81.

[24] L. Gan, E. Abd-Elrady, and G. Kubin, "A simplified predistorter for distortion compensation of parallel Wiener-type systems based on direct learning architecture," in *IEEE 13th Digital Signal Processing Workshop and 5th IEEE Signal Processing Education Workshop, 2009. DSP/SPE 2009.*, 2009, pp. 72–77. 1Cited on page 3.

[25] D. Morgan, Z. Ma, and L. Ding, "Reducing measurement noise effects in digital predistortion of RF power amplifiers," in *Communications, 2003. ICC '03. IEEE International Conference on*, vol. 4, may 2003, pp. 2436 – 2439 vol.4. 1Cited on pages 3, 53, 64, and 79.

[26] S. Amin, E. Zenteno, P. Landin, D. Ronnow, M. Isaksson, and P. Handel, "Noise impact on the identification of digital predistorter parameters in the indirect learning architecture," in *2012 Swedish Communication Technologies Workshop (Swe-CTW)*, 2012, pp. 36–39. 1Cited on pages 3 and 64.

[27] Y.-J. Liu, W. Chen, J. Zhou, B.-H. Zhou, F. Ghannouchi, and Y.-N. Liu, "Modified least squares extraction for Volterra-series digital predistorter in the presence of feedback measurement errors," *IEEE Trans. Microwave Theory Tech.*, vol. 60, no. 11, pp. 3559–3570, 2012. 1Cited on pages 3 and 53.

[28] B. Widrow and S. Sterns, *Adaptive Signal processing*. Prentice Hall Inc., 1985. 1Cited on pages 3 and 54.

[29] S. M. Kuo and D. R. Morgan, "Active noise control: a tutorial review," *Proceedings of the IEEE*, vol. 87, no. 6, pp. 943–973, Jun 1999. 1Cited on pages 3 and 54.

[30] M. Abi Hussein, V. Bohara, and O. Venard, "On the system level convergence of ILA and DLA for digital predistortion," in *2012 International Symposium on Wireless Communication Systems (ISWCS),*, 2012, pp. 870–874. 1Cited on page 3.

[31] P. Júlian, M. Jordan, and A. Desages, "Canonical piecewise linear approximation of smooth funtions," *IEEE Trans. Circuits and Syst. I*, vol. 45, no. 5, pp. 567–571, 1998. 1Cited on page 4.

[32] P. Julián, A. C. Desages, and O. E. Agamennoni, "High-level canonical piecewise linear representation using a simplicial partition," *IEEE Trans. Circuits Syst. I*, vol. 46, pp. 463–480, Apr. 1999. 1Cited on pages 4 and 40.

[33] P. S. R. Diniz, *Adaptive Filtering: Algorithms and Practical Implementation*, ser. The Kluwer international series in engineering and computer science. Kluwer Academic Publishers, 2002. 1Cited on pages 5 and 32.

[34] A. Hagenblad, "Aspects of the identification of Wiener models," Lic. thesis, 1999. 1Cited on pages 5, 38, and 58.

[35] T. Wigren, *Recursive Identification Based on The Nonlinear Wiener Model*. PhD Dissertation, Uppsala, Sweden, 1990. 1Cited on pages 5 and 58.

[36] ——, "Recursive prediction error identification using the nonlinear wiener model," *Automatica*, vol. 29, no. 4, pp. 1011–1025, 1993. 1Cited on pages 5 and 58.

[37] S. C. Cripps, *Advanced Techniques in RF Power Amplifier Design*. Artech House, 2002. 1Cited on pages 11, 14, 19, and 20.

[38] J. Vuolevi and T. Rahkonen, *Distortion in RF Amplifier*. Artech House Inc., 2003. 1Cited on pages 11, 14, 19, 20, and 31.

[39] D. Schreurs, M. O'Droma, A. A. Goacher, and M. Gadringer, *RF Power Amplifier Behavioral Modeling*, 1st ed. New York, NY, USA: Cambridge University Press, 2008. 1Cited on pages 16, 19, 20, and 31.

[40] A. A. M. Saleh, "Frequency-independent and frequency-dependent nonlinear models of TWT amplifiers," *IEEE Trans. Commun.*, vol. 29, pp. 1715–1720, Nov. 1981. 1Cited on pages 16, 33, and 86.

[41] V. T. D. Dardari and A. Vaccari, "Analytical evaluation of total degradation for OFDM systems with TWTA or SSPA," Tech. Rep. CSITE-003-99, 1999. 1Cited on page 18.

[42] J. Vuolevi, T. Rahkonen, and J. Manninen, "Measurement technique for characterizing memory effects in RF power amplifiers," *IEEE Trans. Microwave Theory Tech.*, vol. 49, no. 8, pp. 1383–1389, 2001. 1Cited on pages 19, 20, and 22.

[43] J. Vuolevi, "Analysis, measurement and cancellation of bandwidth and amplitude dependence of intermodulation distortion in RF power amplifiers," PhD. thesis, 2001. 1Cited on page 19.

[44] G. Gamez, "Measurements for modelling of wideband nonlinear power amplifiers for wireless communications," Master's thesis, 2004. 1Cited on page 21.

[45] R. V. Nee and R. Prasad, *OFDM for Wireless Communications*. Artech House, 2000. 1Cited on page 24.

[46] S. B. Weinstein and P. M. Ebert, "Data transmission by frequency division multiplexing using the discrete fourier transform," *IEEE Transaction on Communication Technology*, vol. COM-19, no. 5, pp. 628–634, Oct. 1971. 1Cited on page 25.

[47] H. Saeedi, H. S. M. Sharif, and F. Marvasti, "Clipping noise cancellation in OFDM systems using oversampled signal reconstruction," *IEEE Communications Letters*, vol. 6, no. 2, pp. 73–75, 2002. 1Cited on page 26.

[48] N. Aizawa, O. Muta, Y. Akaiwa, and M. Sawahashi, "Effect of peak power suppression and adaptive predistortion on power amplification of an OFDM signal," in *Proc. IEEE 61st Veh. Tech. Conf. 2005 (VTC spring 2005)*, vol. 3, Stockholm, Sweden, May 2005, pp. 1783 – 1787. 1Cited on page 26.

[49] R. Van Nee and A. de Wild, "Reducing the peak-to-average power ratio of OFDM," in *Vehicular Technology Conference, 1998. VTC 98. 48th IEEE*, vol. 3, May 1998, pp. 2072–2076. 1Cited on page 26.

[50] G. Chen, R. Ansari, and Y. Yao, "Improved peak windowing for PAPR reduction in OFDM," in *Vehicular Technology Conference, 2009. VTC Spring 2009. IEEE 69th*, April 2009, pp. 1–5. 1Cited on page 26.

[51] S. H. Müller, , and J. B. Huber, "OFDM with reduced peak-to-average power ratio by optimum combination of partial transmit sequences," *IEE Elect. Lett.*, vol. 33, pp. 368–369, Feb. 1997. 1Cited on page 26.

[52] A. D. S. Jayalath and C. Tellambura, "SLM and PTS peak-power reduction of OFDM signals without side information," *IEEE Trans. Wireless Commun.*, vol. 4, no. 5, pp. 2006–2013, Sep. 2003. 1Cited on page 26.

[53] R. W. Bäuml, R. F. H. Fischer, and J. B. Huber, "Reducing the peak-to-average power ratio of multicarrier modulation by selected mapping," *IEE Elect. Lett.*, vol. 32, no. 22, pp. 2056–2057, Oct. 1996. 1Cited on pages 26 and 86.

[54] A. D. S. Jayalath and C. Tellambura, "A blind SLM receiver for par-reduced OFDM," in *Proc. 56th IEEE Vehicular Technology Conference 2002 (VTC2002)*, Vancouver, Canada, Sep. 2002, pp. 219–222. 1Cited on page 26.

[55] H. Qian, C. Xiao, N. Chen, and G. T. Zhou, "Dynamic selected mapping for OFDM," in *Proc. IEEE Intl. Conf. on Acoustic, Speech and Signal Processing*, vol. 4, Philadelphia, USA, Mar. 2005, pp. 325–328. 1Cited on page 26.

[56] R. J. Baxley and G. T. Zhou, "MAP metric for blind phase sequence detection in selected mapping," *IEEE Trans. Broadcast.*, vol. 51, no. 4, pp. 565–570, Dec. 2005. 1Cited on page 26.

[57] J. Tellado, "Peak to average power reduction for multcarrier modulation," Ph.D. dissertation, Stanford University, 2000. 1Cited on page 27.

[58] J. A. Davis and J. Jedwab, "Peak-to-mean power control in OFDM, Golay complementary sequences, and reed-muller codes," *IEEE Transactions on Inf. Theory*, vol. 45, no. 7, pp. 2397–2417, Nov. 1999. 1Cited on page 27.

[59] K. U. Schmidt, "On cosets of the generalized first-order Reed-Muller code with low PMEPR," *IEEE Transactions on Inf. Theory*, vol. 52, no. 7, pp. 3220–3232, Jul. 2006. 1Cited on page 27.

[60] Y. Xin and I. Fair, "Error-control selective mapping coding for papr reduction in OFDM systems," in *Vehicular Technology Conference, 2004. VTC2004-Fall. 2004 IEEE 60th*, vol. 1, Sept. 2004, pp. 583–587. 1Cited on page 27.

[61] G. S. Yue and X. D. Wang, "A hybrid PAPR reduction scheme for coded OFDM," *IEEE Transactions on Wireless Commun.*, vol. 5, no. 10, pp. 2712–2722, Oct. 2006. 1Cited on page 27.

[62] C. Tuna and D. L. Jones, "Tone injection with aggressive clipping projection for OFDM PAPR reduction." in *IEEE International Conference on Acoustics, Speech, and Signal Processing (ICASSP-2010)*, Mar., pp. 3278–3281. 1Cited on page 28.

[63] N. Jacklin and Z. Ding, "A linear programming based tone injection algorithm for papr reduction of OFDM and linearly precoded systems," *Circuits and Systems I: Regular Papers, IEEE Transactions on*, vol. 60, no. 7, pp. 1937–1945, July 2013. 1Cited on page 28.

[64] B. Krongold and D. Jones, "PAR reduction in OFDM via active constellation extension," *IEEE Transactions on Broadcasting*, vol. 49, no. 3, pp. 258–268, Sept. 2003. 1Cited on page 28.

[65] Y. Kou, W. S. Lu, and A. Antoniou, "A new peak-to-average power-ratio reduction algorithm for OFDM systems via constellation extension," *Wireless Communications, IEEE Transactions on*, vol. 6, no. 5, pp. 1823–1832, May 2007. 1Cited on page 28.

[66] M. C. Jeruchim, P. Balaban, and K. S. Shanmugan, *Simulation of Communication Systems: Modeling, Methodology and Techniques*, 2nd ed. Kluwer Academic/Plenum Publishers, 2001. 1Cited on page 30.

[67] S. Haykin, *Communication Systems*, 5th ed. Wiley Publishing, 2009. 1Cited on page 30.

[68] G. T. Zhou, H. Qian, L. Ding, and R. Raich, "On the baseband representation of a bandpass nonlinearity," *IEEE Trans. Signal Processing*, vol. 53, no. 8, pp. 2953–2957, Aug. 2005. 1Cited on pages 32 and 42.

[69] R. Raich and G. T. Zhou, "On the modeling of memory nonlinear effects of power amplifiers for communication applications," in *Proc. IEEE 10th DSP Workshop*, Pine Mountain, GA, USA, Oct. 2002, pp. 7–10. 1Cited on page 32.

[70] L. Ding and G. T. Zhou, "Effects of even-order nonlinear terms on power amplifier modeling and predistortion linearizer," *IEEE Trans. Veh. Technol.*, vol. 53, no. 1, pp. 156–162, Jan. 2004. 1Cited on page 32.

[71] R. Raich and G. T. Zhou, "Orthogonal polynomials for complex Gaussian processes," *IEEE Trans. Signal Processing*, vol. 52, no. 10, pp. 2788–2797, Oct. 2004. 1Cited on page 33.

[72] E. Costa, M. Midrio, and S. Pupolin, "Impact of amplifier nonlinearities on OFDM transmission system performance," *IEEE Commun. Lett.*, vol. 3, no. 2, Feb. 1999. 1Cited on page 34.

[73] D.-S. Han and T. Huang, "An adaptive pre-distorter for the compensation of HPA nonlinearity," *IEEE Trans. Broadcast.*, vol. 46, no. 2, pp. 152–157, Jun. 2000. 1Cited on page 34.

[74] E. Aschbacher and M. Rupp, "Modelling and identification of nonlinear power amplifier with memory for nonlinear digital adaptive pre-distorter," in *Proc. Workshop on Signal Processing Advances in Wireless Communications*, Jun. 2003, pp. 555–559. 1Cited on page 34.

[75] M. Schetzen, *The Volterra and Wiener Theories of Nonlinear Systems*. John Wiley & Sons Inc., 1980. 1Cited on pages 34, 52, and 53.

[76] J. Mathews and G. Sicuranza, *Polynomial Signal Processing*. John Wiley and Sons Inc., 2000. 1Cited on pages 34, 35, and 49.

[77] S. Boyd and L. O. Chua, "Fading memory and the problem of approximating nonlinear operators with Volterra series," *IEEE Trans. Circuits Syst.*, vol. 32, no. 11, pp. 1150–1161, Nov. 1985. 1Cited on page 35.

[78] G. Karam and H. Sari, "Analysis of predistortion, equalization, and ISI cancellation techniques in digital radio systems with nonlinear transmit amplifiers," *IEEE Trans. Commun.*, vol. 37, no. 12, pp. 1245–1253, Dec. 1989. 1Cited on page 35.

[79] H. Ku and J. S. Kenney, "Behavioral modeling of nonlinear RF power amplifiers considering memory effects," *IEEE Trans. on Microwave Theory Tech.*, vol. 51, no. 12, pp. 2495–2504, Dec. 2003. 1Cited on page 35.

[80] A. Zhu and T. Brazil, "Behavioral modeling of RF power amplifiers based on pruned Volterra series," *IEEE Microwave and Wireless Components Letters*, vol. 14, no. 12, pp. 563–565, 2004. 1Cited on page 36.

[81] F. Filicori and G. Vannini, "Mathematical approach to large-signal modelling of electron devices," *Electronics Letters*, vol. 27, no. 4, pp. 357–359, 1991. 1Cited on page 36.

[82] D. Mirri, G. luculano, F. Filicori, G. Pasini, G. Vannini, and G. Gabriella, "A modified Volterra series approach for nonlinear dynamic systems modeling," *Circuits and Systems I: Fundamental Theory and Applications, IEEE Transactions on*, vol. 49, no. 8, pp. 1118–1128, 2002. 1Cited on page 36.

[83] D. Mirri, F. Filicori, G. Iuculano, and G. Pasini, "A nonlinear dynamic model for performance analysis of large-signal amplifiers in communication systems," *Instrumentation and Measurement, IEEE Transactions on*, vol. 53, no. 2, pp. 341–350, 2004. 1Cited on page 36.

[84] E. Ngoya, N. Le Gallou, J. Nebus, H. Buret, and P. Reig, "Accurate RF and microwave system level modeling of wideband nonlinear circuits," in *Microwave Symposium Digest. 2000 IEEE MTT-S International*, vol. 1, 2000, pp. 79–82. 1Cited on page 36.

[85] A. Zhu, J. Pedro, and T. Brazil, "Dynamic deviation reduction-based Volterra behavioral modeling of RF power amplifiers," *IEEE Trans. Microwave Theory Tech.*, vol. 54, no. 12, pp. 4323–4332, 2006. 1Cited on pages 36 and 76.

[86] D. R. Morgan, Z. Ma, J. Kim, M. Zierdt, and J. Pastalan, "A generalized memory polynomial for digital predistortion of RF power amplifiers," *IEEE Trans. Signal Processing*, vol. 54, no. 10, pp. 3852–3860, Oct. 2006. 1Cited on pages 37, 53, 76, and 79.

[87] T. Wigren, "Recursive identification based on the nonlinear Wiener model," PhD. thesis, 1990. 1Cited on pages 38 and 59.

[88] G. A. Pajunen, "Application of a model reference adaptive technique to the identification and control of Wiener type nonlinear processes," Ph.D dissertation, Helsinki Univ. Tech., Helsinki, Finland, 1984. 1Cited on page 38.

[89] H. B. Poza, Z. A. Sarkozy, and H. L. Berger, "A wideband data link computer simulation model," in *NAECON '75; Proceedings of the National Aerospace and Electronics Conference*, 1975, pp. 71–78. 1Cited on page 39.

[90] L. O. Chua and S. M. Kang, "Section-wise piecewise-linear functions: Canonical representation, properties, and applications," vol. 65, no. 6, pp. 915–929, June 1977. 1Cited on page 40.

[91] M. J. Chien and E. S. Kuh, "Solving nonlinear resistive networks using piecewise-linear analysis and simplicial subdivision," *IEEE Trans. Circuits Syst.*, vol. CAS-24, pp. 305–317, Jan. 1977. 1Cited on page 40.

[92] C. Guzelis and I. G. Goknar, "A canonical representation for piecewise-affine maps and its applications to circuit analysis," *IEEE Trans. Circuits Syst.*, vol. 38, no. 11, pp. 1342–1354, Nov. 1991. 1Cited on page 40.

[93] Y. Guo and J. Cavallaro, "A novel adaptive pre-distorter using ls estimation of sspa non-linearity in mobile ofdm systems," in *Circuits and Systems, 2002. ISCAS 2002. IEEE International Symposium on*, vol. 3, 2002, pp. III–453–III–456 vol.3. 1Cited on page 49.

[94] M. Schetzen, *The Volterra and Wiener Theories of Nonlinear Systems*. John Wiley and Sons Inc., 1980. 1Cited on page 49.

[95] L. Ding, Z. Ma, D. R. Morgan, M. Zierdt, and J. Pastalan, "A least-squares/Newton method for digital predistortion of wideband signals," *IEEE Trans. Commun.*, vol. 54, no. 5, pp. 833–840, May 2006. 1Cited on pages 50, 51, 52, and 53.

[96] A. Zhu and T. J. Brazil, "An adaptive volterra predistorter for the linearization of rf high power amplifiers," in *Microwave Symposium Digest, 2002 IEEE MTT-S International*, vol. 1, June 2002, pp. 461–464 vol.1. 1Cited on pages 51 and 52.

[97] S. Choi, E.-R. Jeong, and Y. Lee, "Adaptive predistortion with direct learning based on piecewise linear approximation of amplifier nonlinearity," *Selected Topics in Signal Processing, IEEE Journal of*, vol. 3, no. 3, pp. 397 –404, June 2009. 1Cited on pages 51 and 54.

[98] E. Biglieri, S. Barberis, and M. Catena, "Analysis and compensation of nonlinearities in digital transmission systems," *Selected Areas in Communications, IEEE Journal on*, vol. 6, no. 1, pp. 42–51, Jan 1988. 1Cited on page 52.

[99] K. S. Narendra and P. G. Gallman, "An iterative method for the identification of nonlinear systems using a Hammerstein model," *IEEE Trans. Automat. Contr.*, vol. 11, no. 3, pp. 546–550, July 1966. 1Cited on page 53.

[100] G. Strang, *Introduction to Linear Algebra*. Wellesley-Cambridge Press, 1993. 1Cited on pages 55 and 56.

[101] A. D. Kalafatis, L. Wang, and W. R. Cluett, "Identification of Wiener-type nonlinear systems in noisy environment," *INT. J. Control*, vol. 66, pp. 923–941, 1997. 1Cited on page 59.

[102] S. Haykin, *Adaptive Filter Theory*, 3rd ed. Prentice Hall Inc., 1996. 1Cited on page 59.

[103] P. L. Feintuch, N. J. Bershad, and A. K. Lo, "A frequency domain model for 'filtered' LMS algorithms-stability analysis, design, and elimination of the training mode," *IEEE Trans. on Signal Processing, [see also IEEE Trans. on Acoust., Speech, and Signal Processing]*, vol. 41, no. 4, pp. 1518–1531, Apr 1993. 1Cited on page 60.

[104] G. Chen, T. Sone, N. Sato, M. Abe, and S. Makino, "The stability and convergence characteristics of the delayed-x LMS algorithm in ANC systems," *Journal of Sound and Vibration*, vol. 216, no. 4, pp. 637–648, Oct. 1998. 1Cited on page 60.

[105] O. J. Tobias and R. Seara, "Performance comparison of the FXLMS, nonlinear FXLMS and leaky FXLMS algorithms in nonlinear active control applications," in *Proc. 11th European Signal Processing Conference, EUSIPCO2002*, vol. 1, Toulouse, France, Sep. 2002, pp. 155–158. 1Cited on page 61.

[106] M. Bruno, J. Cousseau, A. Ghadam, and M. Valkama, "On high linearity high efficiency RF amplifier design," in *Argentine School of Micro-Nanoelectronics, Technology and Applications, (EAMTA)*, Oct. 2010, pp. 97–102. 1Cited on pages 67 and 70.

[107] "SMT370 user manual," Sundance Multiprocessor Technology Ltd., Chesham, United Kingdom. 1Cited on page 72.

[108] E.-W. Bai, "An optimal two-stage identification algorithm for Hammerstein-Wiener nonlinear systems," *Automatica*, vol. 34, no. 3, pp. 333–338, 1998. 1Cited on page 77.

Errata

- In [I], Figure 1 should have the dotted arrow (vector b') at the position of the solid arrow (vector b) and vice-versa.
- In [I], Figure 3 should have the dotted curve (inverse nonlinearity) below the linear line and the solid curve (nonlinearity) above the linear line.

Aalto-DD 38/2014

ISBN 978-952-60-5619-7
ISBN 978-952-60-5620-3 (pdf)
ISSN-L 1799-4934
ISSN 1799-4934
ISSN 1799-4942 (pdf)

Aalto University
School of Electrical Engineering
Department of Signal Processing and Acoustics
www.aalto.fi

BUSINESS +
ECONOMY

ART +
DESIGN +
ARCHITECTURE

SCIENCE +
TECHNOLOGY

CROSSOVER

DOCTORAL
DISSERTATIONS